

CLINICAL IMPLEMENTATION OF
MOSFETS FOR ENTRANCE DOSE IN-
VIVO DOSIMETRY WITH HIGH
ENERGY PHOTONS FOR EXTERNAL
BEAM RADIATION THERAPY

Jason Morton
School of Chemistry and Physics
University of Adelaide
September 2006

Table of Contents

ABSTRACT	5
I ACKNOWLEDGEMENTS.....	7
II ABBREVIATIONS.....	8
III DEFINITIONS.....	8
INTRODUCTION	13
1.1 AIM OF PROJECT.....	13
1.2 SCOPE OF PROJECT	13
1.2.1 Literature Review.....	13
1.2.2 Methods.....	13
1.2.3 MOSFET Commissioning and Characterization	14
1.2.4 Clinical Implementation of In-vivo Dosimetry System.....	14
1.2.5 Setting an Action Threshold.....	15
1.2.6 Clinical Results	15
1.2.7 Conclusion	15
1.2.8 Summary of Scope.....	15
2 LITERATURE REVIEW	17
2.1 INTRODUCTION.....	17
2.2 MOSFETS.....	17
2.2.1 Single MOSFET Dosimeters	18
2.2.2 Dual MOSFET Dual Bias Detectors.....	21
2.3 DIODES.....	28
2.3.1 TLDs (Thermoluminescent Dosimeters)	29
2.4 IN VIVO DOSIMETRY (IVD).....	31
2.4.1 Comparison of Detectors Used In IVD.....	33
3 METHODS	36
3.1 INTRODUCTION.....	36
3.2 PRELIMINARY MEASUREMENTS.....	36
3.2.1 Ion Chambers Used.....	37
3.2.2 Transmission Curves.....	38
3.3 TECHNIQUES FOR MEASURING TARGET DOSE.....	39
3.3.1 Mean Dose – An Approximation of Target/Midline Dose.....	39
3.3.2 A Linear Exponential and Linear Equations Method of Approximating Midline Dose.....	40
3.3.3 Estimation of Midline Dose Using TMR's.....	44
3.4 SUMMARY : ENTRANCE AND EXIT DOSE BASED TECHNIQUES	52
3.5 ISOCENTRIC DOSE	53
3.5.1 Introduction	53
3.5.2 Estimation of Isocentric Dose Using TMR's	54
3.6 ISOCENTRIC DOSE IMPLEMENTATION	58
3.6.1 Implementation of Model.....	58
3.6.2 Comparison with Ion Chambers	59
3.6.3 Comparison with a 2D Planning System	60
3.6.4 Correction for an Inhomogeneous Medium	60
3.6.5 Imhomogeneity Correction in a Lung/Thorax Phantom	62
4 MOSFET COMMISSIONING AND CHARACTERISATION	65
4.1 INTRODUCTION:.....	65
4.2 REPRODUCIBILITY	65
4.3 CONSTANCY	68
4.3.1 Short Term Constancy (Less than 3 months)	68
4.3.2 Total Constancy over 6 Month Period (Long term).....	69
4.3.3 Changes in Constancy.....	71
4.4 SKEWNESS AND KURTOSIS	72
4.5 LINEARITY.....	72

4.6	ANGULAR DEPENDENCE.....	74
4.7	ENERGY DEPENDENCE.....	75
4.8	BUILD UP	76
4.9	TEMPERATURE DEPENDENCE	78
4.10	SSD AND DOSE RATE DEPENDENCE.....	80
4.11	FIELD SIZE DEPENDENCE.....	81
4.12	TIME DEPENDENCE.....	82
4.12.1	<i>Warm up Time</i>	82
4.12.2	<i>Time Till Readout</i>	83
4.13	CONCLUSION	84
5	SETTING AN ACTION THRESHOLD	86
5.1	INTRODUCTION	86
5.2	SETTING THE ACTION THRESHOLD FOR MOSFETS.....	87
5.3	A COMPARISON WITH ACTION THRESHOLDS SET IN LITERATURE.....	89
6	CLINICAL IMPLEMENTATION OF MOSFETS	91
6.1	INTRODUCTION	91
6.2	THE BUILD UP CAP.....	92
6.2.1	<i>Build Up Material</i>	92
6.2.2	<i>Custom Built Cap</i>	93
6.2.3	<i>Build Up Cap Shadow</i>	94
6.2.4	CF_{ent} (<i>Entrance Dose Calibration Factor</i>)	95
6.2.5	CF_{SSD} (<i>SSD Correction Factor</i>)	96
6.2.6	CF_{FS} (<i>Field Size Correction Factor</i>)	97
6.2.7	CF_{wedge} (<i>Wedge Correction Factor</i>).....	99
6.2.8	CF_{ang} (<i>Angular Dependence Correction Factor</i>).....	100
6.2.9	CF_{Tray} (<i>Tray Correction Factor</i>).....	101
6.3	CREATION OF A USER FRIENDLY INTERFACE FOR RADIOTHERAPISTS TO USE	102
	A COMMERCIAL SOFTWARE PACKAGE USED FOR MOSFET MEASUREMENTS (RADCALC)	104
6.4	IMPLEMENTATION OF RESULTS IN RADCALC	106
7	CLINICAL RESULTS.....	110
7.1	INTRODUCTION	110
7.2	CLINICAL USE	110
7.2.1	<i>Patient Setup</i>	110
7.2.2	<i>RT Training</i>	110
7.2.3	<i>MOSFET Measurement process and time</i>	111
7.3	CLINICAL RESULTS.....	111
7.3.1	<i>Breasts</i>	111
7.3.2	<i>Prostates and Pelvis</i>	112
7.3.3	<i>Head and Neck, Lung</i>	113
7.3.4	<i>All Results</i>	113
7.3.5	<i>All Results without Breasts</i>	115
7.3.6	<i>Error analysis</i>	116
7.3.7	<i>Typical results for different techniques</i>	118
7.4	CONCLUSION	121
8	CONCLUSION.....	122
8.1	CONSIDERATIONS	122
8.1.1	<i>Time</i>	122
8.1.2	<i>Error and Precision</i>	123
8.1.3	<i>MOSFET Robustness</i>	123
8.1.4	<i>Long Term Stability</i>	123
8.2	FUTURE PROJECT CONSIDERATIONS.....	123
9	REFERENCES.....	125
	APPENDIX A.....	130

A	AN ANALYSIS ON THE EFFECT OF PHANTOM SCATTER ON ISOCENTRIC MIDLINE DOSE ESTIMATES FOR ENTRANCE AND MIDLINE DOSE PREDICTION	130
A.1	<i>Definitions:</i>	130
A.2	<i>Procedure</i>	133

Abstract

In external beam radiotherapy quality assurance is carried out on the individual components of the treatment chain. The patient simulating device, planning system and linear accelerators are tested regularly according to set protocols developed by national and international organizations. Even though these individual systems are tested errors can be made in the transfer between systems. The best quality assurance for the system is at the end of the treatment planning chain. In-vivo dosimetry measures the dose to the target volume through indirect measures at the end of the treatment planning chain and is therefore the most likely method for picking up errors which might occur earlier in the chain.

Metal Oxide Semiconductor Field Effect Transistors (MOSFETs) have been shown to have a similar error in estimating entrance dose for in-vivo dosimetry to diodes, but no studies have been done clinically with entrance dose in-vivo dosimetry with MOSFETs. The time savings for using MOSFETs makes them preferable to TLD's. Due to their small size and versatility in other applications they are useful as more than dedicated in-vivo dosimetry systems using diodes. Clinical implementation of external beam in-vivo dosimetry would add another use to the MOSFETs without purchasing more specialized equipment.

My studies have shown that MOSFETs can be used clinically for external beam in-vivo dosimetry using entrance dose measurements. After the MOSFET measurement system was implemented using a custom built aluminium build up cap clinical measurements were performed. A total of 23 patients and 54 fields were studied. The mean for all clinical measurements was 1.3%, with a standard deviation of 2.6%. Results were normally distributed around a mean with skewness and kurtosis as -0.39 and 0.34 respectively. For breasts the mean was 1.8%, with a standard deviation of 2.7%. For prostates and hips the

mean was 1.3% with a standard deviation of 2.9%. These results are similar to studies conducted with diodes and TLD's. From these results one can conclude that MOSFETs can be used for entrance dose in-vivo dosimetry and are no worse than diodes or TLD's in terms of their measurement accuracy.

Disclaimer

I, Jason Morton declare that the thesis contains no material which has been accepted for the award of any other degree or diploma in any university and that, to the best of my knowledge and belief, the thesis contains no material previously published or written by another person, except where due reference is made in the text of the thesis. I consent to the thesis being made available for photocopying and loan if accepted for the award of the degree.

Signed:.....

I Acknowledgements

I would like to thank the following people and organizations for helping me with this project: Andrew Kovendy for helping me start the project and for giving me ideas for a choice of model.

Madhava Bhat and Tim Williams for assistance with writing and for reviewing my chapters. Katrina Rech and Jenny Argent for organizing radiation therapist support for getting clinical results.

Judith Pollard for helping me navigate the complex ways of University bureaucracy. The Adelaide Radiotherapy Centre for supporting me with this project and providing the equipment necessary for making measurements as well as clinical time and patients for getting results.

II Abbreviations

MOSFET	Metal Oxide Semiconductor Field Effect Transistor
IVD	In-vivo dosimetry
TLD	Thermoluminescent dosimeter
IC	Ion chamber
PMT	Photomultiplier tube
ICRU	International Commission of Radiation Units and Measurements
WHO	World Health Organization
AAPM	American Association of Physicists in Medicine
ESTRO	European Society for Therapeutic Radiology and Oncology
SSD	Source to surface distance
SAD	Source to axis distance

III Definitions

In-Vivo Dosimetry Definitions

Clinical Target Volume (CTV): “*The clinical target volume (CTV) is the tissue volume that contains a demonstrable GTV and/or sub-clinical microscopic malignant disease, which has to be eliminated.*” (ICRU Report No. 50, cited in Andreo et al. 2005).

Discrepancy: The difference (in percent) between the measured entrance dose and the calculated entrance dose based on treatment planning system information.

Entrance Dose (D_{ent}): The dose at D_{max} below the surface on the central axis (Figure 0-1).

Exit Dose (D_{exit}): The dose at D_{max} before the exit surface on the central axis (Figure 0-1).

Isocentric Dose (D_{iso}): The dose to the isocentre.

Midline Dose (D_{mid}): The dose to the midline of a patient or phantom on the central axis (Figure 0-1).

Target: See CTV.

Transmission: The ratio of the dose at a depth on the central axis to the dose at D_{max} on the central axis (See PDD).

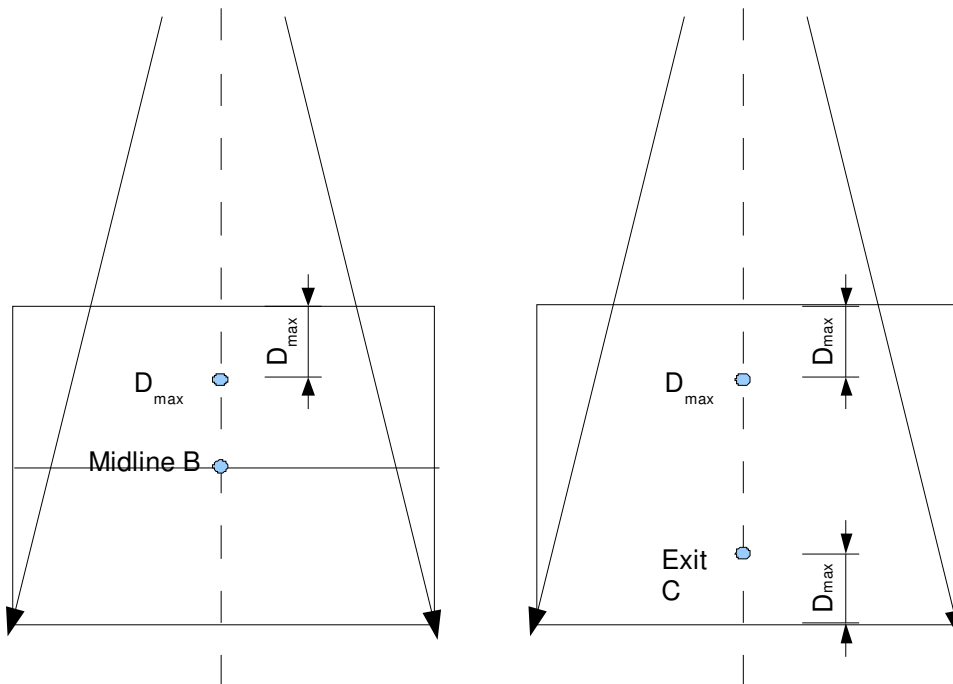
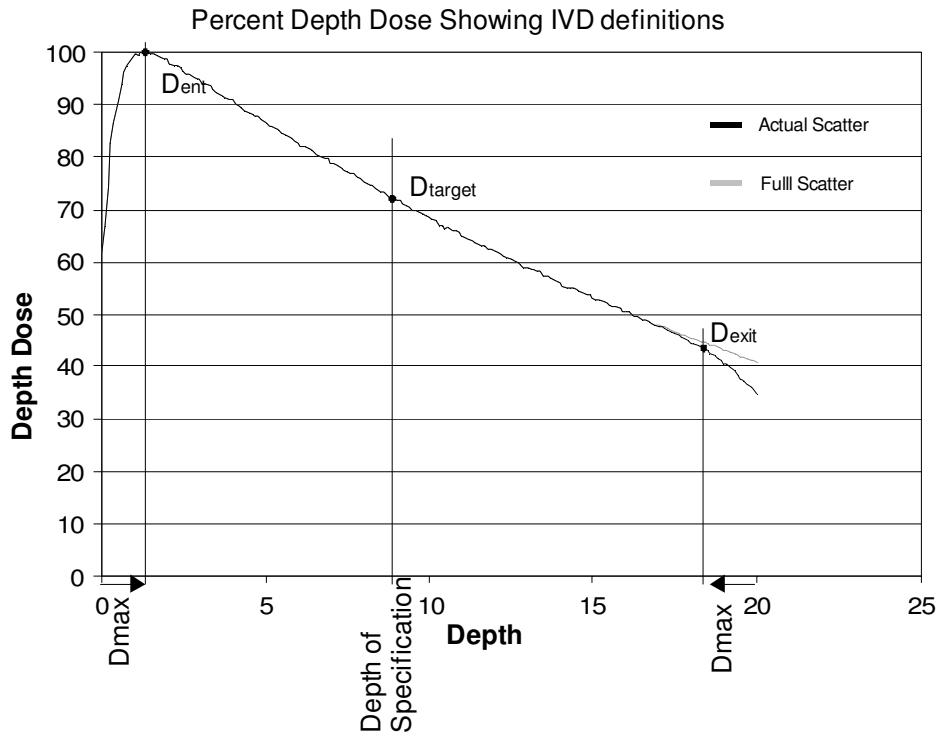


Figure 0-1: In-vivo dosimetry definitions

General Dosimetry Definitions

Depth of Dose Maximum (D_{\max}): The depth of maximum dose on the beam central axis.

Tissue Air Ratio (TAR): $TAR(z, A, h\nu)$ is the ratio of the dose D_Q at point Q on the central axis in the patient or phantom to the dose D_{eQ} , the ‘dose to small mass of water in air’, at the same point Q on the beam central axis (Andreo et al. 2005). The TAR depends on the depth z , field size A , and beam energy $h\nu$ (Figure 0-2).

Percent Depth Dose (PDD): The PDD is defined as follows: $PDD(z, A, f, h\nu) = 100D_Q / D_P$ where D_Q is the dose at point Q at depth z on the central axis of the phantom and D_P is the dose at point P at D_{\max} on the central axis of the phantom (Andreo et al. 2005). $z, A, f, h\nu$ are depth, field size, SSD and energy respectively.

Tissue Phantom Ratio (TPR): The TPR is defined as follows: $TPR(z, A, h\nu) = \frac{D_Q}{D_{Qref}}$,

where D_Q and is dose in a phantom at arbitrary point Q on the beam central axis and D_{Qref} is the dose in a phantom at a reference depth z_{ref} (typically 5 or 10 cm) on the beam central axis (Andreo et al. 2005).

Tissue Maximum ratio (TMR): The TMR is a special case of a TPR, where the reference point depth is D_{\max} (Figure 0-3).

Peak Scatter Factor (PSF): $PSF(A, h\nu)$ is the ratio of the dose to D_{\max} in a phantom at a point on the central axis to the dose in a mini-phantom at the same point. The PSF is a special case of the TAR, where the reference depth is at D_{\max} .

PSF: Ratio of the dose in a mini phantom to the dose at D_{max}

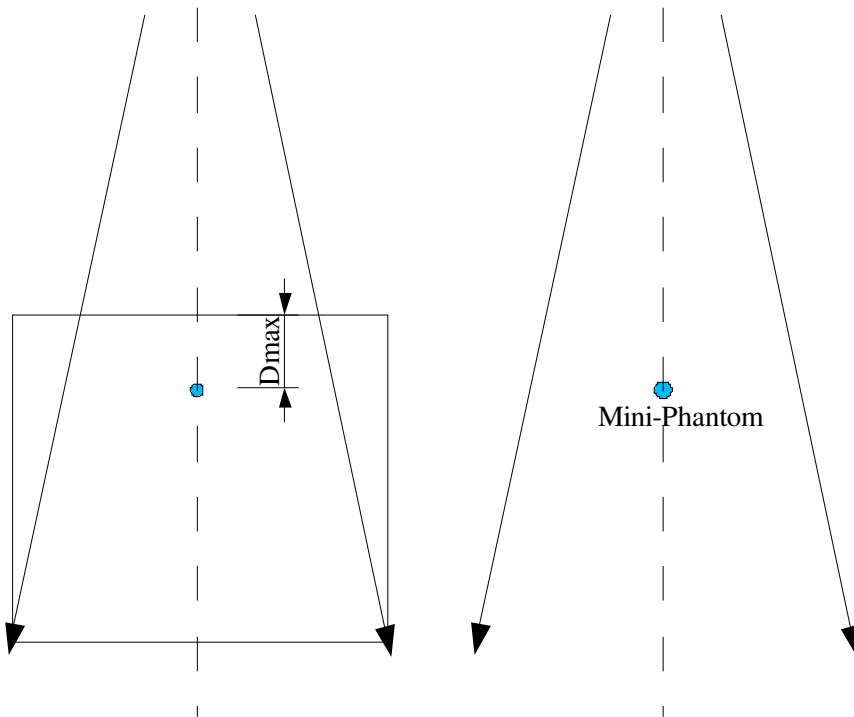


Figure 0-2: PSF Measurement setup

TMR: Ratio of the dose at depth z to the dose at D_{max}

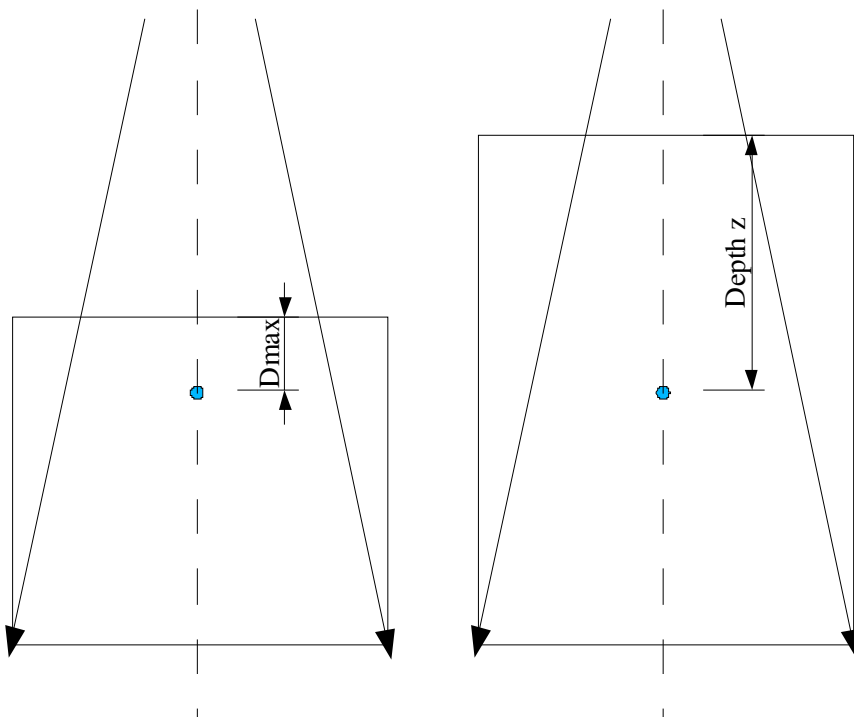


Figure 0-3: Setup for measuring TMR

Total scatter correction factor $S_{c,p}(A)$: The scatter contribution to the dose at depth originating from the collimating system and the phantom for field size r (Khan et al. 1980).

Collimator scatter correction factor $S_c(A)$: The ratio of the effective primary dose for a given collimator field size r (Khan et al. 1980).

Effective primary dose $P_c(A)$: Dose due to the primary beam as well as photons scattered from the collimating system (including source, target, flattening filter, collimator and other scatterers in the beam) (Khan et al. 1980).

Back Scatter Factor $BSF(A)$: see **Peak Scatter Factor** $PSF(A)$.

Off Axis Ratio (OAR): The ratio of the dose off the central axis to the dose on the central axis at a given depth.

Expression of Uncertainties

Error: An error is the difference between a measured value and the true value (IAEA TRS 398 2000). If errors were known exactly the true value could be determined by correcting the errors. Errors can be the result of calculation, transcription or setup errors in in vivo dosimetry.

Uncertainty: the uncertainty associated with a measurement is a parameter that characterizes the dispersion of the values ‘that could reasonably be attributed to the measurand’ (IAEA TRS 398 2000). Uncertainties may also be referred to as random errors. This is normally an estimated standard deviation and is assumed to be symmetrical. It has no sign. There are 2 types of uncertainty, type A and type B. Type A are based on means of measurements and statistical observations, while type B are based on means other than statistical observations (TRS 398). Because type A and type B uncertainties are both estimated standard deviations, they are combined using the statistical rules for combining variances (which are squares of standard deviations).

Introduction

1.1 Aim of Project

Thomson and Nielsen MOSFETs have been shown to be suitable dosimeters for in-vivo dosimetry (Jornet et al. 2004). To date no papers have been published with clinical results for in-vivo dosimetry with high energy photons. The aim of this project is to clinically implement MOSFETs for in-vivo dosimetry (IVD) for high energy photons.

1.2 Scope of Project

1.2.1 Literature Review

A literature review is conducted introducing MOSFETs and their current uses. It discusses the specific characteristics of the different types of MOSFETs in use. The other two devices used regularly in entrance dose in-vivo dosimetry (Diodes and Thermoluminescent dosimeters (TLDs)) are also discussed. Entrance dose in-vivo dosimetry is discussed and a justification for the use of in-vivo dosimetry is given. MOSFETs are then compared to the other two types of detectors as a suitable in-vivo dosimeter. Note that more complex in-vivo dosimetry techniques such as critical structure dosimetry and complex field dosimetry are not compared in this study, and that when in-vivo dosimetry is used it means entrance dose in-vivo dosimetry.

1.2.2 Methods

Current in-vivo dosimetry techniques are investigated to find the technique that would best suit MOSFET dosimetry. The techniques investigated include entrance dose, as well as, entrance and exit dose combined, techniques.

The models investigated are mean entrance and exit dose, a continuous equation approximation, a tissue maximum ratio (TMR) based approximation based on entrance and

exit dose, and an isocentric dose model based on entrance dose and TMR's. The best technique is the method of choice for MOSFETs.

1.2.3 MOSFET Commissioning and Characterization

Thomson and Nielsen MOSFETs are used with their normal bias setting. They are commissioned and investigated for suitability for in-vivo dosimetry. The commissioning process involves investigating:

- Error
- Constancy
- Skewness and Kurtosis of constancy
- Linearity
- Angular Dependence
- Energy Dependence
- Accuracy in the build up region
- Temperature dependence
- SSD dependence (dose rate dependence)
- Field size dependence
- Time dependence
- Total Dose

1.2.4 Clinical Implementation of In-vivo Dosimetry System

The MOSFETs are commissioned with a specially designed build up cap following current diode in-vivo dosimetry commissioning techniques. The choice of build up cap material, shape and size are discussed. The following correction factors are investigated for the MOSFET in the build up cap as these are the standard correction factors investigated for diode in-vivo dosimetry.

- Build up cap shadow
- Entrance dose calibration factor
- SSD correction factor
- Field size correction factor
- Wedge correction factor
- Angular dependence correction factor
- Tray correction factor

A specially designed spreadsheet is made to implement the model of choice. The spreadsheet is compared to a radiotherapy planning system (Pinnacle 3D) as well as an MU checker (Radcalc) for both 6 MV and 10 MV. Radcalc is then commissioned for MOSFET in-vivo dosimetry using the built in diode facility in the program.

1.2.5 Setting an Action Threshold

An action threshold is set based on phantom measurements. This threshold is used for deciding whether a second check of patient dose is necessary. It is then compared to other action thresholds set in literature.

1.2.6 Clinical Results

Clinical trials are carried out on patients and the results compared to other clinical studies with diodes and TLD's.

1.2.7 Conclusion

A conclusion is drawn about the suitability of MOSFETs for entrance dose in-vivo dosimetry for high energy photons, and future areas of study using MOSFETs discussed.

1.2.8 Summary of Scope

A flow diagram showing the manner in which the project is carried out in is shown in Figure 1-1.

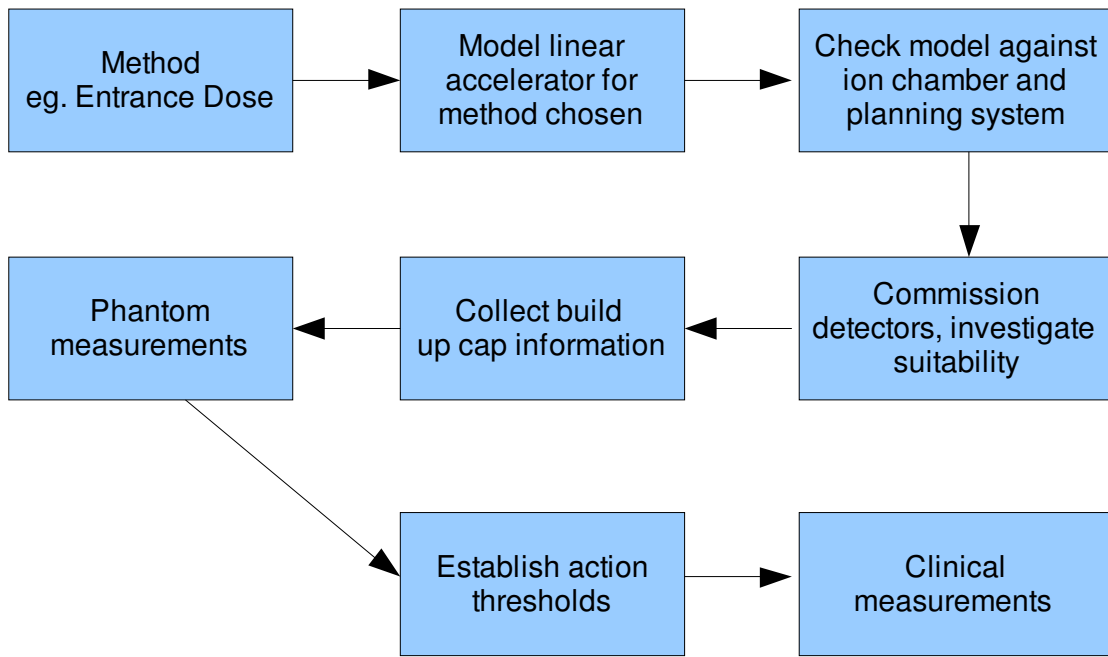


Figure 1-1: Flow diagram of project outline

2 Literature Review

2.1 Introduction

This chapter first outlines the types of dosimeters used in in-vivo dosimetry (IVD) as well as their properties. IVD is then explained and justified. A comparison is then made between the detectors used in IVD.

2.2 MOSFETs

The general MOSFET dosimeter used today is based on a p channel MOSFET. This is a MOSFET with a negatively doped (n-type) Si substrate. Above this substrate sits two positively doped Si substrates (Figure 2-1 p-type). These two terminals are called the source (s) and the drain (d) . Between these 2 terminals is an insulating layer of SiO₂. On top of this insulating layer is the third terminal called the gate. Without a bias voltage applied across the gate the SiO₂ acts as an insulator. When a negatively charged bias voltage is applied across the gate holes are attracted from the source, drain and the bulk oxide layer to the gate (Figure 2-2). Once a threshold voltage (V_{th}) has been reached the number of holes necessary for current to flow between the source and the drain will be reached. As the negative bias across the gate increases the current channel will increase in size and more current will flow. For radiation dosimetry the threshold voltage is often the voltage required across the gate before a set current is reached (say 10 μ A) between the source and the drain.

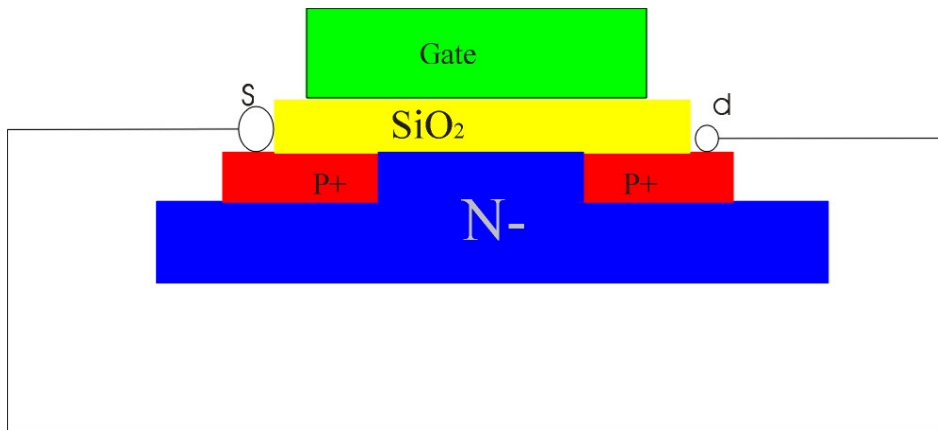


Figure 2-1: A typical MOSFET

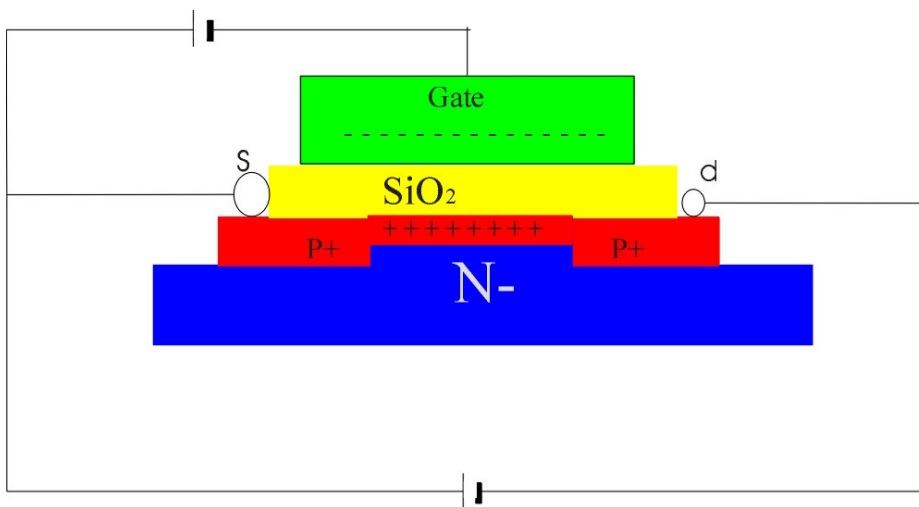


Figure 2-2: A MOSFET with bias across the gate

2.2.1 Single MOSFET Dosimeters

2.2.1.1 Introduction to MOSFETs

MOSFETs were first introduced as a possible radiation dosimeter by Holms-Siedel (1974).

Since then other researchers have investigated the use of the MOSFET as a radiation dosimeter (Gladstone and Chin 1991, Streubel et al. 1998).

When the MOSFET is irradiated three mechanisms contribute to a shift in threshold voltage (Bensen et al. 2004, Chueng et al.2004, Soubra et al.1991, Ramani et al.1994, Thomson and Nielsen Tech Note #4 1996). These mechanisms are:

- The build up of trapped charge in the oxide.

- The increase in the number of interface traps.
- And the increase in the number of bulk oxide traps.

Electrons from ionising radiation which are generated in the SiO₂ layer travel quickly to the positively charged bias contacts (p+). Some of these electrons will recombine with holes (which move more slowly than the electrons), but the holes that fail to recombine are relatively immobile and remain near their point of creation. Over a period of about 1 second the holes undergo stochastic hopping as a result of the biased electric field. When they reach the Si-SiO₂ boundary some are trapped in long term trapping sites that can last for years. This leads to a negative voltage shift in situ that is not sensitive to the Si surface potential. This is the voltage shift (ΔV_{th}) that is measured and is indicative of the dose received by the MOSFET. The voltage threshold is therefore proportional to the formation of long term holes at the Si-SiO₂ interface and can therefore be increased by applying a bias voltage across the gate during irradiation. This will increase the rate at which electrons are removed. By increasing the thickness of the bulk oxide the volume over which the holes are produced is larger leading to a greater shift in threshold voltage. It is easier to increase the bias voltage than the bulk oxide thickness. Manufacturing quality decreases with an increase in bulk oxide thickness. Therefore the way to increase sensitivity is by increasing the bias voltage. Increasing the thickness of bulk oxide can also lead to larger stresses at the Si-SiO₂ interface. This will result in fast surface states and threshold instability (Soubra and Cygler 1994).

2.2.1.2 Advantages and Disadvantages of MOSFETs

MOSFET dosimeters give instantaneous readout, have dose memory, and dose rate independence (Gladstone and Chin 1991). There are, however limitations that make MOSFET dosimetry less user friendly than diodes. Single MOSFETs have temperature dependence. A 1 °C change in ambient temperature can lead to a 4-5 mV shift in V_{th} with a gate oxide

thickness appropriate for a sensor (Soubra et al. 1994, Thomson et al. 1990). A linear dependence of $7.4 \text{ mV}/^\circ\text{C}$ has been published for MOSFETs (Gladstone et al. 1994). The post irradiation voltage shift was greater at higher temperatures (Gladstone et al. 1994). If the MOSFET reading temperature is kept constant there is no significant difference in threshold voltage, even if the MOSFET is irradiated at a different temperature (Cheung et al. 2004). A note is that Cheung et al. 2004 contradicts Gladstone et al. 1994. This is because the two MOSFETs studied are different types of MOSFETs and temperature dependence depends on manufacturing design and quality. As the MOSFET takes approximately 30 seconds for the temperature to stabilise (Cheung et al. 2004) there is no need to measure temperature dependence.

At high doses of radiation the dose to threshold shift relationship becomes non-linear as the positive charge in the oxide traps create an electric field which will negate the effect of the field created by the bias voltage (Soubra et al. 1994, Benson et al. 2004). There will therefore be a decrease in the electron transport and therefore a decrease in the change in voltage threshold (V_{th}) with dose (Soubra et al. 1994). The dose/voltage threshold relationship in p type MOSFET dosimeters is never linear, but instead follows the exponential relationship $V_t(D) = \alpha(1 - e^{-\beta D})$, where α and β are constants for small doses (Benson et al. 2004). This voltage threshold follows the power law relationship $V_t(D) = kD^n$ for larger doses. Dosimeters should be replaced prior to the departure from linearity becoming significant (Benson et al. 2004). The easiest approximation for non-linearity would be a quadratic (Benson et al. 2004, Gladstone et al. 1994).

After irradiation there is an exchange of charge between slow traps at the Si-SiO₂ boundary. This is known as drift and can be several mV. It is therefore important to try to take a measurement at a set time after irradiation to minimise the effect of drift (Benson et al. 2004). Fading is the long term change in RADFET (a p-type MOSFET used to measure radiation)

after irradiation. It is generally less than 2% over a period of months and can therefore be ignored for IVD (Benson et al. 2004). Drift is dependent on MOSFET temperature and time after exposure (Gladstone et al. 1994). After about 100 minutes the relative voltage threshold increases linearly. As measurement is taken shortly after irradiation (within 20 minutes) drift can be ignored.

2.2.2 Dual MOSFET Dual Bias Detectors

The use of single bias MOSFETs in dosimetry was then extended to the use of a dual MOSFET dual bias dosimetry system, where two identical MOSFETs are placed on the same Si substrate. Different bias voltages are applied across each MOSFET on the substrate. As the slope of the voltage threshold depends on the bias they will have different slopes for the same dose (Figure 2-3). The difference in threshold voltages across both MOSFETs is used to obtain the dose delivered to the MOSFETs. The current source (Figure 2-2) is common to both MOSFETs as is the Si substrate. The voltage threshold graphs will therefore remain parallel with dose and different bias voltages. This is because the number of holes trapped near the Si and SiO₂ interface remains constant for both biases and MOSFETs. This is only true until a limit has been reached, after which sensitivity will drop off (Soubra et al. 1994). The implication of this is that the linearity of the voltage threshold with dose is maintained over a larger dose range. This method greatly reduces dependencies such as temperature dependence.

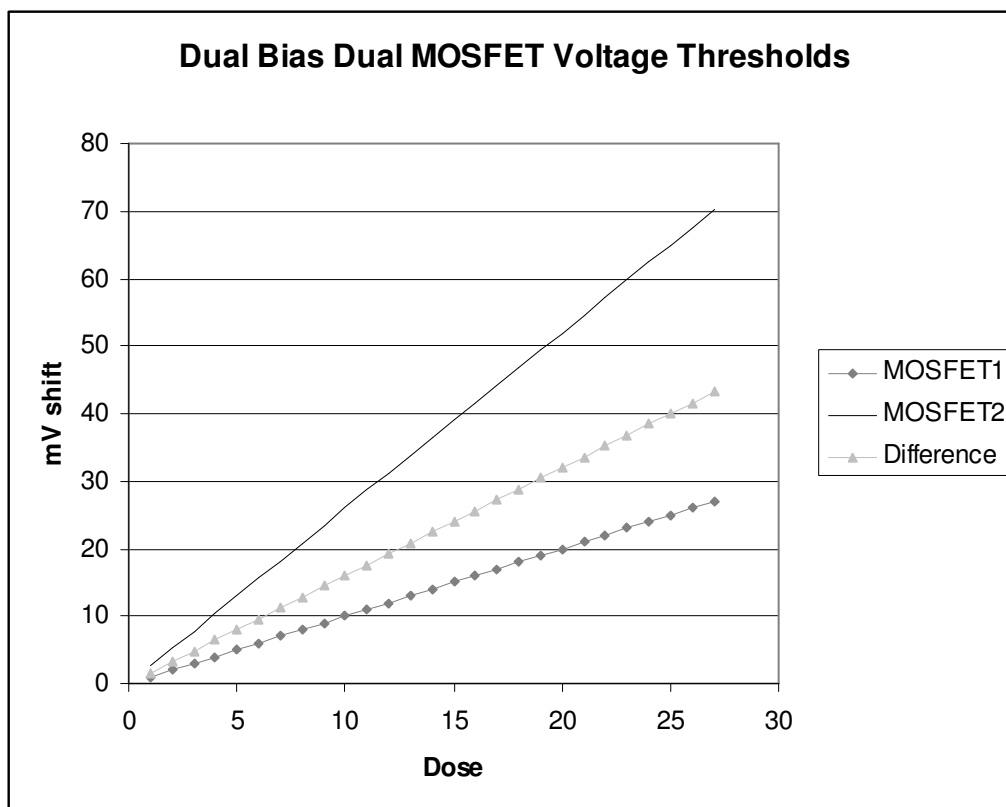


Figure 2-3: Dual Bias Dual MOSFET description

2.2.2.1 Thomson and Nielsen MOSFET Dosimeters

A commercially available MOSFET made by Thomson and Nielsen is an example of a dual MOSFET dual bias “MOSFET”. The gate voltage across the two MOSFETs is +1V and +15V while the MOSFETs are being irradiated (Chuang et al. 2002). The MOSFET system comes with two bias supplies, or one dual purpose bias supply. The MOSFETs used in this study were the Thomson and Nielsen TN502RD low sensitivity MOSFETs and the TN1002RDM high sensitivity microMOSFET. Both of these MOSFETs have been shown to be useful in current radiotherapy practice. Of all the MOSFETs commercially available to date Thomson and Nielsen have been cited the most. These MOSFETs have also been included in more studies relating to radiation therapy, diagnostic radiology and energy dependence studies than any other MOSFET.) The TN502RD isotropic MOSFET can be useful in IMRT verification when combined with a film technique (Chuang et al. 2002). TN502RD isotropic MOSFETs

can be used in high energy x-ray beams as in-vivo dosimeters (Jornet et al. 2004). TN1002RDM microMOSFET is suitable as an in- vivo dosimeter in radiotherapy (Ramaseshan et al. 2004).

2.2.2.2 Dose Consistency and Error

Thomson and Nielsen MOSFETs have dose reproducibility with a 3σ (standard deviation) error of 4.6% at 200 cGy with the bias setting set to normal and a 3σ error of 2.3% at 200 cGy with the bias supply set to high sensitivity (T&N Technical Note #3 2002). The finding of Chuang et al. 2004 of about 5% (3σ) is consistent with the results found by Benson et al. 2004. There is skewness associated with the error distribution implying that the average would be more than one defined with a Gaussian distribution (Benson et al. 2004). Interestingly, while constancy measurements are provided in some papers (Chuang et al. 2002, Soubra and Cygler 1991), histograms have only been provided in one paper (Benson et al. 2004). The MOSFETs used by Benson are RADFETs, not Thomson and Nielsen MOSFETs. Jornet et al. 2004 managed to measure entrance dose to 2.9% (1σ) with the MOSFETs set to high sensitivity. The intrinsic precision of MOSFETs was 0.7% (1σ) when set to high sensitivity mode (Jornet et al. 2004). This is less than the 2% recommended for TLD's (Van Dam et al. 1994). MOSFETs can measure entrance dose to within 5%, and found that the MOSFET are stable within +/- 2% (Ramaseshan et al. 2004).

2.2.2.3 Linearity

In spite of the findings of Benson et al. 2004 studies done on commercially available dual MOSFET dual bias MOSFET systems such as the TN502RD or TN RDM type MOSFETs have excellent linearity with a stated linearity correlation coefficient between 0.998 (Chuang

et al. 2002) over the range 5-420 cGy, 0.999 over the range 5 to 500 cGy (Ramaseshan et al. 2004), and 1.000 from 25-400 cGy (Jornet et al. 2004).

2.2.2.4 Angular Dependence

MOSFETs exhibit angular dependence even though they are small in size. This is because the Si layer of the MOSFET has a higher atomic number than water (or epoxy) leading to increased electron backscatter in one direction (Figure 2-4). In the other direction the Si layer has a lower mass energy absorption coefficient therefore reduced kerma (Figure 2-5). These two effects combine to create a directional dependence (Francescon et al. 1998).

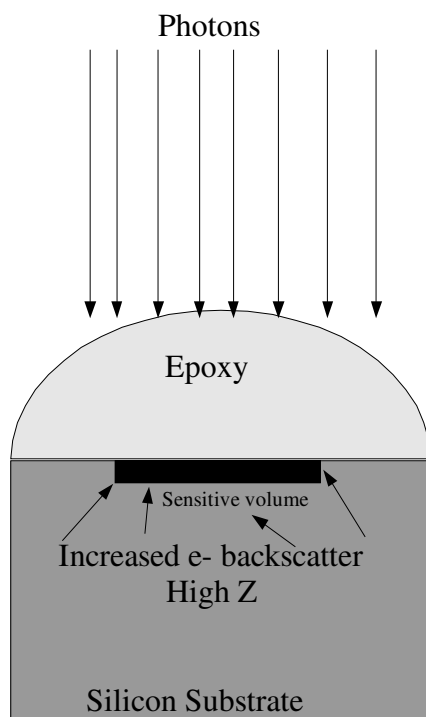


Figure 2-4: MOSFET irradiated from above

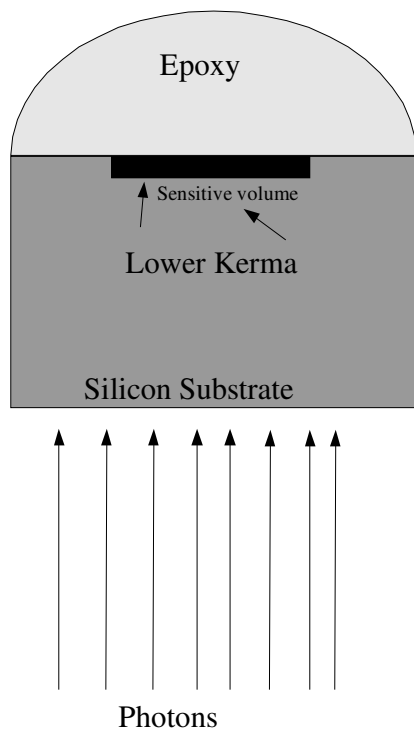


Figure 2-5: MOSFET irradiated from below

Directional dependence of TN-502RD MOSFETs in air changed by 18% over 180 degrees in a 6MV beam (Ramani et al. 1997). MOSFET response differed by 7% with beams from 0 to 90 degrees with a 6MV beam (Scalachi et al. 1998). These angular dependencies are large indeed and would require accurate modelling of the angular response before the MOSFET was used clinically. There have been significant improvements in Thomson and Nielsen MOSFET angular response and at present the Thomson and Nielsen web site states that their angular dependence is <2% over the full range of energies that the detector would be used in. This has been confirmed for high energy photons by many researchers, with Chuang et al. (2002), Jornet et al. (2004), Rowbottom and Jaffray (2004) all stating an angular dependence of less than 2% for energies of 6 to 18 MV. For lower energy photons the angular dependence is greater than 2% (Rowbottom and Jaffray 2004).

2.2.2.5 Temperature Dependence

Thomson and Nielsen MOSFETs do not have any noticeable temperature dependence (Ramaseshan et al. 2004, Jornet et al. 2004, Soubra et al. 1994).

2.2.2.6 Energy Dependence

MOSFETs have a uniform energy response over the MeV range for both photons and electrons, but the energy dependence is observed as energy decreases to about 10keV. In the keV range where photoelectric absorption in Si is the main process there is an over response of the MOSFET. This is because the Si has far more photoelectric interactions than water due to its higher Z. By comparing the mass stopping power ratios μ_{en}/ρ for water and Si one would expect an over response up to 6 times at about 10 keV (Figure 2-6), and up to 4 times at about 40 keV. As the MOSFET is made of Si, Kapton, Si Dioxide (SiO₂), and epoxy (Wang et al. 2004) there is a contribution from all these materials. The model would also have to look at the sensitive volume 1 μ m thick. This was done by Monte Carlo modelling (Wang et al. 2004). They stated that at energies less than 100 keV the energy dependence of MOSFETs increased to a maximum of 6.6 times that of water at 40 keV. These results are similar to the Thomson and Nielsen Tech note #3 (1995) which shows an increase in energy dependence starting at about 200keV and increasing rapidly from 100 keV to a maximum of 4.4 to 12.4 at 45 keV depending on bias, with an increase in over-response corresponding to an increase in bias voltage. Ramaseshan et al. (2004) also noted a strong dose dependence on energy in the keV range, measuring a maximum of 4 to 4.5 times the dose with a 75 kV (2 mm Al) beam and a 100 kV (3.2 mm Al) beam from an orthovoltage machine when compared to a calibrated ion chamber measurement. Kron et al. (1998) noted an increase in energy dependence of up to 3 times at 80 keV energies for Thomson and Nielsen MOSFETs. Edwards et al. (1997) found that Thomson and Nielsen MOSFETs had a relative sensitivity of

around 4.3 at around 40 keV tapering off and becoming stable around 100 keV for quasi-monoenergetic x-rays. He also compared two separate Thomson and Nielsen MOSFETs and found their detector to detector energy dependence was similar.

These results show that energy dependence should be accounted for when measuring dose with MOSFETs; especially if there is a low energy x-ray component. It also means that MOSFETs would be poor measuring devices for dose that is close to high density materials with characteristic x-rays around the MOSFET sensitivity range. Any metal such as tin (K edge 29.2 keV) and lead in the vicinity of the MOSFET will lead to an over estimation of dose at that point. The energy dependence of MOSFETs in the keV would require measuring separately to the MeV range.

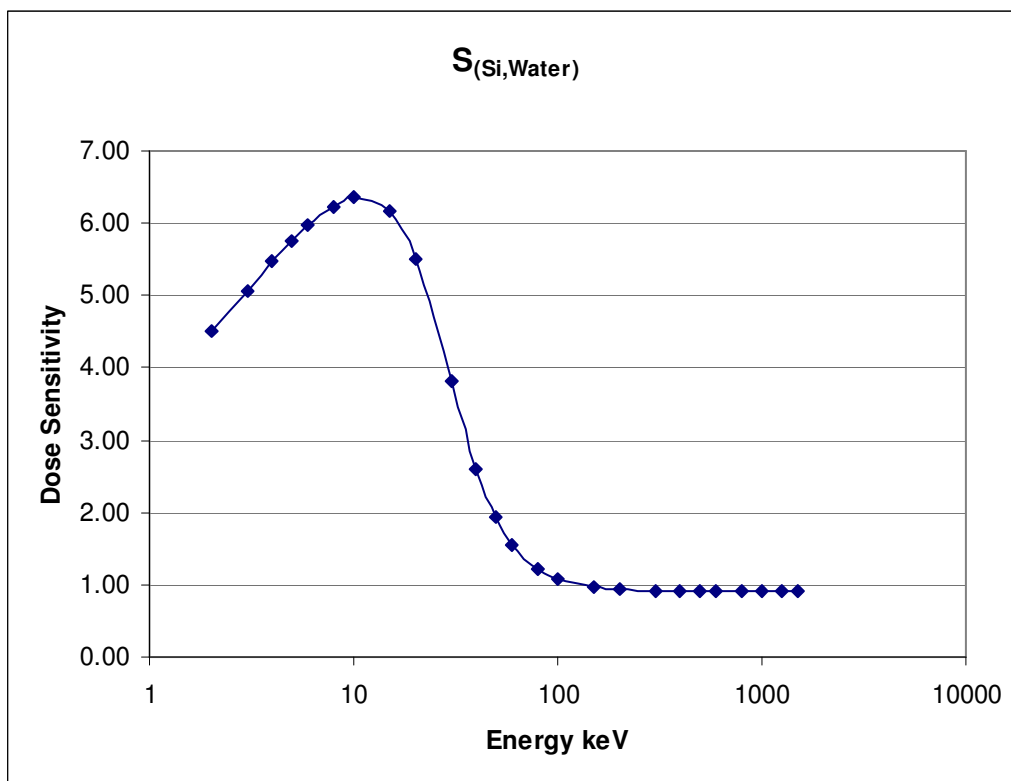


Figure 2-6: Energy Dependence of Dose Response in Si

2.3 Diodes

A diode is a semi-conductor like a MOSFET. There is a p-type and an n-type layer on a piece of Si. Between these two layers there is a depletion layer where there is no charge. When irradiated, electrons and holes will form in the depletion layer. These electrons and holes will then be transported to the p and n end of the diode respectively and current will flow (Figure 2-7). As there are a lot of crystal imperfections on the n side of the diode, as well as the fact that holes move far slower than electrons the probability of recombination centres being encountered is large and therefore minority charge carriers (electrons) contribute to most of the current. The current produced will therefore be proportional to the number of minority charge carriers produced, which in turn is proportional to dose.

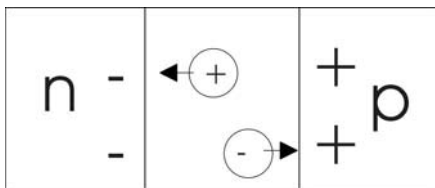


Figure 2-7: A Typical Diode

The detector signal depends on the lifetime of charge carriers, which depends on the doping level, radiation damage, and detector type (p or n) (Huyskens et al. 2001, p13.). Radiation damage induces recombination centres in the crystal lattice resulting in a greater chance of recombination of charges thereby reducing the resulting current. Sensitivity therefore is reduced with dose (Huyskens et al. 2001, p14). At higher dose rates recombination centres become “occupied” this means that there is less recombination and that more current flows. An over-response will therefore become apparent with high instantaneous dose rate. This effect is more pronounced in n type diodes than in p type diodes (Heukelom 1991). As

temperature increases so does the response of the diode. This effect is less at lower doses, but as dose increases the response becomes more pronounced. The temperature dependence depends on dose received. Temperature dependence decreases with accumulated dose (Grusell et al. 1986). Diodes are therefore often pre-irradiated to reduce the temperature dependent effect (Jornet et al. 2004). The diode will also have energy dependence due to the high Z material (Si) as with MOSFETs (Kron et al. 1998, Edwards et al. 1997). All of these characteristics need to be modelled accurately to get a useful IVD program (Huyskens et al. 2001). Dependency on Source to surface distance (SSD), accessories, wedges and field size also need to be measured before the MOSFET is used as a dosimeter. As the dose depends on a current, once the measurement has been made the detector will not keep a history of dose. The readout is instantaneous and cables need to be used to measure the dose.

2.3.1 TLDs (Thermoluminescent Dosimeters)

Thermoluminescent dosimetry is based on the ability of imperfect crystals to absorb and store energy delivered by ionizing radiation. In a perfect crystal an electron would be allowed in certain energy bands separated by bands where it is not allowed (“allowed” bands and “forbidden bands”). As the TLD is not a perfect crystal the electrons can be trapped in the forbidden bands where there are lattice defects or impurities. These are local regions in the forbidden bands where electrons can become trapped. The ease with which the electron can become free from the local trap depends on the depth of the trap. Some electrons may become free at room temperature, while electrons in a deeper trap will need a higher temperature to be released and emit electromagnetic radiation. The electromagnetic radiation released depends on the dose received as well as the temperature of the crystal. This electromagnetic radiation is mainly in the visible spectrum and is detected by a photomultiplier tube when the thermoluminescent (TL) material is heated (normally by a stream of hot gas). The visible light

emitted is correlated to the dose received by the TL material (cited in Van Dam 1994 McKinley 1981, McKeever 1985). The EM radiation is detected by a photomultiplier (PM) and correlated with a dose (Van Dam et al. 1994). These peaks depend on the temperature and composition of the TL crystal, as well as the heating rate of the crystal. Realistically there are several peaks as the energy released comes from metastable energy states between the “discreet” energy bands of the crystal. As there are several discreet states the peaks will correspond to energy trapped between these states. The peaks which are released at lower temperatures are called unstable curves as the glow curve depends strongly on the time after irradiation as they decay naturally. These peaks are therefore not useful. Often pre-heating to 100 degrees for several minutes is done after irradiation to remove unstable peaks (Hosseini-Pooya and Jafarizadeh 2004). Only the peaks which remain after this are read and are stable over time. These are called dosimetric peaks. The sum of all the peaks is called the glow curve. Some institutions only start reading glow curves after a certain temperature has been reached. The system that heats the TLD material and collects the light emitted is called a reader. It is actually a combination of a heater, photomultiplier tube and computer to analyse glow curves.

TLDs can be doped to improve sensitivity. The doping process increases the amount of traps in the crystal lattice that the electrons can be stored in. Typical TLDs used in radiotherapy are LiF. These have a dose sensitivity of 10 μ Gy (micro-Gray) to 20 Gy. LiF is often doped with magnesium and titanium to increase sensitivity. TLDs are produced in a chip form or in powder form.

For TLD dosimetry to be accurate, quality assurance of the system should be performed periodically. TLD accuracy depends on the annealing process. The annealing process involves heating in order to remove all trapped electrons in the crystal, so that it is primed for receiving radiation again. During annealing, the linearity of the heating and cooling, as well as heating

and cooling time periods affect the sensitivity of the TLD. The TLD should therefore be annealed in the same way every time. The reader heating linearity and time should be kept constant, as should the gain on the PMT (Photomultiplier tube). Glow curve analysis is so sensitive to variation that if different metallic trays of the same composition are used the results will be affected by as much as 7% (Wood and Males 1994). To maximise sensitivity TLDs should therefore always be measured in the same tray.

TLDs are not linear in their glow curve output as the dose increases. The dose is generally super-linear till a saturation point is reached after which the dose tapers off as all the traps are full and are therefore less likely to accept electrons (saturation region). The useful range of the TLDs is therefore an important factor when measuring dose. TLDs suffer from fade which means that after irradiation they lose electrons in the trapped regions through random processes over time. The fading of a TLD is small (5-10% per year for LiF) when used in in-vivo dosimetry.

TLDs have a similar constancy to MOSFETs on a measurement to measurement basis with typically 1σ being 2% for radiotherapy applications (Kirby et al. 1992). TLDs have excellent water equivalence and are less susceptible to low energy radiation than other dosimeters in the 30 to 100keV range (Kron et al. 1998). They also do not require cables for measurement which makes them ideal for mail based studies. TLDs have no dose rate or temperature dependence (Van Dam 1994).

2.4 In Vivo Dosimetry (IVD)

The International Commission of Radiation Units and Measurements (ICRU, 1976) recommends that the dose be delivered within 5% of the prescribed dose. This means that at

the end of the planning and treatment “chain” the total error in dose delivered is less than 5%. Each stage in the planning process has an inherent error, so it is therefore hard to meet this requirement. As IVD is at the end of the planning chain any errors made in the treatment chain (such as patient positioning, calculation, accessory insertion etc.) can be detected. Although IVD is extremely useful in the detection of any errors along the chain it is underused, and should be put into practice more often (Mayles et al. 1999). There should be feedback in all steps in the radiotherapy chain as any problems at one point will require a change at another point (Leunens et al.1992). Mayles et al. (1999) also recommend that in situations where a higher than normal dose is given IVD is desirable and portal imaging is essential. In Australia, as in the rest of the world, IVD is often used to check field edges and dose to more radical treatments (Mayles et al. 1999, AAPM TG40 1994). IVD is seldom used to estimate dose to the tumour volume, despite the fact that it was a recommendation of WHO (1988).

Work done by the Leunens group has found that considerable benefits can be achieved by the implementation of regular IVD (Leunens et al. 1990, Heukelom et al. 1991), and that errors that would otherwise have been missed have been found. On the other hand, the inherent errors in IVD make it difficult to identify sources of error (Mayles et al. 1999). It is therefore important to set realistic error boundaries so that time is not wasted looking into errors in the measurement chain that do not exist.

IVD is the only way to actually measure dose given to a patient (Mayles et al. 1999). Errors in the treatment chain have been found that could have been detected by phantom measurements, while some errors have been found that could only have been measured with IVD on a patient. Any new technique should be checked on a phantom before it is implemented clinically (Mayles et al.1999).

2.4.1 Comparison of Detectors Used In IVD

The details involved in implementing IVD have been detailed by several authors (Van Dam and Marinello 1994, Huyskens et al. 2001, AAPM presentation 2003). There are two main types of detector used in IVD today. These are the Thermoluminescent Dosimeter (TLD) and the diode. Despite the fact that ion chambers (ICs) would have lower measurement errors the use of high voltage poses too much of a safety risk to the patient. ICs are therefore never used as a dose measuring device in IVD (Mayles et al. 1999).

TLDs and diodes are used with entrance dose or exit dose measurements to verify the entire planning process to delivery. There are obvious errors associated with exit dose measurement such as detector placement on the exit surface. Measurement error is also harder to trace back to the source of the problem (IAEA 1999) when making exit dose measurements. Entrance dose is far easier to predict. For these reasons entrance dose has been the favourite choice for institutions measuring IVD (Masterson-McGary 2003). Recently MOSFETs have started to be seriously considered as an in-vivo dosimeter as they have few dependencies and therefore require less modelling to implement (Masterson-McGary 2003, Jornet et al. 2004, Ramaseshan et al. 2004). Below is a reproduction of a table given in a presentation by Masterson-McGary 2003 (Table 2-1).

Implementation of IVD can be a long and difficult process. Each characteristic of the detector has to be modelled so that the dose is as accurate as possible. Some detectors such as diodes change dependencies with accumulated dose and therefore require frequent calibrations. This will be discussed in more detail later.

Design Trait	TLD	IC	Diode	MOSFET
Accurate	+	+	+	+
Safe	+	-	+	+
Independent	+	+	+	+
Rugged and Reliable	+	-	+	+
Real Time	-	+	+	+
Comprehensive	+	-	+	+
Efficient to Use	-	+	+	+
Efficient to Calibrate	-	+	+	+
Efficient to QA	-	+	+	+
Affordable	+	+	+	+

Table 2-1: Masterson-McGary comparison

From Table 2-1 MOSFETs and diodes are preferable for IVD as they have fewer negative traits. Another table from Jan Van Dam (1994) has been updated to include MOSFETs (Table 2-2). Table 2-2 compares the measurement drawbacks of each type of detector. As one can see there are five areas with no concern for MOSFETs and TLDs, while diodes have three areas. From this table it would appear that MOSFETs or TLDs would be the preferred choice of in-vivo dosimetry detector.

	Cable	High Voltage	Delay in Results	Dose	Dose accum	Dose Rate	Temp	Energy	Direction
IC	XX	XX	0	0	0	X	X	X	0
Diode	X	0	0	0	XX	XX	X	XX	X
TLD	0	0	X	0 or X	X	0	0	X	0
MOSFET	X	0	0	0 or X	X	0	0	X	0

Table 2-2: Adaptation of Van Dam

0 Means that there is no concern

X Means that there is a mild concern of this factor

XX Means that this factor is a major concern

Many of the negative traits in Table 2-2 can be removed by experiment. Once diodes have been modelled and have had their dependencies accounted for they are very reliable (Van Dam 1994, Jornet et al. 2004, Leunens et al. 1992). The intrinsic sensitivity of the detector is of importance as well. This sensitivity will determine the spread of results that the detector

would give clinically (Jornet et al. 2004). Diodes have a proven track record for giving in-vivo dose with a low intrinsic error. IVD measurement error for diodes, TLDs and MOSFETs is similar, with diodes and MOSFETs having an intrinsic error of 2.0% and 2.9% respectively (Jornet et al. 2004), and TLD about 4.9% (Loncol et al. 1996).

Another factor influencing choice of dosimeter is man-hours per readout. TLDs require the greatest amount of time per readout, while MOSFETs and Diodes require shorter times, as preparation of these detectors consists of placing detector on the patient and pressing a button once the initial calibration of the relevant factors has been made.

As MOSFETs require the modelling of fewer correction factors than diodes and fewer calibrations once prepared, MOSFETs show a slight advantage as an in-vivo dosimeter over diodes and TLDs as they are comparable to the better choice of detector in Van Dam and Marinello 1994 and Masterson-McGary 2003. There is no huge advantage over the other types of dosimeters for in-vivo dosimetry.

The implementation of in-vivo dosimetry with MOSFETs will be discussed in the next chapter. Finding a useful model for approximating dose to the tumour will be explored with several techniques essentially employed are compared, as well as a new technique introduced. This technique is similar to that employed by other authors, (Van Dam 1994, Masterson-McGary 2003) will also be introduced.

3 Methods

3.1 Introduction

Van Dam et al.1994 states that “*a check of entrance and exit dose is, also an indirect check of target dose*”. The primary aim of in vivo dosimetry in radiotherapy is to check that the target (tumour) dose is delivered accurately. There are several techniques employed at present to check the target dose from entrance and exit doses.

- The use of the entrance dose (D_{\max} dose) and exit dose (Dose at D_{\max} depth from the exit surface) to measure the midline dose.
- The use of entrance dose to measure the dose to the isocentre (tumour).

Van Dam et al. 1994 p10. outlines the use of midline dose as an approximation of target dose. Even though these techniques are old they are still employed today (Huyskens et al. 2001, AAPM Report 87 2005), showing the usefulness of these techniques. In order to assess the accuracy of these models a sample set of data was taken for entrance, midline and exit doses in water equivalent RW3 with ion chambers.

3.2 Preliminary Measurements

All external IVD point based extrapolation techniques use entrance or exit dose measurements or a combination of the two to predict the target dose. Entrance, exit and midline dose measurements need to be taken with the greatest accuracy possible. Ion chambers were used in water equivalent RW3 (Tello et al. 1995) in a 6 MV photon beam. Ion chambers were placed at a depth of D_{\max} , D_{mid} (depth of middle of phantom), and D_{exit} (depth of D_{\max} before the exit surface of the phantom). For midline dose measurements the midline was taken at the isocentric depth as most clinical techniques with photons use isocentric techniques with multiple fields (Dobbs et al. 1999 p21.) . The measurement depth of the ion chamber was the depth of the effective point of measurements z_{eff} for that ion chamber as per IAEA TRS 398 (2000).

- For cylindrical ion chambers z_{eff} is the depth of the centre of the ion chamber $-0.6r$, where r is the radius of the cavity of the ion chamber (IAEA TRS 398, 2000 p78).
- For parallel plate ion chambers (PPICs) the depth of the effective point of measurement is the depth of the inner surface of the entrance window (IEAE TRS 398, 2000 p31).

As ion chambers have a much better photon ionisation accuracy it is better to use ion chambers to create midline and exit transmission curves than other types of detectors (IAEA TRS 398 2000 p78). For high energy photons the change in stopping power ratio for water to air with depth is small enough to be considered negligible (IAEA TRS 398, 2000 p78). For this reason the depth ionisation curve measured with an ion chamber is very close to the depth dose curve. Depth ionisation curves can therefore be used as depth dose curves when normalised to D_{max} .

Preliminary measurements were made on a 6 MV photon beam in RW3 phantoms of different water equivalent thicknesses. These measurements were then used to compare several models to find a suitable model for approximating midline dose.

TMR's used later in this chapter are constructed from PDD's, collimator scatter factors and phantom scatter factors, taken during machine commissioning, as per Khan et al. (1980).

3.2.1 Ion Chambers Used

The cylindrical ion chamber used was a NE2571 type ion chamber. The effective point of measurement was taken as 2 mm above the centre of the ion chamber. The parallel plate ion chamber used was a ROOS type ion chamber. The effective point of measurement was taken as 1mm below the upper surface of the detector. These displacements were derived from the cavity radius of 3.2 mm for the Farmer chamber (IAEA TRS 398, 2000, p33) and window thickness of 1.18 mm for the ROOS chamber (IAEA TRS 398, 2000, p37).

3.2.2 Transmission Curves

Definition:

- Midline Transmission (T_{mid}): The ratio of the dose to the middle of a phantom to the dose at D_{max} in the same phantom.
- Exit Transmission (T_{exit}): The ratio of the dose to the depth D_{max} before the exit surface of the phantom to the dose at D_{max} in the same phantom.

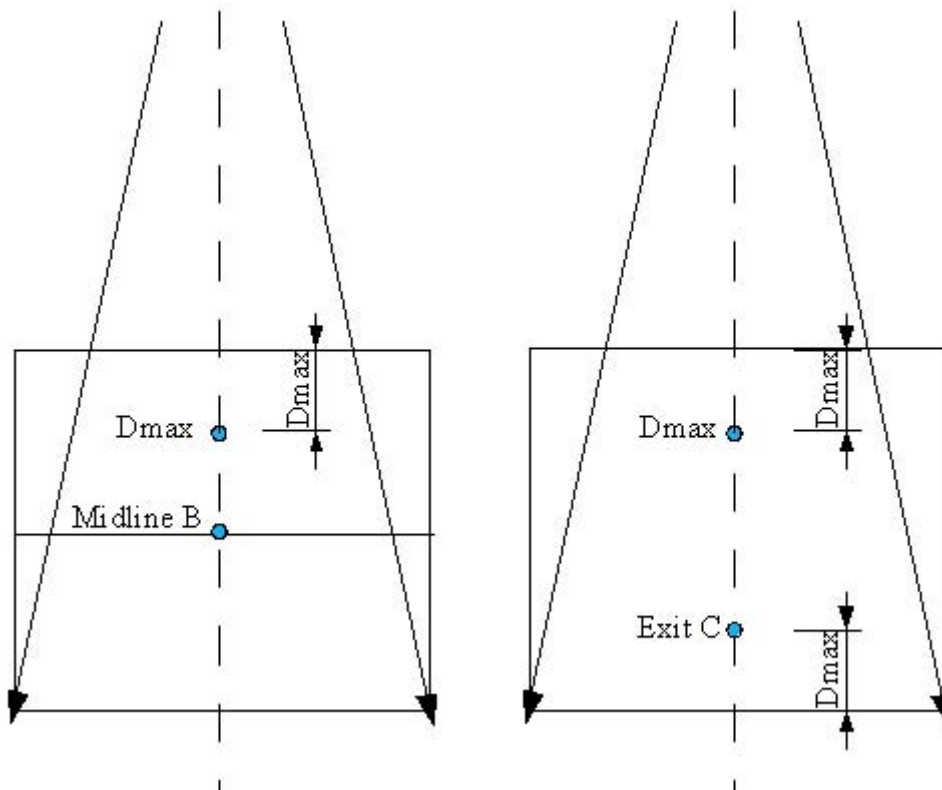


Figure 3-1: Transmission through a phantom

From (Figure 3-1),

$$T_{mid} = \frac{B}{D_{max}}, \quad (3.2.1)$$

$$T_{exit} = \frac{C}{D_{max}} \quad (3.2.2)$$

Midline and exit transmission curves were created from ion chamber measurements.

The results of the ion chamber measurements are in the graphs below. The midline transmission curve is approximately linear (Figure 3-2). The exit transmission curve is approximately exponential (Figure 3-2). The curves for these depend on field size.

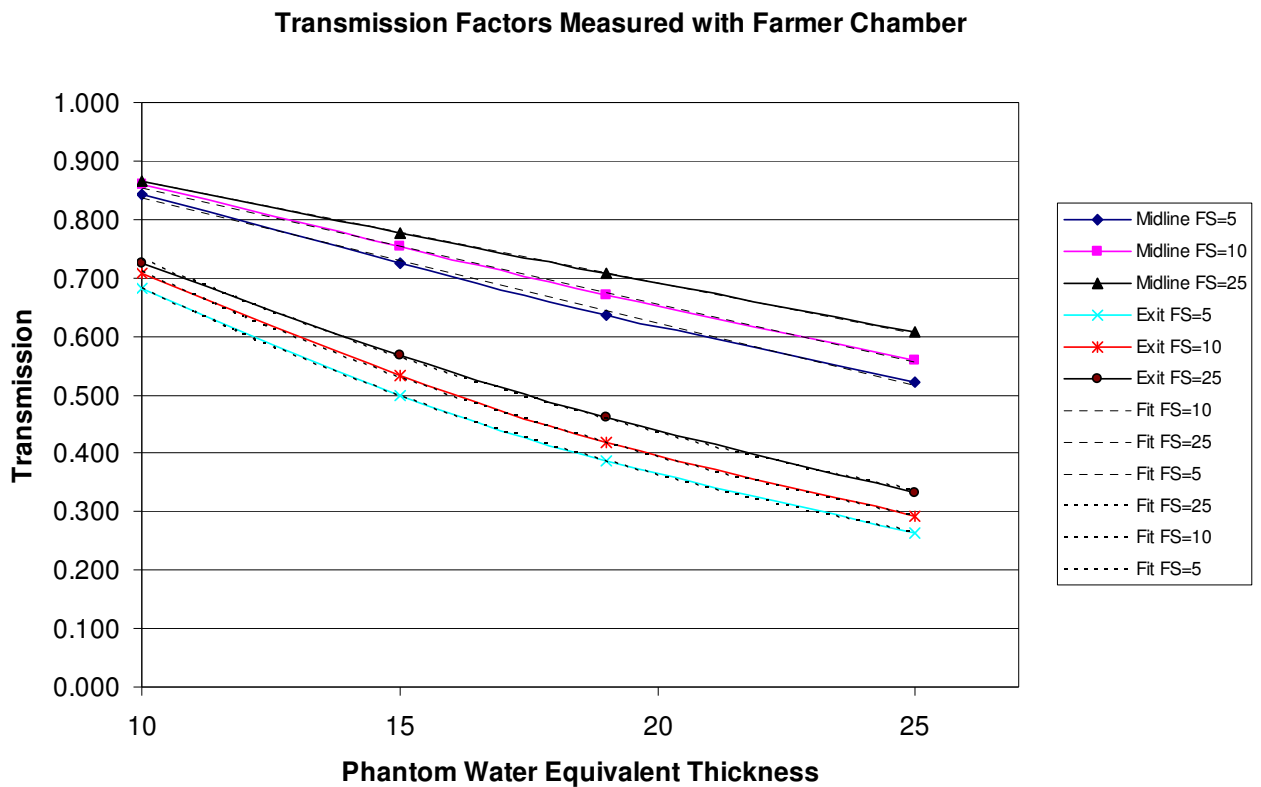


Figure 3-2: Midline and Exit Transmission curves measured with an ion chamber

From the above graph (Figure 3-2) it is likely that the midline and exit transmission curves can be approximated by linear and exponential equations respectively that depend on field size.

3.3 Techniques for Measuring Target Dose

3.3.1 Mean Dose – An Approximation of Target/Midline Dose

A simplified approach to measure the midline dose is found in Van Dam 1994 p12.

$$D_{mid} = \frac{D_{ent} + D_{exit}}{2} \tag{3.3.1}$$

The mean dose of the entrance and exit is sufficient for approximating the midline dose most clinical cases.

This method is accurate over a small range of patient thicknesses for 6 MV and would be more useful for higher energy photon beams. For 6 MV it performs poorly for thicker patients with an exponential increase in error with patient thickness (Figure 3-3). From Figure 3-3 and Figure 3-1, a patient that is equivalent to 20cm water would have an error of 6%, while a patient with an equivalence of 25cm thickness would have an error of up to 12%. A patient that is about 17cm water equivalent or less would agree within 2%. Therefore most 6 MV beams which pass through the patient laterally will have an error that exceeds the recommendations of ICRU 1976 (<5%) even if there was no error associated with the entrance and exit dose measurements.

This model has limited usefulness as it would not work for a patient >17 g/cm² thick (Figure 3-3) for 6 MV.

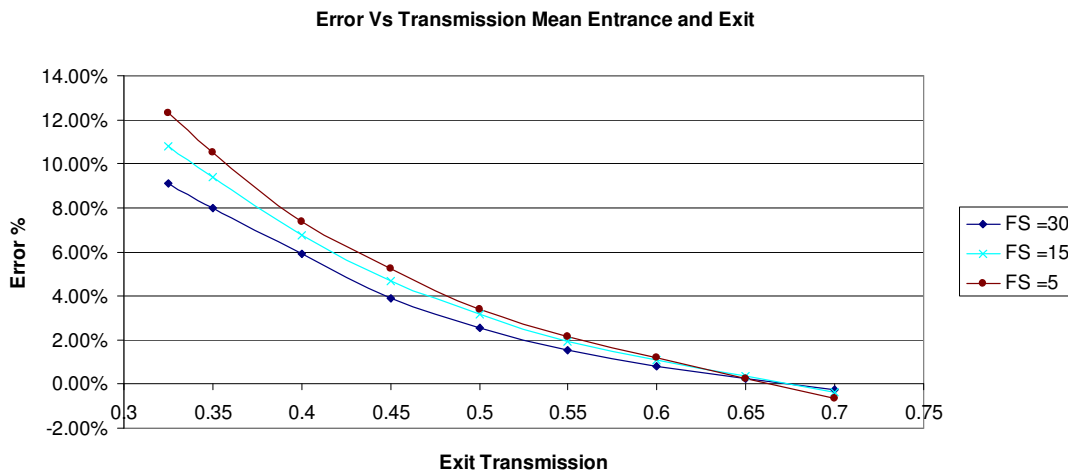


Figure 3-3: Percent difference between ion chamber measured midline transmission to mean model

3.3.2 A Linear Exponential and Linear Equations Method of Approximating Midline Dose

As the previous method has a potentially large error when the beam passes through a large thickness another method was devised using continuous equations. This method assumes that

midline transmission is linear and exit transmission is exponential. Both of these transmission factors depend on depth and field size. A continuous equation based model can then be made to approximate midline transmission using exit transmission and entrance dose.

Assume exit transmission is exponential.

$$T_{exit} = Ae^{-\mu d}, \quad (3.3.2.1)$$

- T_{exit} is the exit transmission.
- μ is the exponential fit to the exit transmission curve and is a function of field size.
- d is the water equivalent depth of the patient or phantom.

A is approximated with a linear function depending on field size and μ with a quadratic (Figure 3-4).

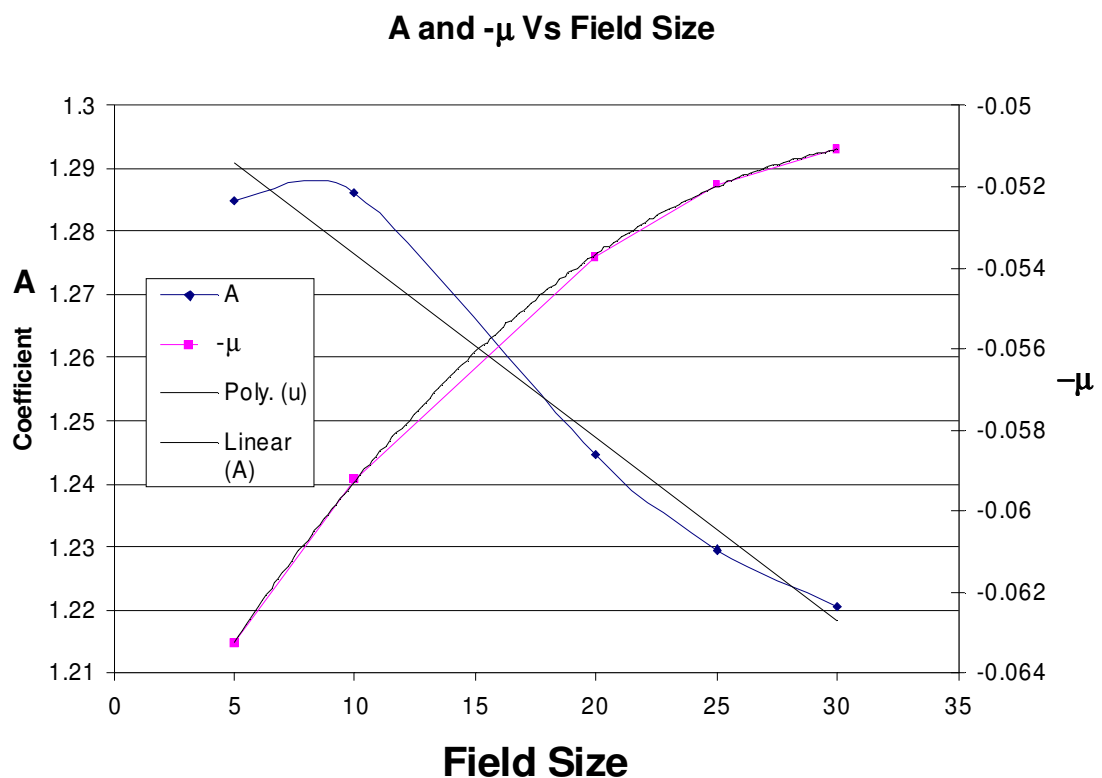


Figure 3-4: A and μ versus field size

Similarly if the midline dose is linear then

$$T_{mid} = Bd + C \quad (3.3.2.2)$$

- T_{mid} is the midline transmission
- B and C are the coefficients of the linear approximation and are a function of field size.

Plotting B and C versus field size shows that there is a field size dependence on these factors as one would expect (Figure 3-5). A is approximated with a linear function depending on field size and B with a quadratic

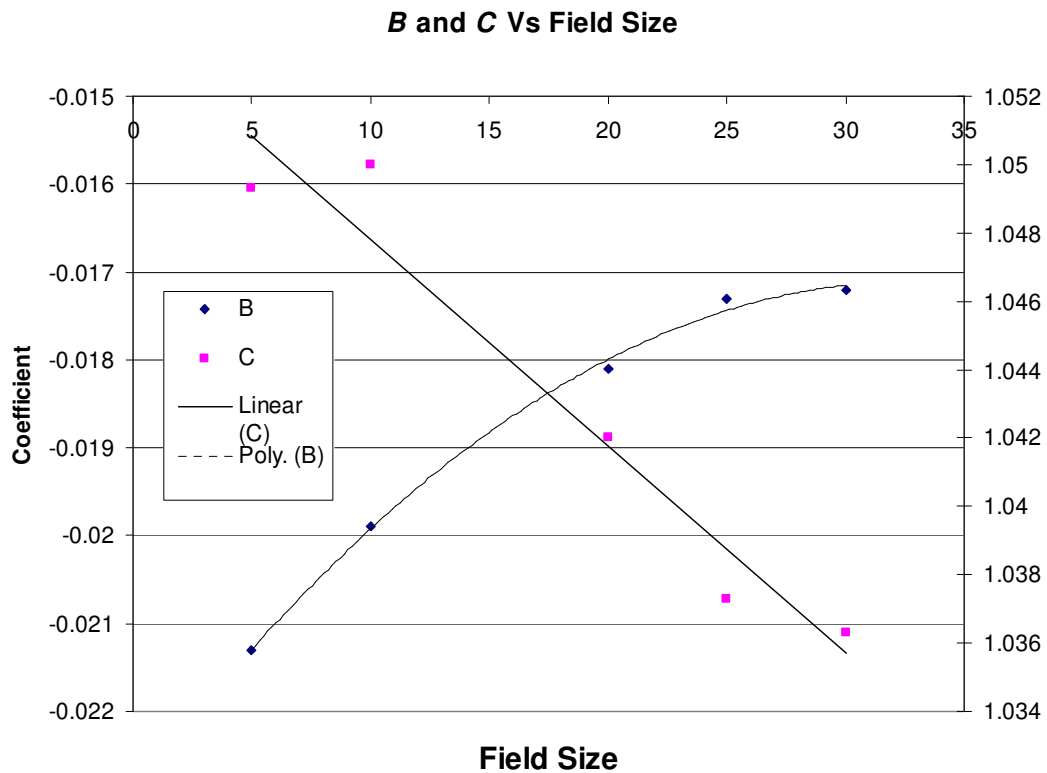


Figure 3-5: B and C versus field size

One can then use the exit transmission to determine the water equivalent depth and then use this to get the midline transmission.

$$T_{exit} = A_{fs} e^{-\mu_{fs}d}, \quad (3.3.2.3)$$

Therefore from equation 3.3.2.3

$$d = -\ln \left[\frac{T_{exit}}{\mu_{fs}} \right] A_{fs} \quad (3.3.2.4)$$

Substituting d into the equation (3.3.2.5) below will give the midline dose.

$$T_{mid} = B_{fs} d + C_{fs} \quad (3.3.2.5)$$

This gives an approximation of the midline dose based on the entrance and exit doses. When compared with the measurements made with the Farmer chamber the error in the midline transmission is up to 1.5% over the range of ion chamber measurements (Figure 3-6). These results are also considerably better than the model used in section 3.3.1.

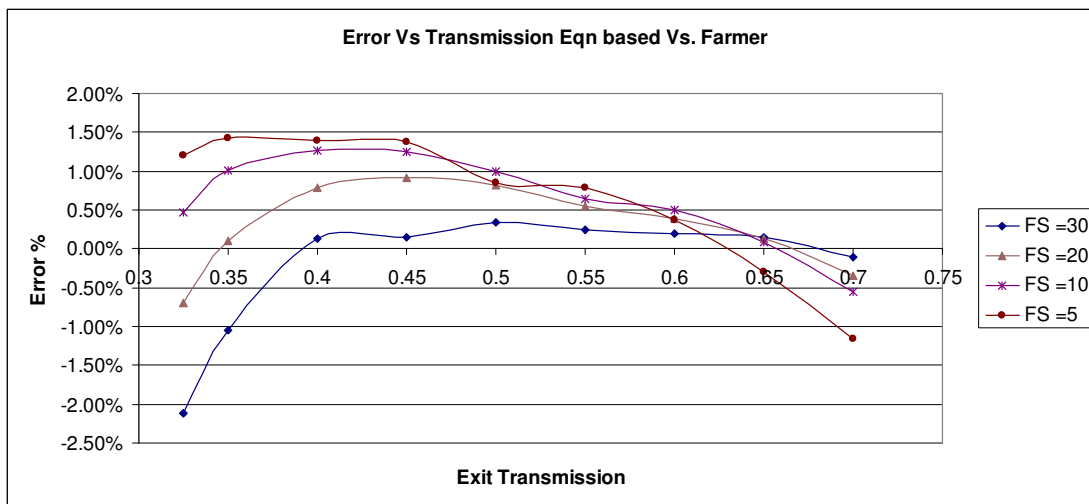


Figure 3-6: Error in model calculated transmission compared to ion chamber transmission

This gives a good approximation based on the measurements in the transmission range of 0.325 to 0.7, or a phantom thickness of 25 cm to 10 cm respectively.

There are several concerns about this model. At the ends of the graph (in particular the 0.3 transmission end) the slope of the error is steep (Figure 3-6). This means that this model could fail quite drastically at transmission less than 0.325, or about 30cm water equivalent thickness. There is also quite a distinctive shape to the curve. This means that it is likely that the model will continue to underestimate the midline dose outside the bounds measured with the ion chamber.

The model is based on the assumption that the midline dose is linear and the exit dose is exponential (which is not true), and although the fit is excellent for these curves the assumption does not fully address the fact that the midline dose/transmission is closer to exponential than linear.

This method would be the fastest way to accurately estimate the midline dose without using interpolation tables from beam data or complex algorithms as it uses the smallest number of calculations and continuous functions to approximate the dose. It relies on the use of ion chambers to get the midline and exit transmission curves, and is therefore more of an exercise in a-posteriori logic. One needs to construct a model based on sound physical phenomena that will result in excellent agreement for all patient thicknesses.

3.3.3 Estimation of Midline Dose Using TMR's

The midline dose to a phantom/patient can be estimated using Tissue Phantom Ratios (TPR's). A method is outlined by Van Dam J, (1994), p12-13, which relates the exit dose and midline dose using TPR's and backscatter factors. This model is very similar to Khan et al.1980, using TPR's in high energy photon beams.

Figure 3-7 illustrates a radiation beam passing through a phantom. The TPR's are corrected for inverse square law taking into consideration the difference in distance between the dose points (D_{max} , Isocentre, and D_{exit}). B_A , $B_{A'}$ and B_{A_0} are the backscatter factors for the field sized A, A' and A_0 respectively at the isocentre, the exit dose point and the entrance dose point. The factor $B_{A'}$ accounts for the lack of material (backscatter) after the exit surface of the phantom. As backscatter from A' and A_0 have a small effect on the predicted midline transmission (Appendix A) the ratio A'/A_0 has been assumed to be 1.00. The Source to Axis Distance (SAD) is 100cm for all linear accelerators and used, therefore the midline point is taken as 100cm from the source (isocentre). As TMR's are measured with the ion chamber at

the isocentre the TPR's can be replaced with TMR's. The TMR at maximum is 1.00, this helps simplify the TPR model.

TPR Approximation for Midline Dose

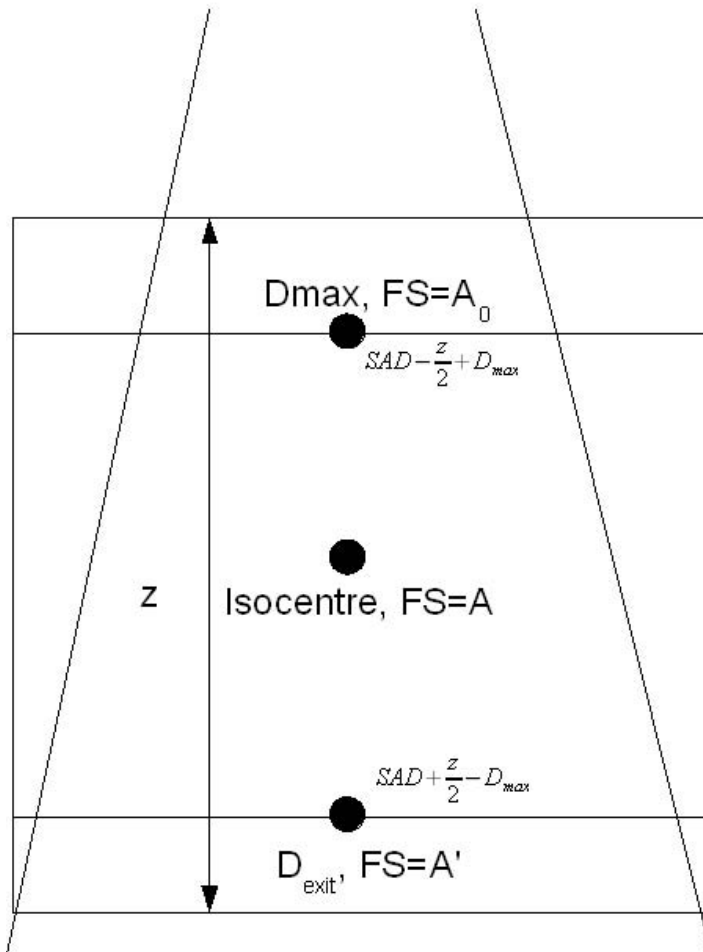


Figure 3-7: Setup for Midline Dose approximation

The relationship between TPR's and transmission are in Van Dam et al. (1994). Equations 3.1 and 3.2 are taken from Van Dam et al. (1994).

$$T_{exit} = \frac{TPR_{(A',z-d_{max})} \times f_1 \times B_{A',A_0}}{TPR_{(A',d_{max})} \times f_2 \times B'_{A'}} \quad (3.3.3.1)$$

Where

- $TPR_{(A,x)}$ is the TPR for the field size A at the depth x
- f_1 is $(SAD - \frac{z}{2} + d_{max})^2$
- f_2 is $(SAD + \frac{z}{2} - d_{max})^2$, so $\frac{f_1}{f_2}$ is the SSD correction
- B_A , $B_{A'}$ and B_{A_0} are the backscatter factors for the field sized A, A' and A₀ respectively at the isocentre
- $B_{A',A_0} = \frac{B_{A'}}{B_{A_0}}$ is the back scatter correction due to the fact that there is more back scatter for a larger field size.
- $B'_{A'}$ is the correction factor for the lack of back scatter from the exit surface of the phantom.
- z is the phantom thickness

$$T_{mid} = \frac{TPR_{(A,\frac{z}{2})} \times f_1 \times B_{A,A_0}}{TPR_{(A,d_{max})} \times (SAD)^2} \quad (3.3.3.2)$$

As the treatment is isocentric the TPR's above can be replaced with TMR's, therefore

$$T_{exit} = \frac{TMR_{(A',z-d_{max})} \times f_1 \times B_{A',A_0}}{TMR_{(A',d_{max})} \times f_2 \times B'_{A'}} \quad (3.3.3.3)$$

$$T_{mid} = \frac{TMR_{(A,\frac{z}{2})} \times f_1 \times B_{A,A_0}}{TMR_{(A,d_{max})} \times (SAD)^2} \quad (3.3.3.4)$$

As $TMR_{(A',d_{\max})} = TMR_{(A,d_{\max})} = 1.00$, 3.3.3.3 and 3.3.3.4 become

$$T_{exit} = \frac{TMR_{(A',Z-d_{\max})} \times f_1 \times B_{A',A_0}}{f_2 \times B'_{A'}} \quad (3.3.3.5)$$

$$T_{mid} = \frac{TMR_{(A,\frac{z}{2})} \times f_1 \times B_{A,A_0}}{(SAD)^2} \quad (3.3.3.6)$$

One can also assume that $B_A/B_{A_0} = 1$ and $B_{A'}/B_{A_0} = 1$ (See Proof in Appendix A). Thus 3.3.3.5 and 3.3.3.6 become.

$$T_{exit} = \frac{TMR_{(A',Z-d_{\max})} \times f_1}{f_2 \times B'_{A'}} \quad (3.3.3.7)$$

$$T_{mid} = \frac{TMR_{(A,\frac{z}{2})} \times f_1}{(SAD)^2} \quad (3.3.3.8)$$

The SAD is 100cm, therefore 3.3.3.7 and 3.3.3.8 reduce to.

$$T_{exit} = \frac{TMR_{(A',Z-d_{\max})} * (100 - \frac{z}{2} + d_{\max})^2}{(100 + \frac{z}{2} + d_{\max})^2 * B'_{A'}} \quad (3.3.3.9)$$

$$T_{mid} = \frac{TMR_{(A,\frac{z}{2})} * (100 - \frac{z}{2} + d_{\max})^2}{(100)^2} \quad (3.3.3.10)$$

3.3.3.1 Midline Transmission

T_{mid} is easily calculated once commissioning data (TMR's) are obtained as the amount of medium below the ion chamber is large and therefore there would be full back scatter. Measurements with the NE2571 farmer type chamber give results within 1.5% of doses predicted using TMR's (Figure 3-8).

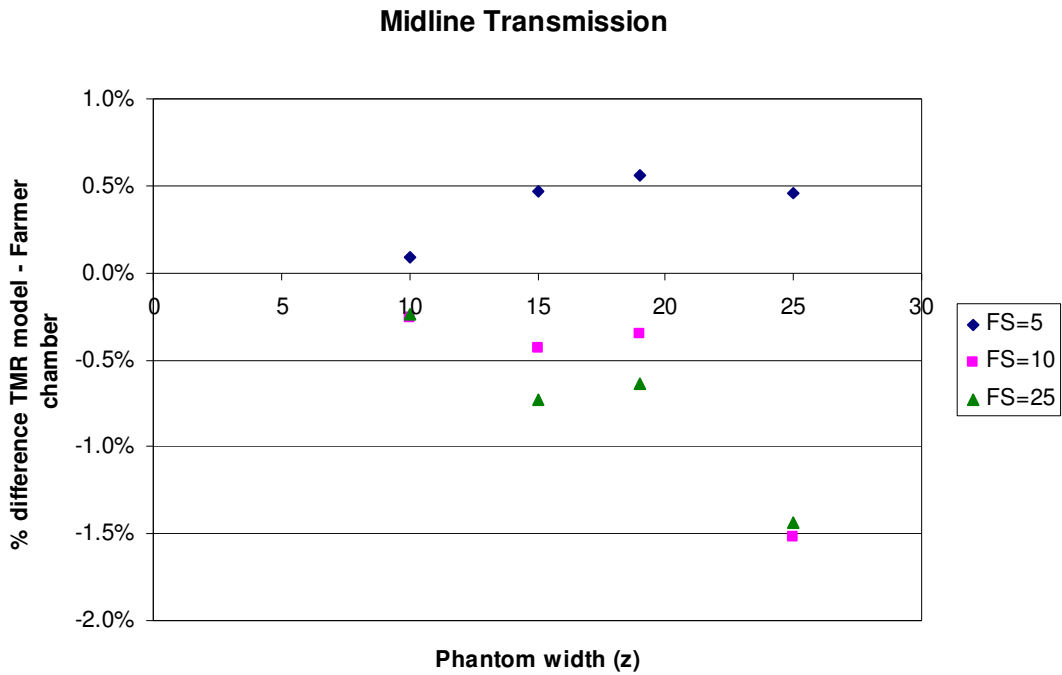


Figure 3-8

3.3.3.2 Exit Transmission

The error of the exit transmission (equation 3.3.3.9) based on the depth of the phantom and without the factor $B'_{A'}$ (BSF from the lack of material past the exit surface) yields results that are inaccurate to up to 5%. The error is smallest for small field sizes as the contribution from backscatter is greater for larger field sizes.

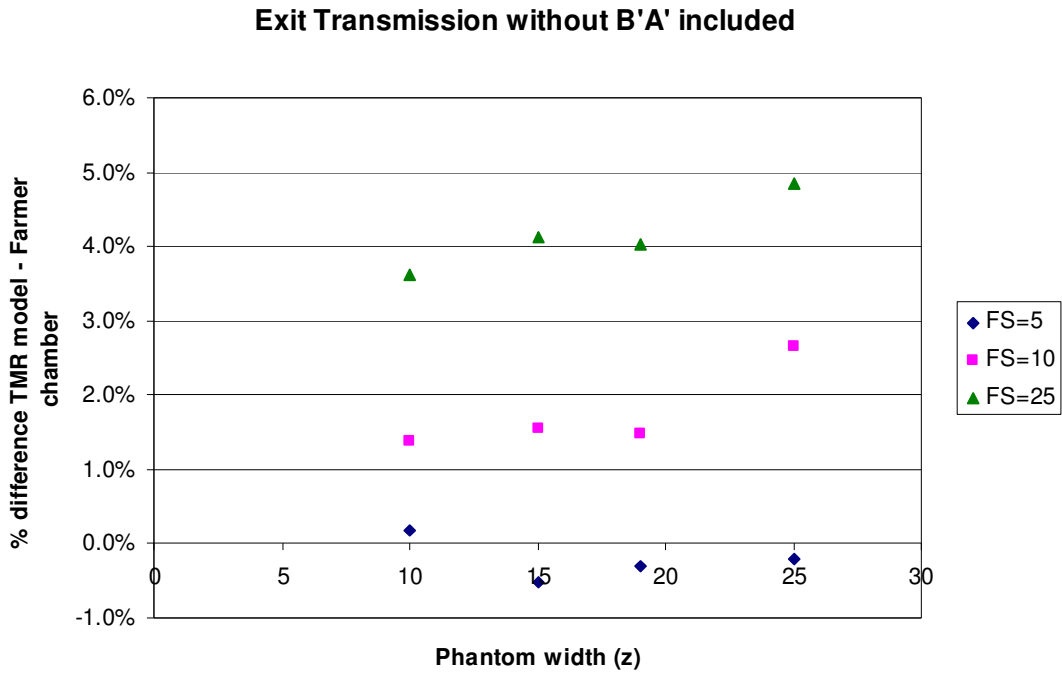


Figure 3-9

The above graph (Figure 3-9) also gives a good indication of what to expect for the factor B'_A , as equation 3.3.3.9 would be accurate if multiplied by this factor. If the exit dose is modified by a correction factor the exit dose agrees well with the Farmer measurements.

B'_A was measured with a NE2571 type Farmer chamber and was placed in the TMR model. Exit transmission values agree to within 1.5% when B'_A is put into consideration. The back scatter factor was measured for a 5x5 cm, 10x10 cm and a 20x20 cm field size and 15cm RW3. The back scatter factors for the 3 field sizes were 0.3%, 1.1% and 3.3%.

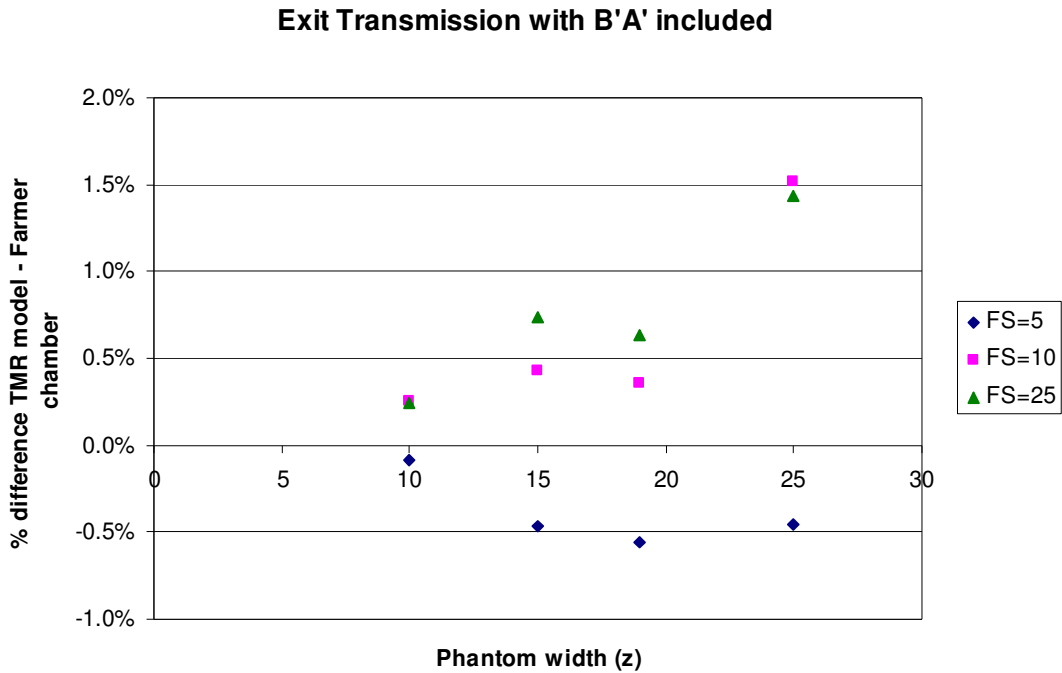


Figure 3-10

The exit transmission agreed to within 1.5% of measured values once back scatter was taken into account (Figure 3-10).

3.3.3.3 Midline Transmission from Exit Transmission Curves

With equation 3.3.3.9 and equation 3.3.3.10 properly modelled (Figure 3-8 and Figure 3-10) the theoretical transmission curves can then be used to estimate the midline dose based on entrance and exit doses (Figure 3-11).

The transmission curve for the exit dose is used to approximate the phantom depth. The depth is then used to approximate the midline transmission (Figure 3-11).

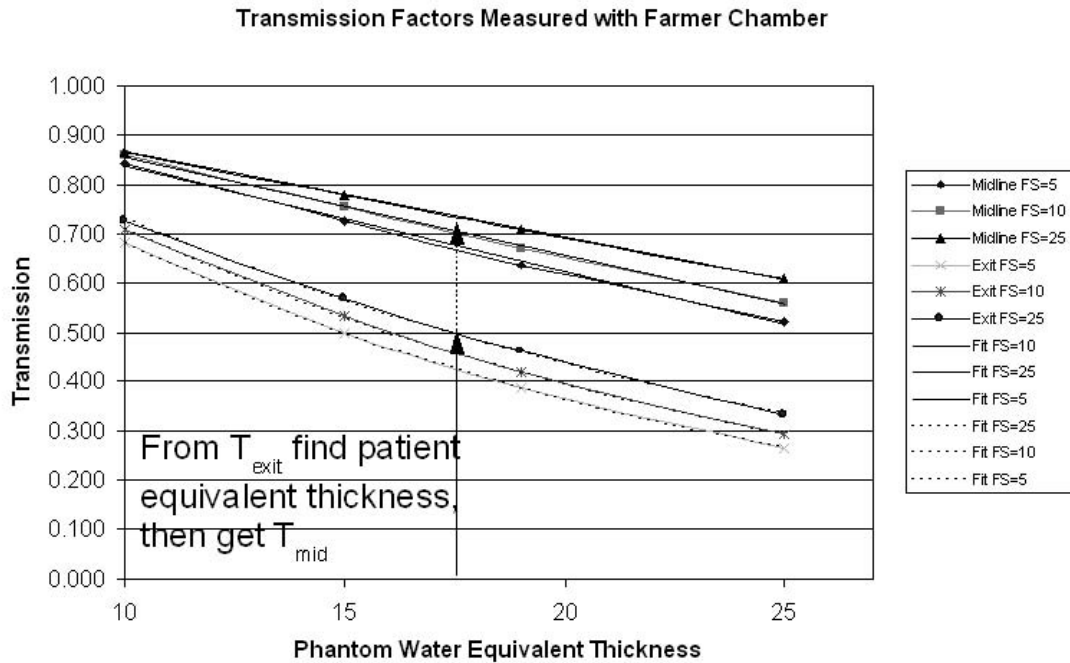


Figure 3-11

This agrees with the ion chamber measurements to within <1.5% for field sizes less than 25 cmx25 cm (the majority of cases in radiotherapy)(Figure 3-12). These results could be improved by measuring the backscatter as a function of field size as well as phantom thickness, but by choosing a single thickness these results are within the tolerance of error required for clinical implementation of the model. This is especially the case when one considers the fact that the TMR's are approximated by PDD's and PSF's (Khan et al. 1980).

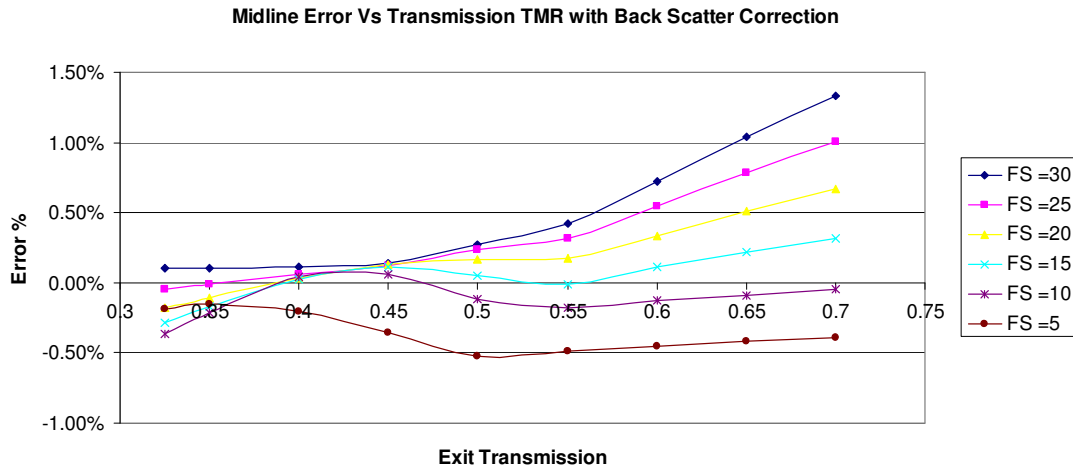


Figure 3-12: Midline Transmission Prediction TMR Entrance and Exit Dose Measurement Model vs. Farmer IC

The advantage of using this method is that standard TMR's or PDD's with S_c and S_p taken during the commissioning of the linear accelerator can be used to predict the midline dose.

The factor that needs to be measured is the backscatter factor B'_A . This factor does not need to be measured over a range of field sizes.

3.4 Summary : Entrance and Exit Dose Based Techniques

All techniques used so far require exit as well as entrance dose measurements. To implement these techniques would require the use of two detectors for each midline dose approximation. These techniques also assume that the patient is uniform in density (water equivalent) and would fail if the beam passed through bone (higher density) or lung (lower density). If there are any asymmetries in patient anatomy the midline dose approximation will no longer be on the midline. SSD as well as density corrections would therefore have to be applied for these models to be of use. Placing a detector on the surface would lead to a dose “shadow” past the detector. That is the detector acts as extra material and the dose below the detector is therefore less than it would be if the detector was not there. Placing another detector in the shadow would therefore reduce the dose at the shadow. Care should therefore be taken when

performing entrance/exit dose measurements to ensure that the exit detector is not in the shadow of the entrance detector. SSD corrections and modelling of the build up cap would have to be performed on the entrance as well as the exit side of the patient as the detector can not be physically placed in the patient at D_{\max} . It is therefore better to find a technique which removes the use of both entrance and exit doses.

3.5 Isocentric Dose

3.5.1 Introduction

The midline dose approximation introduced previously requires both an entrance and exit measurement point and would be independent of treatment planning system calculations. It will, however fall short for irregularly shaped fields and for patients with lack of homogeneity or symmetry of beam passage, as well as for patients where the tumour is not in the midline of the patient. Treatment planning systems are capable of calculating the effective depth within a patient and it is common practice to export effective depth from a 3D planning system to a secondary checker (Radcalc Users Guide). A similar model to the previous one (i.e. a model that uses TMRs/TPRs) is proposed to predict the midline dose. This model will use the effective depth of the point of measurement, equivalent square field size, and entrance dose measurement for determining the dose to the isocentre (tumour). The isocentric dose for each measurement can be summed to give the total dose to the isocentre.

Below is a concept diagram illustrating a 4 field treatment (Figure 3-13).

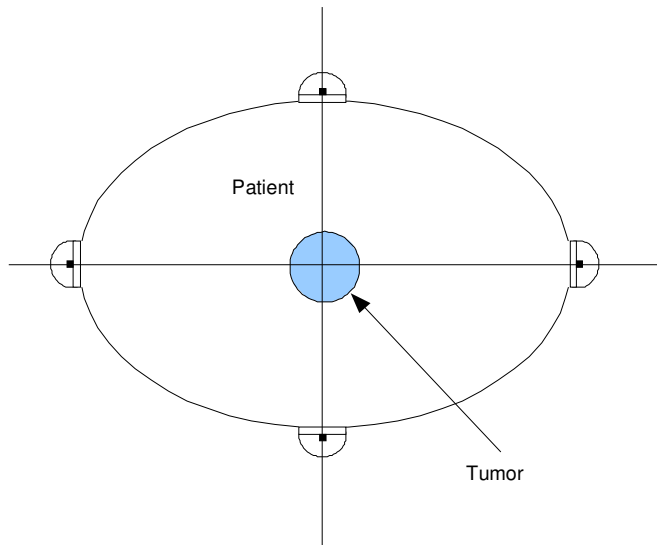


Figure 3-13: Entrance Dose Model Setup

Each of the 4 fields 1,2,3,4 will have the entrance dose measured separately. The effective depth, real depth and equivalent field size will be obtained from the treatment plan.

3.5.2 Estimation of Isocentric Dose Using TMR's

Consider a patient/phantom with surface normal to the gantry and the target at the isocentre (Figure 3-14). The depth to the isocentre is designated z , the source to axis distance (SAD) is 100 cm, and the field size at D_{\max} is A_0 , while the field size at the SAD is A . The back scatter factor from the phantom at A_0 and A is designated B_{A_0} and B_A respectively.

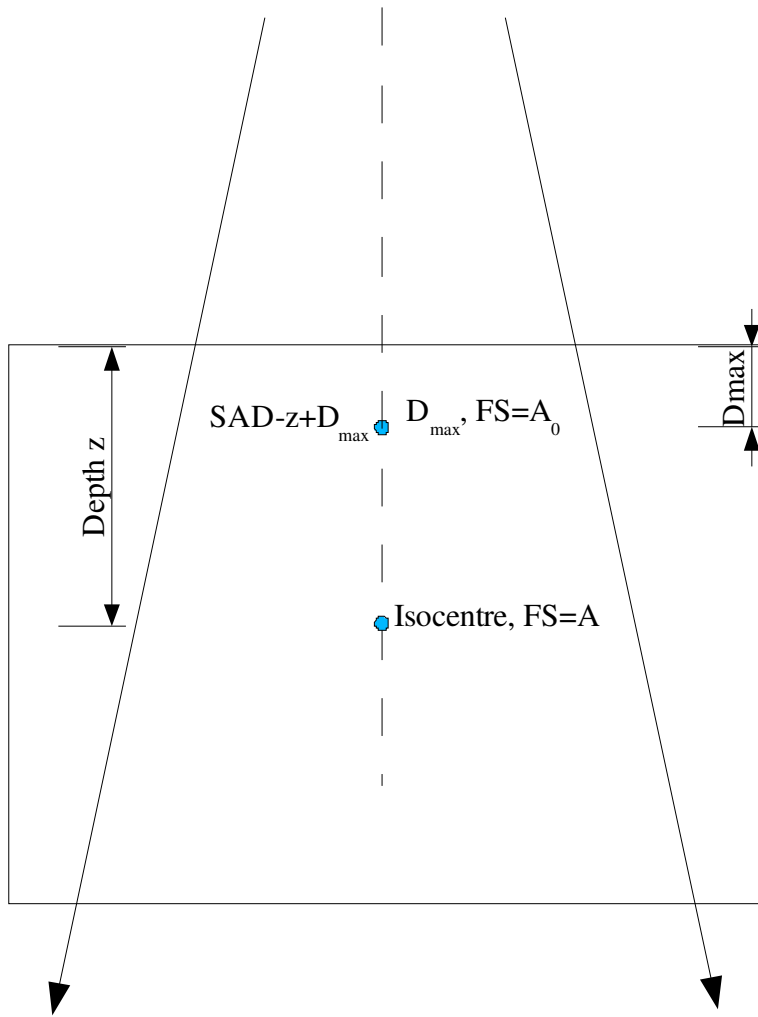


Figure 3-14: Setup for TMR Based Model Using Entrance Dose

Using TPRs the isocentric transmission is,

$$T_{iso} = \frac{TPR_{(A,z)} \times f_1 \times B_A}{TPR_{(A,d_{max})} \times (SAD)^2 \times B_{A_0}} \quad (3.5.2.1)$$

- $TPR_{(A,x)}$ is the TPR for the field size A at the depth x
- f_1 is $(SAD - z + d_{max})^2$
- B_A , and B_{A_0} are the backscatter factors for the field sized A and A_0 respectively at the isocentre

- $B_{A,A_0} = \frac{B_A}{B_{A_0}}$ is the back scatter correction due to the fact that there is more back scatter for a larger field size.

As the treatment is isocentric the TPR's above can be replaced with TMR's, T_{iso} then becomes

$$T_{iso} = \frac{TMR_{(A,z)} \times f_1 \times B_{A,A_0}}{TMR_{(A,d_{max})} \times (SAD)^2} \quad (3.5.2.2)$$

As $TMR_{(A,d_{max})}=1.00$, the equation (3.5.2.2) above becomes

$$T_{iso} = \frac{TMR_{(A,z)} \times f_1 \times B_{A,A_0}}{(SAD)^2} \quad (3.5.2.3)$$

One can also assume that $B_{A,A_0} = \frac{B_A}{B_{A_0}} = 1.00$ (Appendix A). If the isocentre was close to the exit surface B_{A,A_0} would not be 1.00 as there would be incomplete backscatter from behind the isocentre.

$$T_{iso} = \frac{TMR_{(A,z)} \times f_1}{(SAD)^2} \quad (3.5.2.4)$$

As the SAD=100 cm

$$T_{iso} = \frac{TMR_{(A,z)} \times f_1}{(100)^2} \quad (3.5.2.5)$$

If the effective depth of the target is known and the SSD is known then the dose at the isocentre can be shown to be approximately the same as T_{iso} , with d_{eff} , the effective depth of the isocentre as z .

When the isocentre is close to the exit surface there will be incomplete backscatter. A backscatter correction factor will therefore need to be applied to the isocentric transmission to compensate for this. The back scatter factor would depend on field size and depth from the exit surface to the isocentre. Equation 3.5.2.5 will then become.

$$T_{iso} = \frac{TMR_{(A,z)} \times f_1}{(100)^2 * B'_A} \quad (3.5.2.6)$$

Where B'_A is the back scatter factor for the field size A at depth $D_{exit,eff}$, the effective depth to the exit surface of the patient from the isocentre.

3.5.2.1 Isocentric Transmission

This method can be adapted to include wedged fields. The TMR's can be taken for wedges from commissioning measurements.

The total dose to the isocentre will be

$$D_{iso} = \sum T_{iso} \times D_{ent} \quad (3.5.2.1.1)$$

The entrance dose can be measured on the entrance surface of the patient using a MOSFET dosimeter.

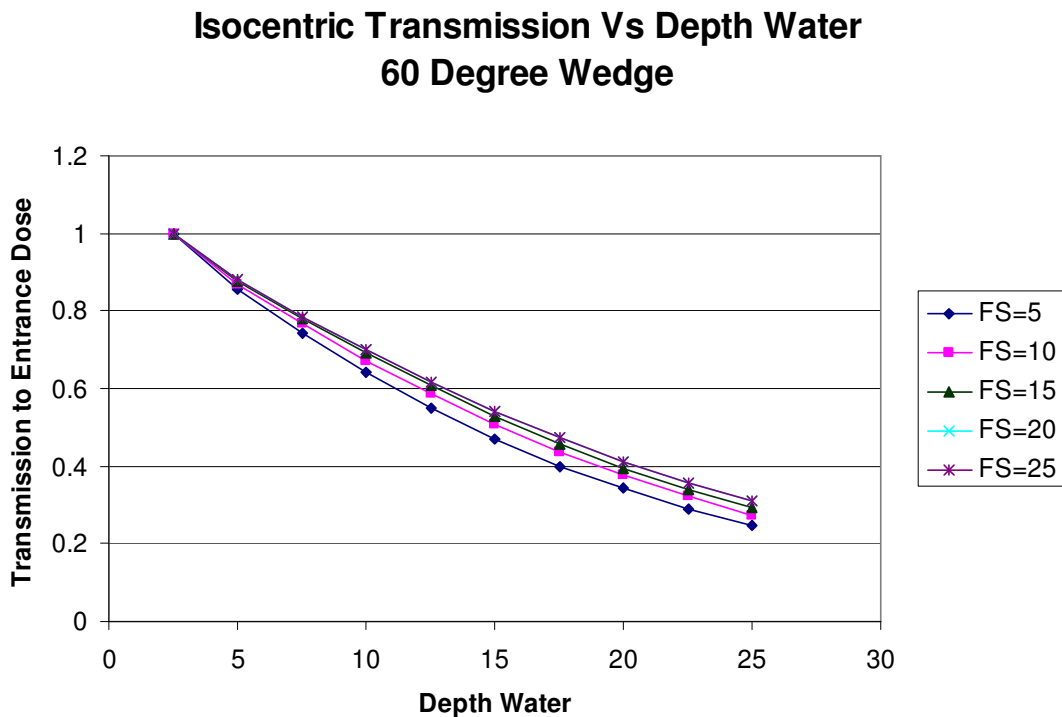
This technique is also similar to the technique used by Masterson-McGary 2003, where the dose at D_{max} is calculated by the relationship.

$$D_{d_{max}} = D_{iso} \times \frac{1}{TMR(depth)} \times \frac{100^2}{(SSD + D_{Max})^2}$$

3.6 Isocentric Dose Implementation

3.6.1 Implementation of Model

To reduce calculation time and simplify the model isocentric transmission curves were produced from TMR's. These curves were then interpolated at the equivalent depth to get the transmission of the entrance dose.



3-15: Isocentric Transmission

This turns the three step process

- Get entrance dose
- From the entrance dose and effective depth calculate the TMR's and back scatter factors required with SSD correction to give the isocentric transmission.
- From this transmission calculate the isocentric dose.

Into a two step process

- Get entrance dose
- From the transmission calculate the isocentric dose.

From the above graph (3-15) the isocentric transmission depends on the effective depth within the patient as well as the equivalent field size.

3.6.2 Comparison with Ion Chambers

The TMR model was tested with a Farmer chamber with the effective point of measurement being the point of dose measurement. The dose at isocentre was compared to the dose at D_{max} for a 6 MV beam with an open field as well as a 30 degree wedge (Figure 3-14). The depth, z , was varied and the isocentre was greater than 5cm away from the exit surface to reduce the effect created by the loss of back scatter.

Measurements were made in RW3 in a dedicated Farmer chamber holder.

The Farmer chamber measurements were then compared to the TMR model. Measurement differences were less than 1.1% for all open field measurements and 1.0% for the 30 degree wedge (Table 3-1, Table 3-2).

This error similar as the TMR model with entrance and exit doses considered.

Ratio Measured/Calculated Isocentric Transmission			
Depth	Field Size		
	5	10	20
5	1.006	1.010	1.003
10	1.004	0.995	0.997
15	1.003	0.997	0.992

Table 3-1: 30 Degree Wedge Isocentric Transmission

Ratio Measured/Calculated Isocentric Transmission			
Depth	Field Size		
	5	10	20
4	1.004	1.001	0.999
6	1.004	1.000	0.995
7	1.007	1.000	0.997
10	1.003	1.001	0.990
15	1.006	0.999	0.989

Table 3-2: Open Field Isocentric

3.6.3 Comparison with a 2D Planning System

Although ion chamber measurements show that the model agrees well for open fields as well as with a 30 degree wedged field for 6 MV, this does not mean that the model will work for all depths and field sizes for both 6 MV and 10 MV, with any wedge. Errors entering the correct PDD data or PSF's would result in erroneous results. More rigorous testing would be necessary to ensure that the MOSFET spreadsheet has no errors. All energies and wedges were tested at different depths to ensure that no incorrect data was entered into the spreadsheet. The MOSFET spreadsheet was tested against an MU check program (Radcalc), which also calculates dose. Results were generally less than 1% different over the depth range of 2.5 cm to 25 cm and field size range of 5 cm² to 30 cm². 6MV with a 30 degree wedge and 10 MV with a 45 degree wedge exceeded 1%, but were less than 2% different to the spreadsheet.

3.6.4 Correction for an Inhomogeneous Medium

Agreement between the model and ion chamber measurements in water equivalent material are within 2%, however, this does not guarantee that results will be as good in situations where there is a difference in density of the material through which the beam passes. This is especially important when the beam passes through lung or bone. Per cm traversed through

lung the dose will need to be corrected anywhere between 3 to 1.5% for ^{60}Co to 20 MV photons respectively (Williams and Thwaites 1993). It is therefore vital that differences in dose are accounted for when the beam passes through lung.

The planning system accounts for the difference in density of the material along the beam path and calculates an effective depth Z_{eff} of water equivalent material from the surface to the depth of the dose point. The point of measurement is therefore effectively not on the surface of the patient when the tissue is not water equivalent. The difference between the effective depth and the actual depth therefore needs to be considered. In order to account for this an SSD correction made. The point will no longer be SAD-z, but at SAD-z_{eff}. The dose at SAD-z can be corrected with an inverse square relationship (Williams and Thwaites 1993). In a phantom the back scatter from the phantom for the different field size (as we are now closer or further away from the source) also needs to be accounted for. Therefore the dose for each

field needs to be multiplied by $\frac{(100 - z)^2}{(100 - z_{\text{eff}})^2}$ and B_A/B_{A_0} where B_A and B_{A_0} are the backscatter

from the field at the entrance at z and z_{eff} respectively (Figure 3-14). The backscatter factor can be ignored as the beam passing through bone or lung would not contribute to a difference in SSD of more than 10cm. This would contribute less than 0.5% from backscatter (Appendix A). If the density in the patient through which the beam passes is, on average, less than water the effective depth will be less than the actual depth and the surface dose will be measured too close to the source. The inverse squared correction will therefore be less than unity. For patients with high density material in the beam path the effective depth will be greater than the actual depth and the reading on the surface will be too far away from the source. The inverse square correction will therefore be greater than 1.00.

The dose can be calculated from

$$D_{iso} = \frac{TMR(A, z) * (100 - z + d_{max})^2 (100 - z)^2}{(100)^2 * B'_A * (100 - z_{eff})^2} * D_{ent}$$

This factor would be used for estimation of the correct dose when the beam passes through say dense bones or less dense lungs. Dose differences calculated would be large if the beam passed through a large portion of lung or bone, for instance (Table 3-3). The difference in SSD could be up to several centimetres, this could contribute several percent to the error of the dose approximation.

Verification in an Inhomogeneous Phantom

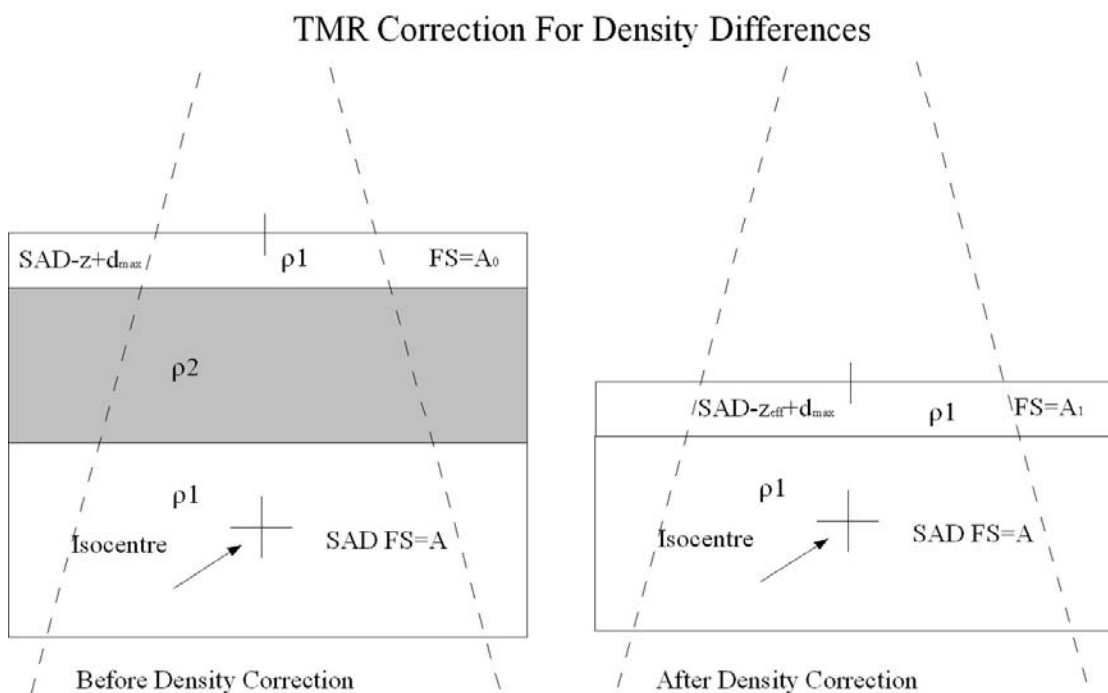


Figure 3-16: Density Correction

3.6.5 Inhomogeneity Correction in a Lung/Thorax Phantom

Pinnacle 3D planning system was used to place lateral beams on a lung/thorax phantom. These plans were complex and involved the use of wedges as well as surface obliquity. A plan was designed that had beams passing through lung tissue. The difference in lung density led to a large difference between the actual depth and effective depth. When density

corrections were applied results were within the usual standard deviation of measurements that is to be expected (less than 8%, chapter 5). When there is no density correction the average dose measured for fields that passed through lung was 13% below the predicted dose with Pinnacle 3D planning system for 6 MV, while the difference in dose was 9% below the planning system dose for 10 MV (Table 3-3). After the density correction was applied the dose differences were 2.2% and 3.3% for 6 MV and 10 MV respectively. As the error in the dose is 4% (1SD) based on the standard deviation of the group of phantom measurements it is safe to say that the density corrected values would be within acceptable tolerances for this group of measurements, while measurements that have no density correction will fall outside the acceptable level of tolerance.

Energy	Field No	Wedge Angle	Depth	Effective Depth	Planned Dose	%Difference No Density Correction	%Difference Density Correction
6 MV	1	15	6.72	6.81	0.664	-0.53%	-0.82%
	2	30	18.29	13.9	0.658	-14.26%	1.61%
	3	30	10.42	5.87	0.677	-12.08%	2.91%
10 MV	1	15	6.72	6.81	0.902	-1.10%	-1.32%
	2	30	18.29	13.9	0.898	-13.15%	-1.11%
	3	30	10.42	5.87	1.197	-10.69%	0.53%

Table 3-3: Thorax Phantom Results

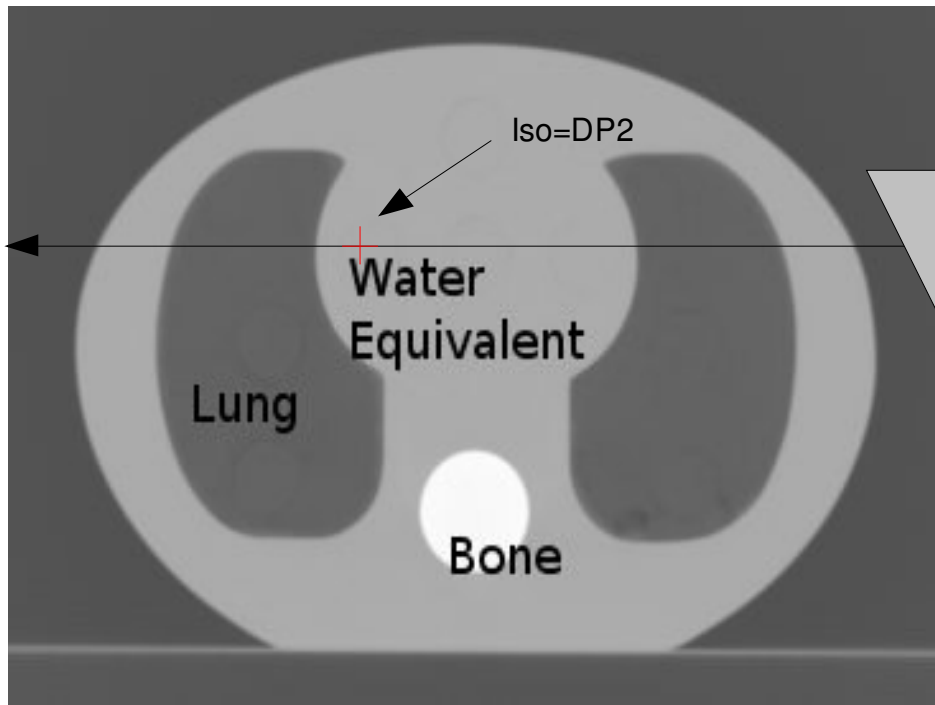


Figure 3-17: Lung/Thorax phantom with beam 2

4 MOSFET Commissioning and Characterisation

4.1 Introduction:

MOSFETs, like any other detector have characteristics that could affect dosimetry.

It is not entirely accurate to assume that isotropic MOSFETs do not have any angular or energy dependence. Even though the manufacturers state that the energy response is flat in the MeV range it is worth checking. MOSFETs have several undesirable characteristics such as dose non-linearity, temperature dependence and angular dependence (Andreo et al. 2005 p. 90-91).

The parameters that could affect dosimetry with MOSFETs that were studied were error, constancy, skewness and kurtosis, linearity, angular dependence, energy dependence, temperature dependence, field size dependence, SSD dependence, and time related factors such as fade.

A standard setup was created so that measurements could be compared. The MOSFETs were placed in a water equivalent RW3 jig at 5 cm and irradiated with a 6 MV beam at 100 cm SSD and a 10x10 cm field size. The PDD of the 6 MV beam is 86.2% at 5.0 cm with 100 cm SSD. From this point onwards this as the *standard setup*.

4.2 Reproducibility

Setup: The MOSFETs were placed in the *standard setup* and irradiated with 100MU (0.862Gy +/- 1%). The output of the linac was measured daily and was within 1.00%.

The reproducibility for a 0.86 Gy reading is taken from the constancy readings. When multiple measurements were made the uncertainty is the standard deviation for the group of measurements. When one measurement was taken the uncertainty is assumed to be the reproducibility stated by the manufacturer (2.6%). This is greater than the standard deviation

of the whole group for isotropic MOSFETs, and about the same as the microMOSFET reproducibility (Table 4-3). An uncertainty at 95% confidence would be 1.64*Standard Error (1 σ) and 3.09*Standard Error (1 σ) for 99.9% confidence. The percentage uncertainty of a standard deviation for a group of measurements is less for larger doses (Chuang et al. 2002, Thomson and Nielsen Technical Note #3. 2002). The standard deviation of a measurement from constancy and linearity measurements is very similar to Thomson and Nielsen (Table 4-1). Comparisons were also made for N measurements of the same dose (0.86 Gy). The standard deviation on the average of N measurements compared to constancy measurements was made for 1 to 32 measurements. The results showed that the error decreases faster than $\frac{1}{\sqrt{N}}$, where N is the number of measurements, and 2.6% (1 σ) for 1 measurement of 0.86Gy. From the graphs in Figure 4-1, and Figure 4-2, a single large measurement will have a smaller uncertainty than several measurements amounting to the same dose. Random and systematic errors such as setup, readout time and electrometer stability/gain will also affect the dose measurement, so one would expect the average of multiple measurements will therefore have a lower error than a single large measurement. The fact that measurements behave in this way is probably because there are two sources of error inherent in the measurement process. The first is reading the mV shift, and the second is the error in dose deposition by the radiation ($\frac{1}{\sqrt{N}}$ (Attix 1986 p7.)). At low doses the first source of error becomes dominant as it is an absolute source of error and not subject to the random nature of radiation. As it is not correctable it is considered a random error, and therefore an uncertainty. The reader can read the MOSFET voltage threshold to say +/-2 mV (T&N Users Manual 2002), factors such as drift can affect MOSFET readings by several mV. The absolute uncertainty of these will therefore be assumed to be constant. The percentage error will therefore taper off at a rate of C/N, where C is a constant. At high doses the error

from reading becomes less and the error from radiation becomes dominant as the error from the random nature of radiation is proportional to $\frac{1}{\sqrt{N}}$ (Attix 1986 p7.). The error will therefore decrease at greater than $\frac{1}{\sqrt{N}}$ for single or multiple measurements. As a power law relationship fits the change in uncertainty with dose a simplification was made based on measurements. The 3σ uncertainty of a measurement over the clinical range of 20cGy to 400cGy was therefore taken as $3\sigma = 1.283x^{-0.6485}$.

Dose	Measured Reproducibility	T & N Tech Note Reproducibility
	3 σ (based on eqn)	3 σ
18.8cGy	19%	22%
100cGy	6.5%	7.8%
200cGy	4.6%	4.1%

Table 4-1: Comparison of 3 σ error measurements

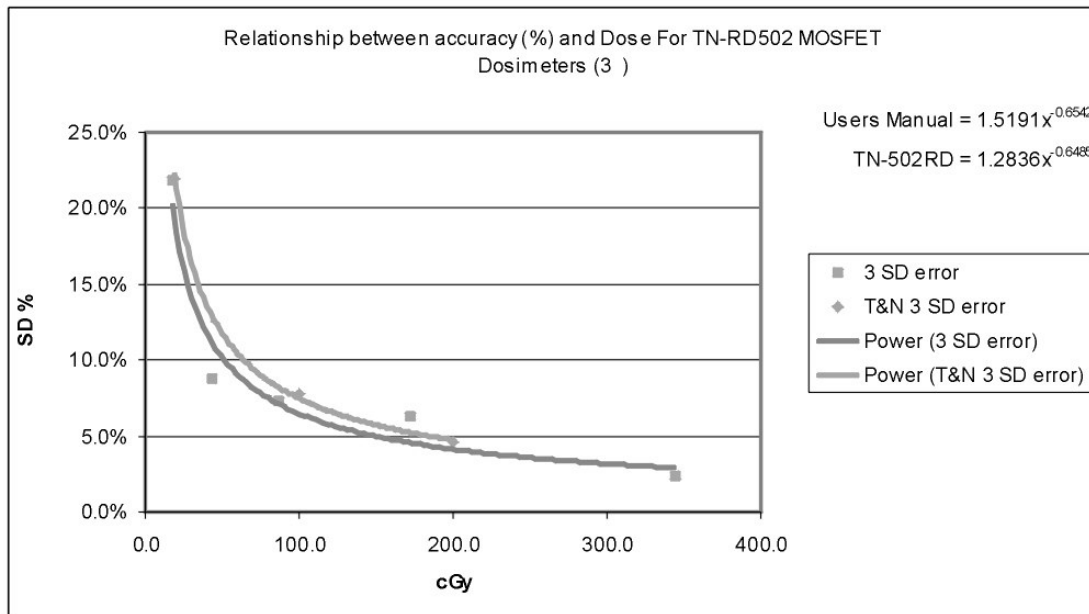


Figure 4-1: 3 σ Uncertainty of one measurement

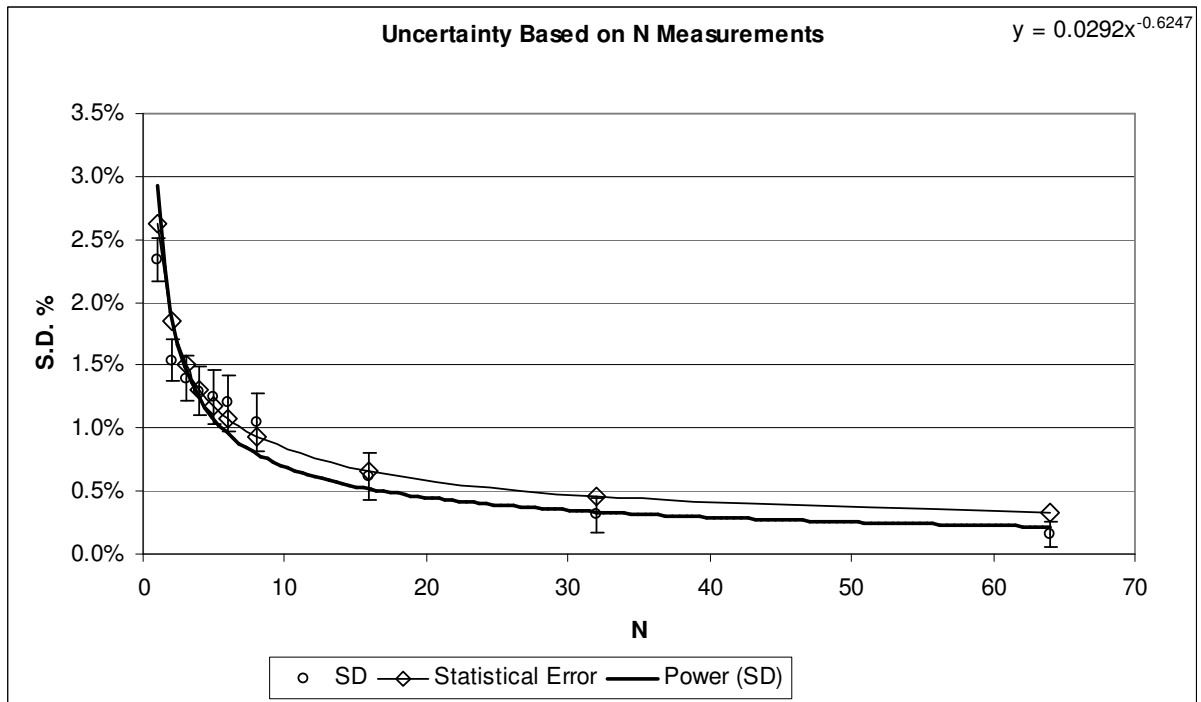


Figure 4-2: 1 σ Uncertainty of N measurements of 0.86Gy

4.3 Constancy

4.3.1 Short Term Constancy (Less than 3 months)

MOSFETs have a reproducibility of 2.6% to 1 σ for 100cGy (Thomson Nielsen technical note #3, 2000). Constancy tests were performed in the *standard setup* for all the 5 MOSFETs (4 isotropic MOSFETs and one micro-MOSFET). Measurements were made over a period of 9 days. A total of 50 measurements were made, 40 with the 4 isotropic MOSFETs and 10 with the micro-MOSFET.

The isotropic MOSFETs had similar response with an average of 110.8 mV/Gy \pm 2.2% (1 σ) for the whole batch. The average for the micro-MOSFET was 294.0 mV/Gy with a σ of 2.6% (Table 4-2). The above results show that if MOSFETs in a batch have similar histories they have similar dose response. They also had a constancy that is within the stated tolerance of 2.6% (Thomson Nielsen Tech note #3).

The results were normally distributed around the mean with a maximum reading of 100 mV/MU and a minimum of 91 mV/MU in the *standard setup* (Figure 4-3: Constancy results for the first 40 Readings).

	MOSFET 1	MOSFET 2	MOSFET 3	MOSFET 4	MOSFET 5
Avg	94.3	96.4	95.1	96.3	253.5
SD	2.31	2.01	1.79	1.89	6.61
SD %	2.5%	2.1%	1.9%	2.0%	2.6%

Table 4-2: Constancy check results

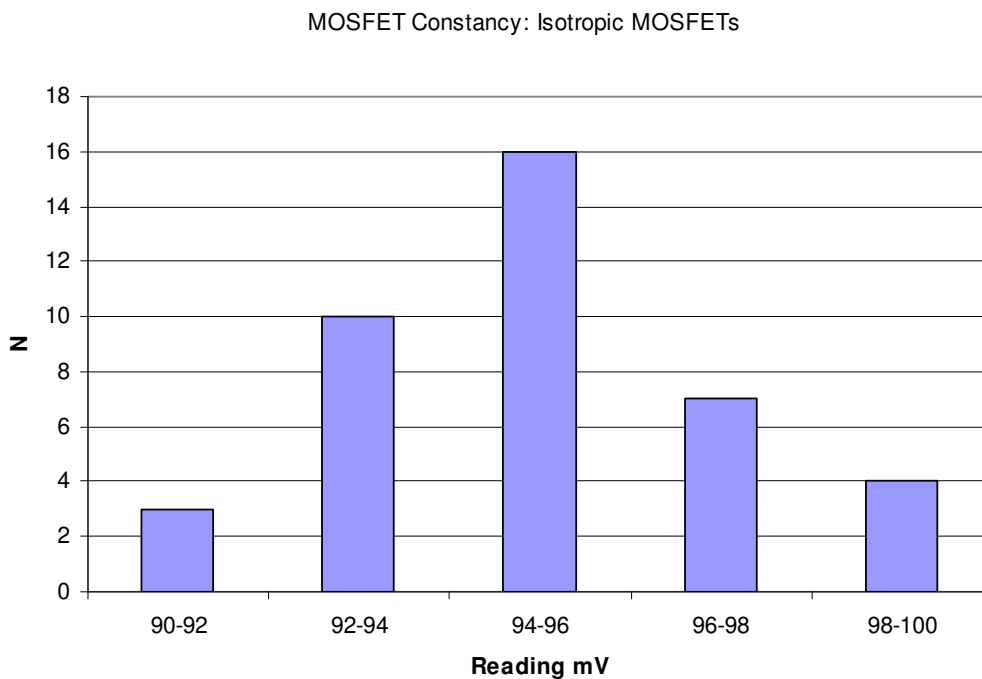


Figure 4-3: Constancy results for the first 40 Readings

4.3.2 Total Constancy over 6 Month Period (Long term)

Over the period from January 2004 to July 2004 twenty five constancy measurements were made. Over that period of time the all readings of the isotropic MOSFETs were normally distributed around a mean of 95.0, with a standard deviation of 2.3% (Figure 4-5). This means that the MOSFETs can be treated as a batch if one chooses. The individual response of the isotropic MOSFETs remained the same (Figure 4-4).

Isotropic MOSFET constancy results Jan 04 to July 04

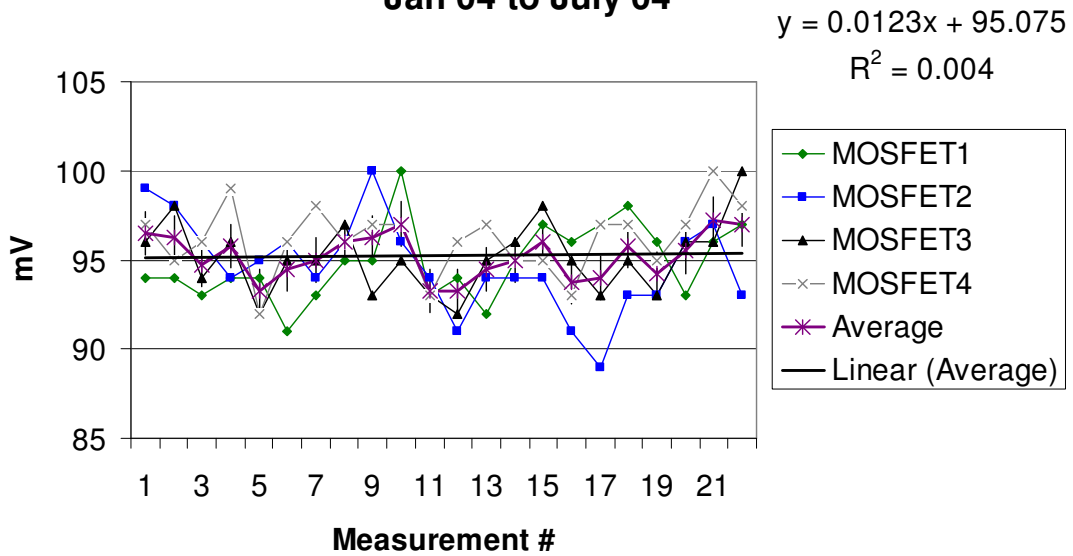


Figure 4-4: Constancy results for the TN-502RD MOSFETs for the first 6 months

MOSFET Constancy Jan 04 to July 04

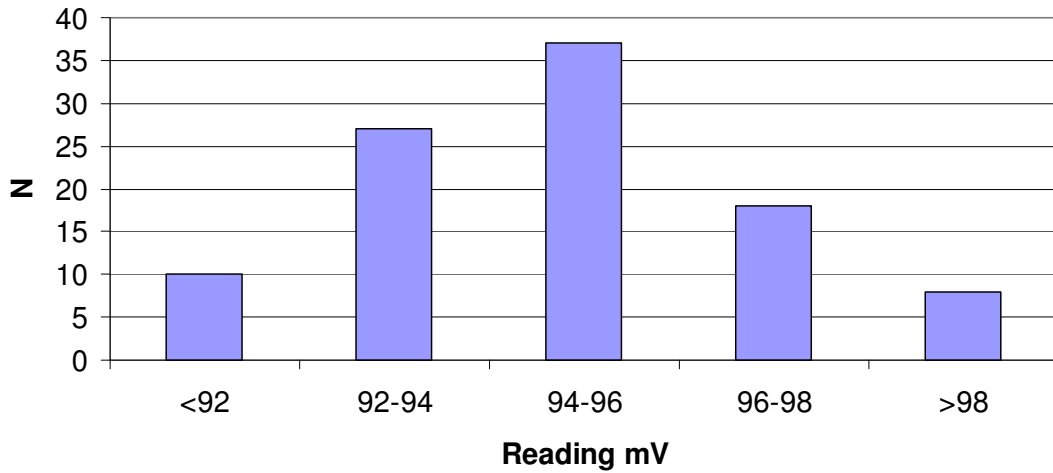


Figure 4-5: MOSFET constancy results for the first 6 months

	MOSFET1	MOSFET 2	MOSFET 3	MOSFET 4	MOSFET 5	All Isotropic as a batch
Mean	95.3	94.7	95.2	96.2	261.6	95.3
SD	2.5	2.5	2.0	1.9	10.1	2.3
1SD%	2.6%	2.6%	2.1%	2.0%	3.9%	2.4%

Table 4-3: MOSFET constancy from all measurements

4.3.3 Changes in Constancy

All isotropic MOSFETs (TN-502 RD) kept their constancy over the six month period. The exception was the micro MOSFET (TN 1002 RDM), which seemed to change sensitivity. After the change the response was stable again (Figure 4-6). These changes could have been the result of damage to the MOSFET which would affect the bias voltage of one of the 2 identical MOSFETs on the same silicon substrate resulting in a gain in sensitivity. After the sensitivity change the MOSFET kept its sensitivity at the same level for the rest of its lifetime (20000 mV). This shows that care should be taken when handling MOSFETs and suspicious results should be checked with a subsequent calibration or constancy check.

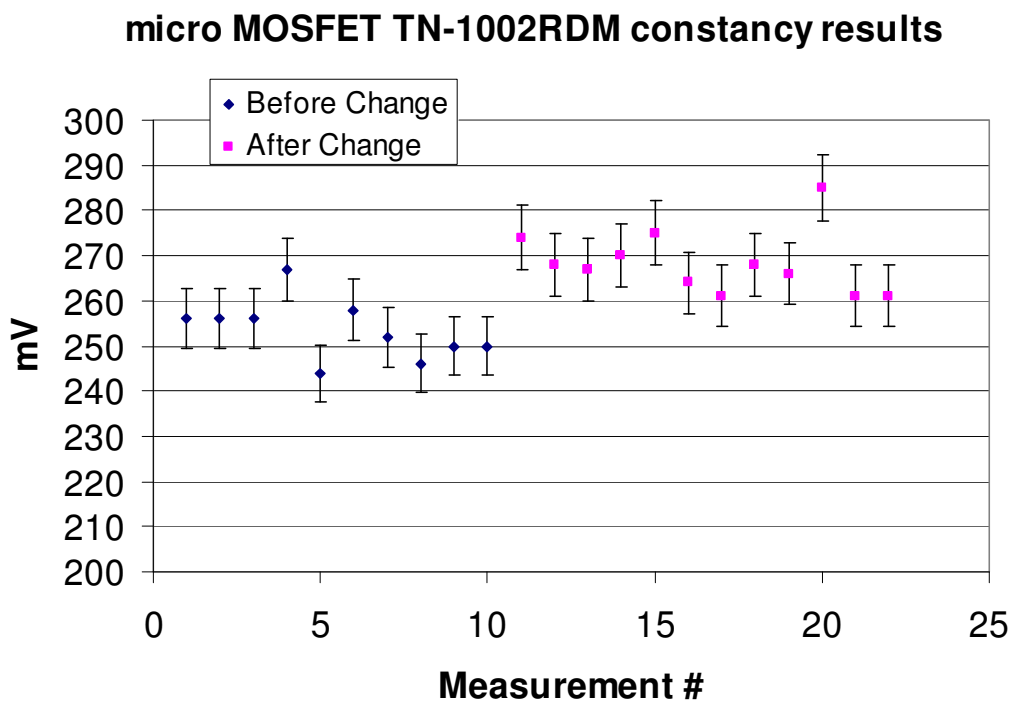


Figure 4-6: Micro MOSFET constancy results

If measurements are taken from the point of change (measurement 10 Jan 04) onwards the mean and standard deviation remain consistent with the manufacturers specifications (Table 4-4).

	MOSFET 1	MOSFET 2	MOSFET 3	MOSFET 4	MOSFET 5
Avg	95.3	93.3	95.2	96.1	268.3

SD	1.92	2.18	2.29	2.02	7.03
SD %	2.0%	2.3%	2.4%	2.1%	2.6%

Table 4-4: MOSFET constancy results after measurement #10

4.4 Skewness and Kurtosis

As the constancy results appeared to have a slight bias towards the negative end of the Gaussian curve, tests for skewness and Kurtosis were conducted on the results. The results showed that skewness was -0.01 (0 being no skewness), and Kurtosis was 2.88 (with 3 being Gaussian). These values were closer to normal than those found by Benson et al. 2004. When using MS Excel Skewness was -0.01, while Kurtosis was -0.086 (0 being Gaussian). When compared to the standard error for Skewness (0.24) and the standard error for Kurtosis (0.49) these values show that the graph has a very Gaussian like distribution (Tabachnick, B. G. and Fidell, L. S. 1996).

4.5 Linearity

MOSFET measurements were made with doses from 20 MU to 400 MU in the *standard setup*.

The dose measured in mV and the dose given in MU are listed in Table 4-5.

MU	MOSFET 1	MOSFET 2	MOSFET 3	MOSFET 4	MOSFET 5	Avg	SD	Number of Measurements	SD % TN-502RD Average
20	19.0	18.1	18.9	17.3	39.0	18.3	0.784	7	4.3%
50	48.4	48.2	48.8	47.8	129.2	48.3	0.41	5	0.9%
100	94.3	96.4	95.2	96.4	253.5	95.6	1.02	10	1.1%
200	194	184.5	190	187.5	506	189	4.02	2	2.1%
400	391	396	390	389	1026	388.7786	3.11	1	0.8%

Table 4-5: MOSFET linearity

For the linearity measurements the standard deviation of the measurements was taken to be the error for the graph. All MOSFETs showed excellent linearity, with a correlation coefficient squared (r^2) of 1.000 (Table 4-6, Figure 4-7, Figure 4-8). This is the same as Jorner et al. (2004), and better than Chuang et al. (2002). Measurements are linear over the full

clinical range. No corrections were made for changes in MOSFET sensitivity as the sensitivity of the TN 502 RD MOSFETs as well as the micro MOSFET were constant while the linearity measurements were being made.

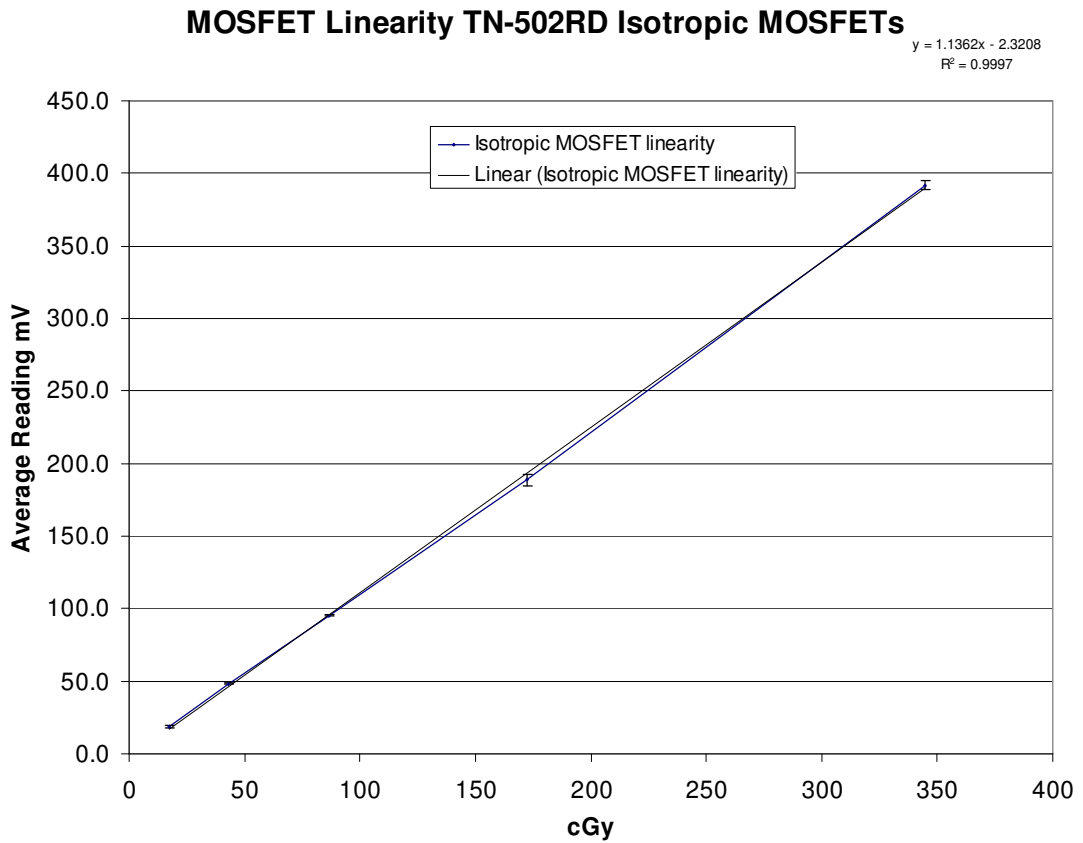


Figure 4-7: Linearity TN-502RD MOSFETs

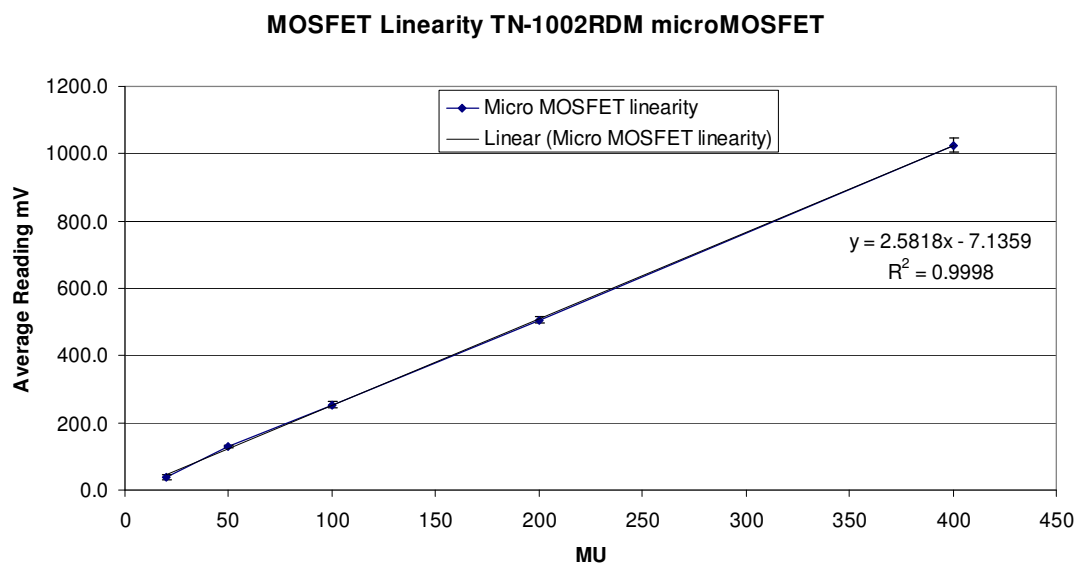


Figure 4-8: Linearity TN-1002RDM micro MOSFET

The correlation coefficient for the detectors is in the table below.

MOSFET1	MOSFET2	MOSFET3	MOSFET4	MOSFET5	Avg of First 4
1.0000	0.9993	0.9999	0.9998	0.9999	0.9999

Table 4-6: Correlation coefficients of linearity

4.6 Angular Dependence

Thomson and Nielsen claim their isotropic MOSFETs exhibit angular dependence of less than 2%. Angular dependence measurements were performed with MV 6 and 10 MV in two separate cylindrically shaped acrylic phantoms 5.2 cm in diameter and 10.2 cm in diameter. The bias used for the MOSFET TN-502RD was the TN-19 High sensitivity bias supply. Measurements were made from -90 degrees to +90 degrees in 15 degree increments for 10 MV and 30 degree increments for 6 MV. The results were recorded and the compared to the average result. For 10 MV the angular dependence was less than 1.5%, while for 6 MV the angular dependence was less than 2.1%. As 6 MV angular dependence was greater than 2.0% the experiment was carried out in a specially designed acrylic phantom which was 10.2 cm diameter. Results were similar, but within the 2% the manufacturers claim. The standard deviation for 10 MV measurements was 0.8%, while the standard deviation for 6 MV measurements was 1.3% and 1.1% for the 2 experiments respectively. Results agree with the manufacturers claims of angular dependence of +/-2%. This has also been confirmed by Chuang et al. (2002) and Ramaseshan et al. (2004) for 18 MV photons and diagnostic energy photons respectively.

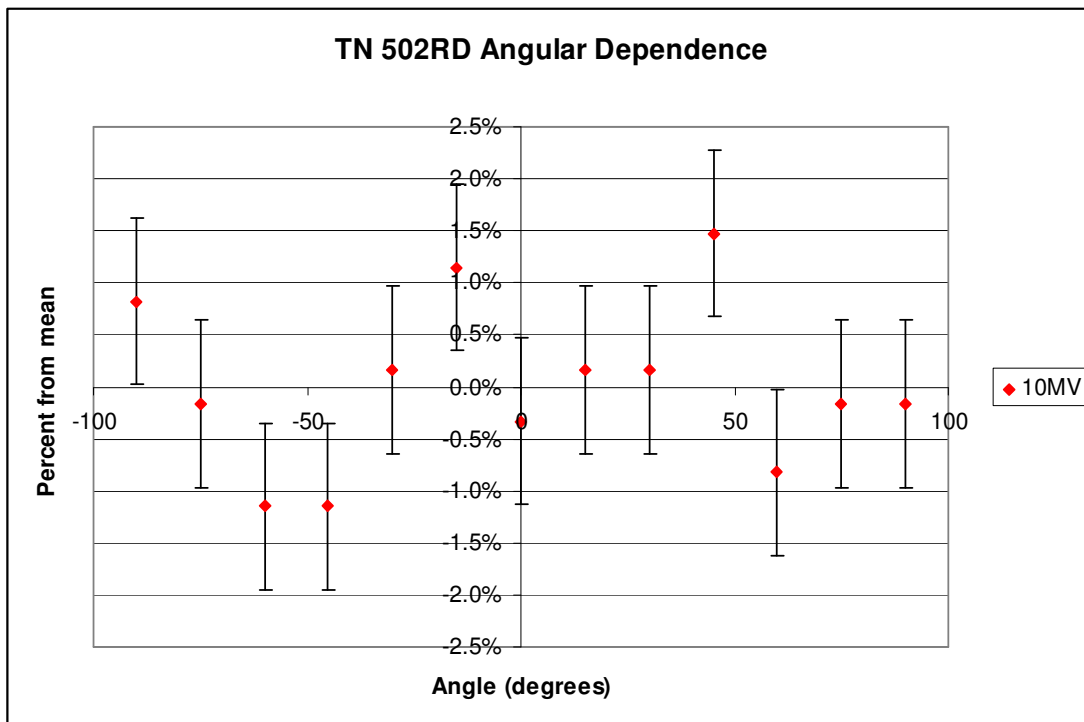


Figure 4-9: Angular dependence 10MV

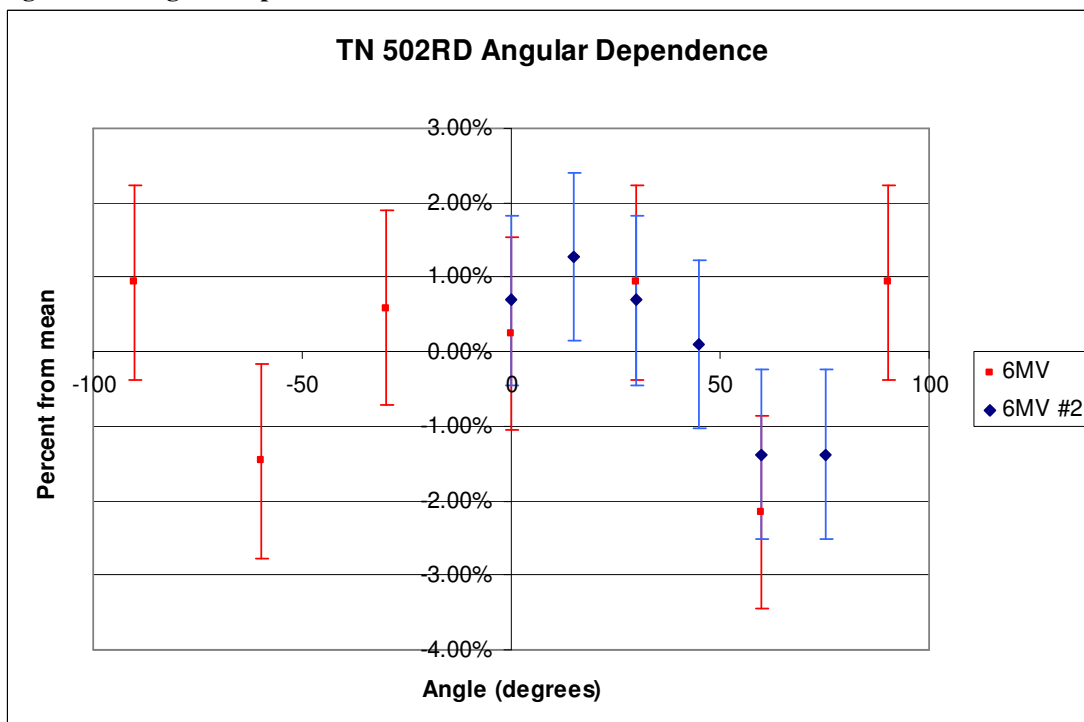


Figure 4-10: Angular dependence 6MV

4.7 Energy Dependence

Thomson and Nielsen claim minimal energy dependence in the MeV range with increased energy dependence in the keV range (Thomson & Nielsen 1995). The dose response of the

energy dependence measurements for the TN-502RD isotropic MOSFETs was excellent, with a 5.4% +/-4.5% difference in mV per Gy over the full range (6 MeV to 21 MeV) of electrons, with an increase in energy dependence with energy (Figure 4-11).

For photons the ratio of 1 Gy to D_{max} in mV for 10 MV to 6 MV photons was 0.986+/-0.015.

This was within the manufacturer's stated 5% energy dependence for MeV photons (Thomson and Nielsen 2002).

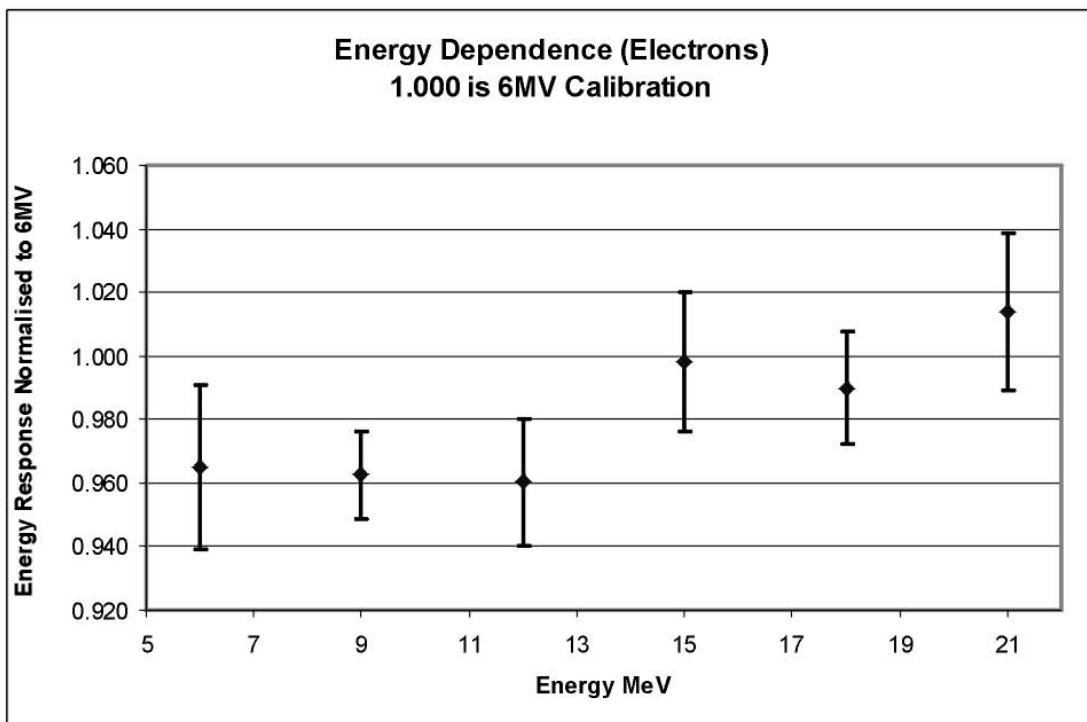


Figure 4-11: Energy Dependence of Electrons 6 to 21 MeV

4.8 Build Up

In the build up region there is an absence of electronic equilibrium. There is also a large amount of low energy electron contamination from Compton scattering in the flattening filter as well as the collimators. Ion chambers can have quite large errors in the build up region as the polarity and guard effects can become significant (IAEA TRS 381 1997).

Experimental Setup: TMR's were measured in RW3 for a 6 MV beam with the ROOS parallel plate ionization chamber (PPIC) with the effective point of measurement $1 \text{ mm} \pm 0.02$

mm below the top surface of the ion chamber (IAEA TRS 398 2000). This was repeated with +360V and -360V and the average (IAEA TRS381 1997 p54).

TMR's were then measured with the MOSFET in RW3 for a 6 MV beam with the build up facing up. No correction was applied for the extra depth of the build up cap. The water equivalent thickness of the build up for the TN 502 RD MOSFET was taken to be $0.9 \text{ mm} \pm 0.02 \text{ mm}$.

Below is a diagram of the experimental setup (Figure 4-12)

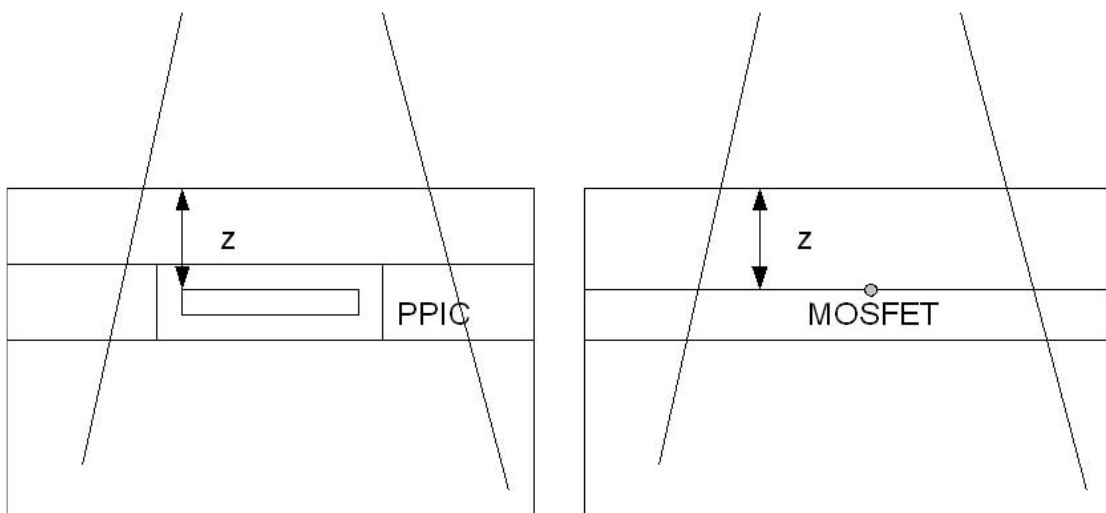


Figure 4-12: BU region setup

All measurements agreed to within the uncertainty of the MOSFET measurement for the TN 502 RD MOSFET and the ROOS ion chamber (Figure 4-13).

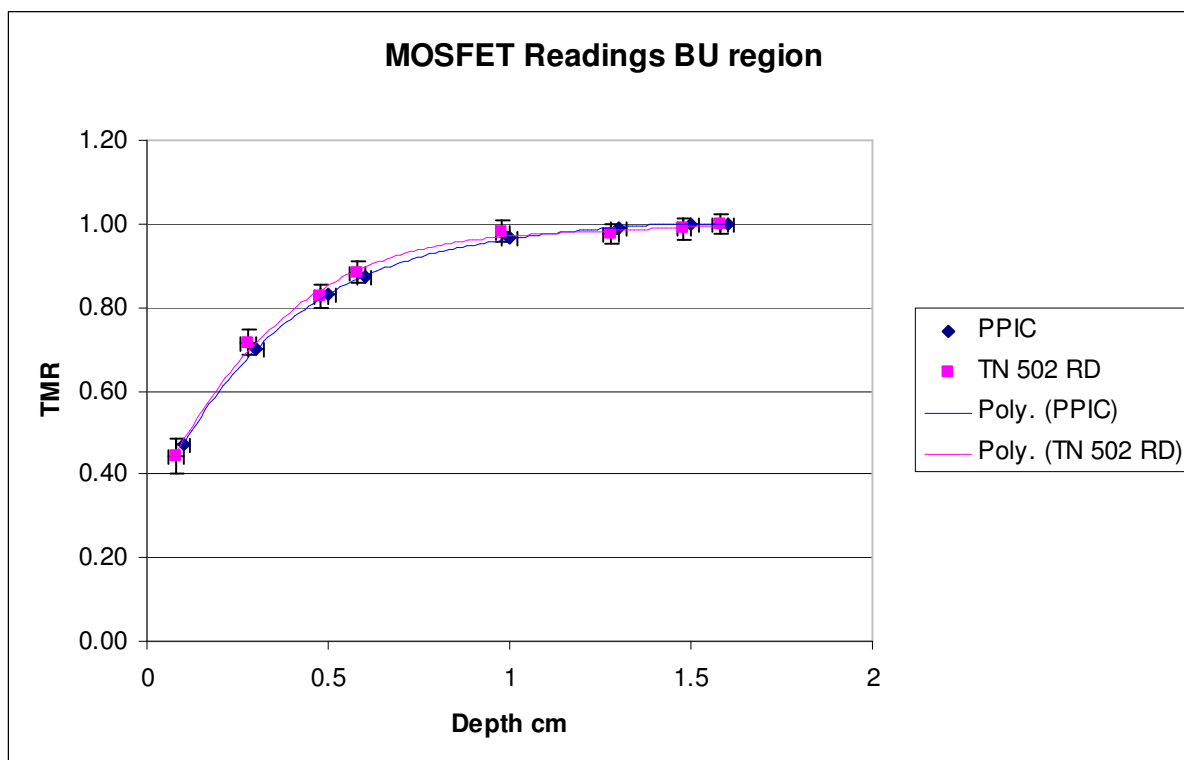


Figure 4-13: TMR measurement of build up region

MOSFETs can therefore be used as a tool for measuring dose in the build up region and on skin surfaces. Care should be taken when placing the MOSFET close to lead as the low energy photons produced by characteristic X-rays are in the energy range where the MOSFET is more sensitive (Kron et al. 1998).

4.9 Temperature Dependence

Temperature dependence of TN 502 RD MOSFETs can not be ruled out (Jornet et al. 2004).

The sensitivity variation with temperature does not have a linear relationship for 18 MV photons over the range of 22 °C to 32 °C (Jornet et al. 2004). This complex behaviour led to temperature dependence experiments to verify whether or not temperature dependence existed. A simple experiment was devised. Two scenarios were constructed.

- The MOSFET was heated under an armpit till it was at body temperature. It was then placed in a phantom and irradiated. This reading was then compared with a reading made without heating the MOSFET.

- The MOSFET was placed in a phantom and irradiated. It was then heated in an armpit and a reading taken. This reading was compared to a MOSFET reading where the MOSFET was at room temperature.

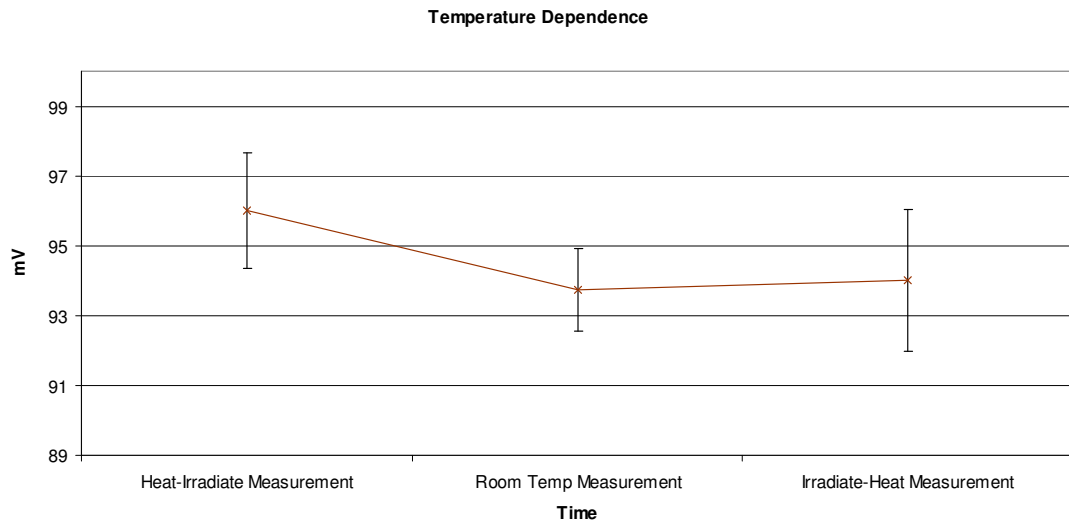


Figure 4-14: Temperature dependence for body temperature

Above are the results of the two scenarios (Figure 4-14). There is no significant difference in the reading obtained between the heated and normal MOSFET. It can therefore be assumed that the temperature dependence of the MOSFETs, if it exists, is small enough not to affect results if the MOSFET is placed on a patient.

Another experiment was then conducted to further investigate the temperature dependence of the MOSFETs. The MOSFET was placed in a water phantom at a set depth in water. The temperature of the water was measured and 3 readings were made with 100 MU. The depth was approximately 1.7 cm and the energy 6 MV. The Temperature dependence was less than 1% over the temperature range 26.2 °C to 30.6 °C (Figure 4-15)

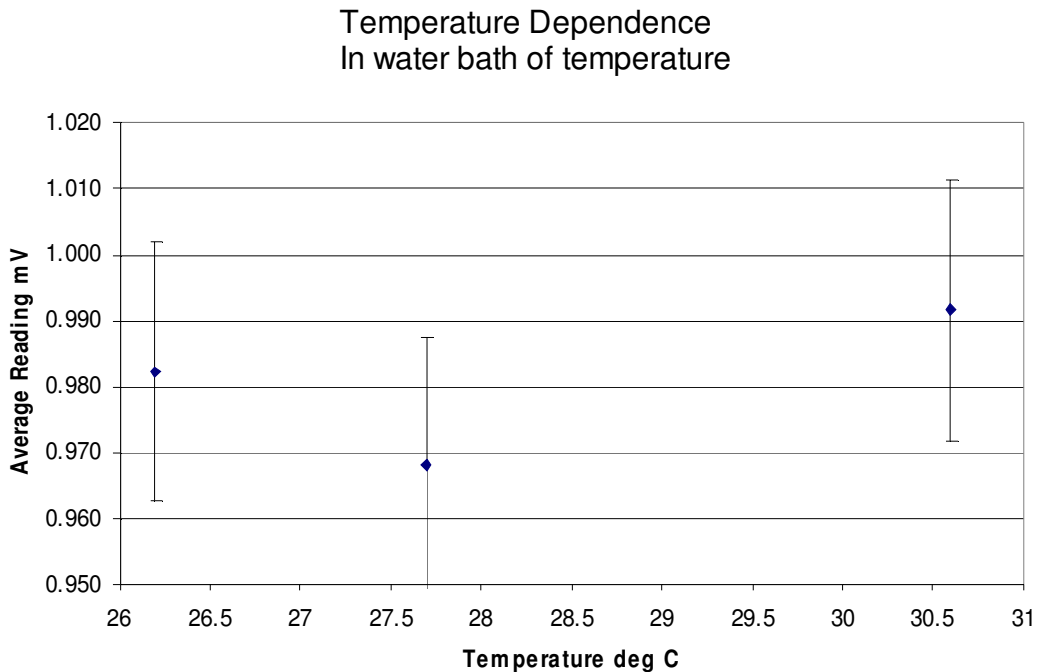


Figure 4-15: Temperature dependence

4.10 SSD and Dose Rate Dependence

Although MOSFETs have no dose rate dependence (Soubra and Cygler 1994) that does not guarantee that there is no SSD dependence. The change in the energy spectrum with collimator distance can affect the dose response of a MOSFET as the MOSFET has an energy dependence at lower energies that can be quite large (Kron et al. 1998, Edwards et al 1997). MOSFET SSD dependence has been noted in literature (Jornet et al. 2004). SSD dependence was tested by placing an ion chamber at 1.5 cm for a 6 MV beam in a plastic water® phantom. The SSD was varied and the reading nC was taken. The MOSFETs were then placed at the same depth in RW3 and irradiated at the same SSD. The ratio of the average MOSFET reading to the ion chamber reading was taken. If there is no SSD dependence the ratio would remain constant. This ratio was normalised to 100.0 cm SSD and the results were

plotted to look for SSD dependence. No noticeable SSD dependence was observed in the range 80.0 cm SSD to 110.0 cm SSD.

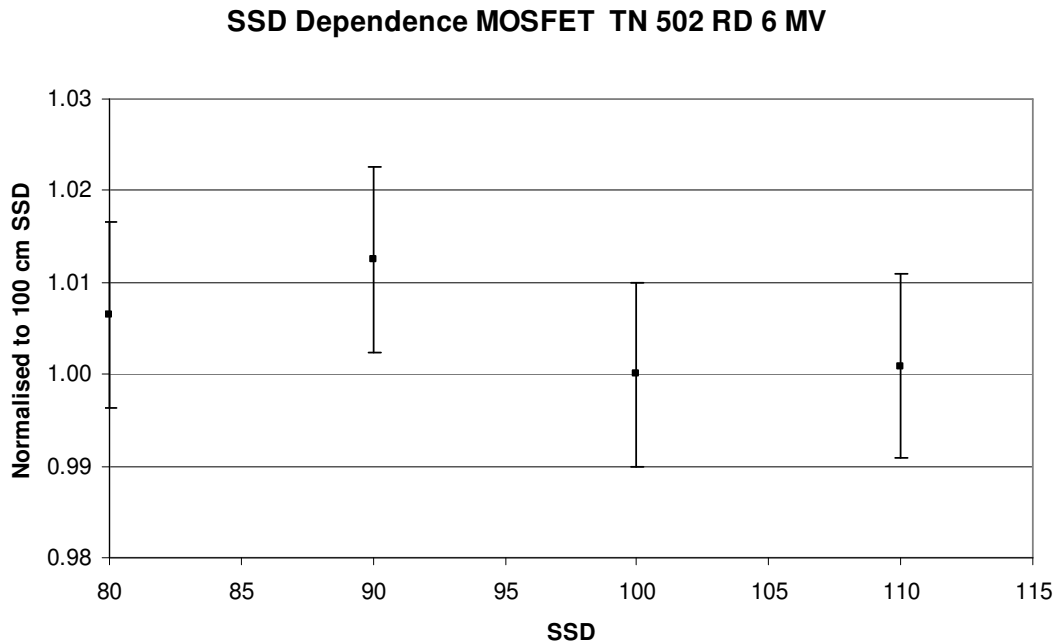


Figure 4-16: SSD dependence

4.11 Field Size Dependence

If the MOSFET exhibited an energy dependence this could result in a field size dependence for the entrance dose. There is no field size dependence for X-rays up to 10 MV, and a slight field size dependence for 18 MV X-Rays (Ramaseshan et al. 2002).

To verify this, MOSFET measurements were made and compared with ion chamber measurements. The depth for field size factor measurements was taken at 5 cm.

Measurements were made in RW3 for the ROOS and MOSFETs, while for the IC15 measurements were made in water.

The MOSFETs agreed with ion chambers to very small field sizes. Even when the larger ion chambers failed the MOSFET still maintained its accuracy. There was no field size dependence in the range 3 cm x 3 cm to 25 cm x 25 cm for 6 MV at 5 cm depth.

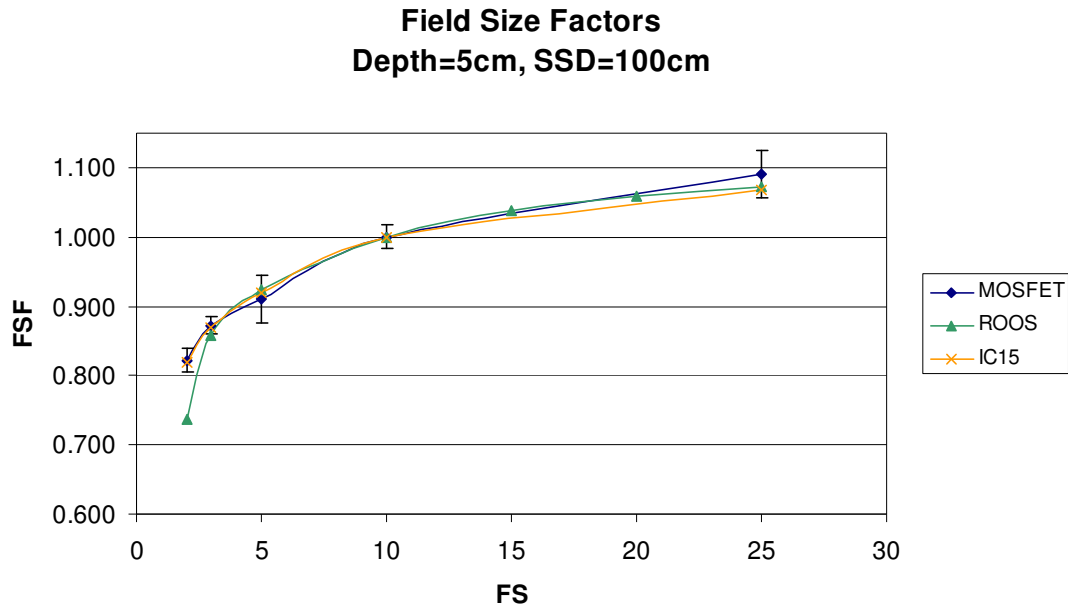


Figure 4-17: Field size dependence

4.12 Time Dependence

4.12.1 Warm up Time

On initial investigation it appeared time was a factor in the reading attained from MOSFETs. One factor that is important is the time it takes for the reader to warm up. The T&N users manual (1998) recommends that the reader should be on for 30 minutes before measurements are taken. This is true for measurement stability as well as measurement accuracy.

Measurements are low and unreliable if the reader has not been on for enough time. Results from a constancy measurement showed that if the reader is not warmed up properly the measured reading will be low. For a set of measurements where the reader was only warmed up for 15 minutes the reading was on average 2.6% low (for all 5 measurements). The

standard error for this set of measurements was taken as $\frac{\sigma}{\sqrt{N}}$, so for 100 MU and 4 readings

this would be $\frac{2.6\%}{\sqrt{4}}$, which is 1.3%. As 2.6% is greater than 2 standard errors from the mean

it can be concluded that the error is not due to random variations in MOSFET readings. All other measurements fell within the standard error (1S.D) of the mean. The next largest difference for a set of measurements was 1.2%.

4.12.2 Time Till Readout

The dependence of time between measurement and reading can be a factor as well. This is known as "fade".

An experiment was conducted to test the time dependence on a measurement. The MOSFETs were irradiated and then left for a period of time before being measured. The results of these measurements were then compared to each other (Figure 4-18). The results of the time dependence measurements were initially an increase in response over time, with less than 1.5% difference in the first 10 minutes. It is more likely that the variation is more the result of measurement uncertainty than a drift with time.

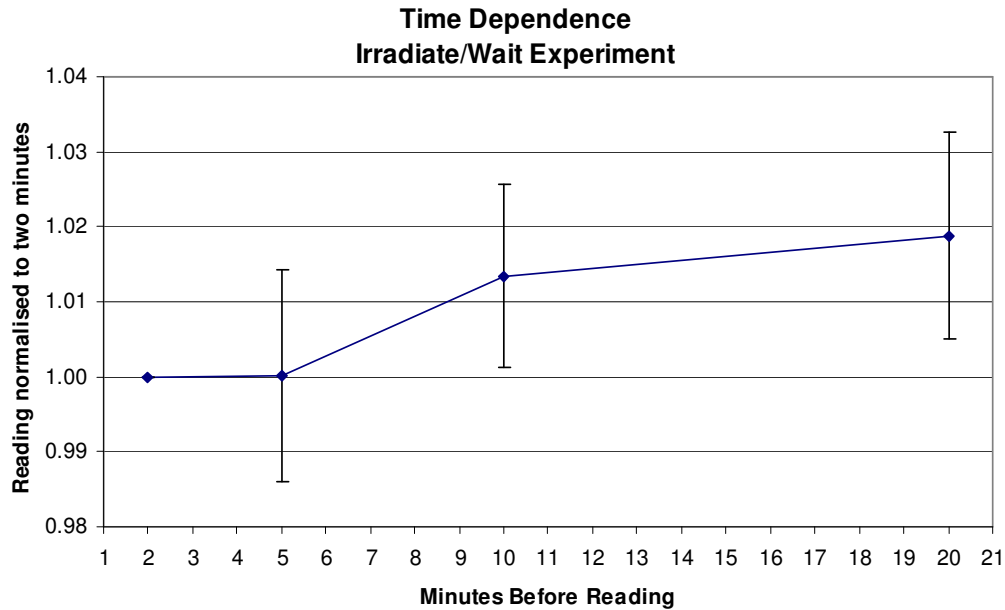


Figure 4-18: Fade measurements

The total difference in time dependence is less than 0.7% for a 20 minute wait based on the two measurements made with a two minute wait and a 20 minute wait. As measurements take place within the first 5 minutes after the MOSFET has been irradiated the time dependence of fade will be negligible.

Time dependence is a factor that can not easily be modelled. It will therefore not be included in any models presented as part of this work.

4.13 Conclusion

Thomson and Nielsen MOSFETs have excellent constancy and linearity. The error is spread evenly around a Gaussian mean and decreases greater than $\frac{1}{\sqrt{N}}$, where N is the number of measurements or the total dose received. They have insignificant field size, angular, or temperature dependence.

Independent calibrations can be performed, and mixed photon energies can be measured at the same time, although this is discouraged, as the energy dependence is similar for 6 MV and 10 MV photons.

5 Setting an Action Threshold

5.1 Introduction

To suitably implement IVD in a clinical setting uncertainties involved in the measurement should be known beforehand. For this reason two thresholds are generally given. An *investigation threshold* above which a repeat of the IVD measurements is made, and an *action threshold*, above which patient setup and treatment delivery is checked (Huyskens et al. 2001, AAPM Report 87 2005). The action threshold should not be chosen arbitrarily as choosing the wrong action threshold can lead to time wasted on investigations into treatment errors which do not exist (Leunens et al. 1994). This in turn leads to lack of confidence in the new techniques being offered. Action levels are based on 2 standard deviations from the mean measurement (Huyskens et al. 2001, Leunens 1994). For a centre with calibrated diodes and a program in place to implement in vivo dosimetry regularly this is about 5 to 8% (Huyskens et al. 2001). Even though Leunens et al. 1994 found the average standard deviation for all measurements was 3.1% (1SD) for corrected tangential breast treatments they chose 5% as the tolerance level. Not surprisingly 10% of patients had deviations greater than 5% (the chosen threshold). Wedged and blocked fields had higher standard deviations. Breasts had higher standard deviations than vertebrae (Huyskens et al. 1992). For MOSFETs the investigation threshold value will be greater given the increase in uncertainty of the measurements (Jornet et al. 2004). Target dose estimation based on entrance and exit dose measurements would have a higher 2σ than entrance dose alone as it involves dose calculation based on a model error, as well as MOSFET reading uncertainty, for two MOSFET readings. For entrance dose measurements the error would come from the model combined with the MOSFET reading uncertainty from one MOSFET reading. For the chosen model error is less than 2% and can not be removed. Even though it is an error which could

theoretically be removed, in practice it can not be removed. It will therefore be considered a random error or uncertainty (see Appendix B).

5.2 Setting the Action Threshold for MOSFETs

For any system of measurements the total error will be at least the random error of the system.

Each model has an intrinsic error, as do the MOSFETs. There will also be an error associated with the treatment type and setup. All these errors need to be taken into consideration and modelled. Systematic errors can also become apparent if, say one of the treatment modelling parameters for the MOSFET were not corrected for properly. For instance an error in F_{ent} (the MOSFET entrance factor) will result in a systematic error for all subsequent measurements.

Very few centres have an average standard deviation of less than 2.9% (1 S.D.) from the expected mean of 1.00 (Huyskens et al. 2001), while the standard deviation and mean of results varies from centre to centre, as well as from one treatment to the next (Huyskens et al. 2001).

Typically the error will be distributed normally around a mean. The standard deviation of this error can then be used to determine the action level that a department needs to check errors in setup or parameters (Huyskens et al. 2001). The action level is recommended at 2σ from the mean (Leunens et al. 1994).

The average of all fields will have a smaller random error than each individual field as random errors associated with the MOSFET will average out.

Consider, for example, the constancy measurements for the MOSFETs. Constancy measurement values range from 89 to 100, with a mean of 95 and a SD of 2.4%. When the first four measurements are averaged the mean is still 95, while the S.D. is 1.3%, almost half the uncertainty of a single measurement. The maximum and minimum errors from the mean measurement were $\pm 5.9\%$ and $\pm 2.2\%$ for one MOSFET and 4 MOSFETs combined

respectively. As the analysis into σ vs. dose shows σ does not obey a square root relationship, but does follow a power law relationship with dose. Analysis of N measurements of the same dose reveals that the uncertainty in measurement is inversely related to the square root of the number of measurements (N). Thus the inherent uncertainty in a measurement without putting into consideration other factors such as patient setup etc. will be approximately

$1.2836 \times Dose^{-0.6485}$. This means that at 2Gy the 3σ uncertainty will be approximately 4.1%, with 1σ at 1.3%.

For the models presented the error is between 1% for TMR based and measurement based approximations to 12% for mean approximation (Chapter 3).

The error in the midline dose of a patient receiving 2 Gy will be at least the uncertainty that is inherent in the system in place. This means that the 3σ uncertainty will be somewhere around 5.1% for the TMR entrance dose based model without considering setup and other related errors. As the standard deviation of the discrepancy in dose predicted of the Lung/Thorax phantom was 3.2% for all measurements made and the error obeys the

relationship $\sigma_T = \sqrt{\sigma_1^2 + \sigma_2^2 + \dots + \sigma_n^2}$, where σ_1 to σ_n are the independent errors contributing to the total error (σ_T), the random error will be about 2.7% 1σ , and the systematic error about 2% (as the mean was about 2%).

Systematic errors such as daily variation of linear accelerator output and calibration transfer factors have not been included, as the purpose of this chapter is to estimate a reasonable tolerance level for MOSFETs for investigation and action thresholds.

Below is a table summarising the typical error contribution per field for a treatment.

Dose Gy	MOSFET Uncertainty	Setup Error	Total Error 1SD	Error 2SD
0.5	3.92	2.7	4.8	9.5
1	2.49	2.7	3.7	7.4
2	1.58	2.7	3.1	6.3

3	1.21	2.7	3.0	5.9
---	------	-----	-----	-----

Table 5-1: Error estimate based on dose

From the relationship above it shows that for any one field a tolerance level of about 8% should be made (Table 5-1) as a typical treatment would deliver a field of about 1 Gy. This is similar to the action threshold of diodes (Table 5-2). For a combination of 3 fields the

uncertainty reduces by $\frac{1}{\sqrt{N}}$, so the 2σ uncertainty will be 4.7%. This is below the

recommended 5% (Huyskens et al. 2001, p 122). For all phantom measurements with the lung/thorax phantom this was the case, with a maximum absolute error for one field of 6.9% (6MV) and a maximum absolute error for 3 fields of 3.9% (6MV). These errors are similar to diode measurement discrepancies on patients (Huyskens et al. 2001, p136).

The errors associated with these in-vivo measurements are within the tolerances set by the AAPM (AAPM Report 87 2005, p 63) and ESTRO (Huyskens et al. 2001, p 136). From this initial analysis of the errors of the lung/thorax phantom one can conclude that MOSFETs will meet the requirements set for diodes in IVD in spite of diodes having a higher intrinsic accuracy (Jornet et al. 2004).

5.3 A Comparison with Action Thresholds set In Literature

Action threshold set in literature vary from one study to the next as well as one institution to another. In Europe the variation between action levels is quite large, ranging from 2.5% to 10% (Table 5-2). Action levels also depend on the complexity of techniques. Techniques using tangential fields with wedges are hard to check and generally have higher action levels (Huyskens et al. 2001, p137). Based on phantom measurements and the uncertainty associated with the MOSFET an action level of 8% is proposed for any one field and an action level of 5% for any 3 fields.

Institution	Technique	Action Level 1	Action Level 2
Leuven	All Techniques	5 - 10%	5 - 10% (6 MV - 18 MV)
Barcelona	All Techniques	5%	5%
Nancy	All Techniques	5%	10%
Copenhagen	Tangential Breast	8%	8%
Copenhagen	Prostate	5%	5%
Amsterdam	Prostate	2.5%	2.5%
Amsterdam	Parotid	4%	4%
Milano	Tangential Wedge	7%	7%
Milano	Other	5%	5%
Edinburgh	Conformal prostate	2.5%	2.5%
Edinburgh	General Entrance	5%	5%
Adelaide	per field	8%	8%
Radiotherapy Centre Adelaide	Per 3 fields	5%	5%
Radiotherapy Centre Adelaide	Breast	8%	8%
Radiotherapy Centre			

Table 5-2: Action Levels ESTRO booklet No.5 2001, and ARC included

6 Clinical Implementation of MOSFETs

6.1 Introduction

The suitability of the MOSFET as an entrance dose in-vivo dosimeter has been investigated in Chapter 4. Suitable measurement tolerances have been set in Chapter 5. For clinical implementation the behaviour of the MOSFET with its build up cap on the surface of the patient is critical. Guidelines for modelling the build up cap properties for diodes are given in AAPM report 87 2005, as well as ESTRO 2001. The models chosen for modelling the entrance and exit dose include these factors in calculating the target dose.

If the MOSFET has no angular dependence, it would exhibit angular dependence when a square build up cap is placed on it. If the build up cap was insufficiently thick enough to shield contaminating electrons arising in the head and collimators, as well as the flattening filters, the MOSFET would show field size as well as SSD dependence (AAPM report 87 2005).

The size of the build up cap could also affect patient comfort, or attenuate too much radiation passing through it resulting in a lower dose to the tumour volume below the build up cap.

As the build up cap is made from material other than water, the photon and electron stopping power ratios would be different, resulting in a different dose in the build up cap than that of water. If the build up cap is made from high Z material photon interactions would lead to an increase in dose due to pair production and photoelectric interactions. Interactions within the material could result in characteristic X-Rays, which would increase the dose to the detector in the sensitive energy range (say, 100keV for lead). Even if characteristic X-rays and low energy scatter comprise a small percentage (say 1%) of the total dose, the increased effect (5 times the sensitivity for MOSFETs (Kron et al. 1998)) of energy dependence in the low X-Ray range would increase the dose read by the MOSFET in comparison to water.

A suitable build up cap needed to be made for entrance dose in-vivo dosimetry which would minimize the measurement of correction factors, provided patient comfort is not compromised and would be easy to manufacture.

All build up caps are generally investigated before implementation of external beam radiotherapy IVD (Huyskens et al. 2001) for parameters which would change near to the surface. This is because the amount of electron fluence near the surface affects the dose to the detector as the build up cap is generally close to the surface of the patient.

6.2 The Build up Cap

6.2.1 Build Up Material

Generally build up caps are made of high Z material so that patient comfort can be achieved by reducing the amount of build up placed on them. For high energy photons they can be flat or hemispherical (Huyskens et al. 2001 p20-22). High Z materials increase the skin dose immediately around themselves as high energy photons provide a greater amount of electron contamination due to the increase in pair production in the MeV range and an increase in photoelectric interactions in the keV range. Build up caps can also be made from water equivalent materials (Jornet et al. 2004, Sun-Nuclear.com, Thomsonsonelec.com). The ideal build up cap would provide a small dose to a small region of the patient's skin, would have electronic equilibrium, and would not be dependent on setup parameters. Jornet et al. 2004 states that the detector should be measuring under electronic equilibrium (Depth $>D_{max}$). Despite these recommendations, in-vivo dosimetry manufacturers use build up that would amount to less than D_{max} for their diodes (Jornet et al. 2004, Huyskens et al. 2001 p.77). As the material of commercial build up caps is of higher Z than water, there will be different proportions of interactions taking place to that of water. The contribution of dose from photoelectric effect and pair production will increase the dose delivered to the measuring

device (diode or MOSFET). It is therefore possible to get doses greater than D_{\max} in the build up cap even though there is an absence of phantom scatter. This is for 2 reasons.

- There is higher μ/ρ for the cap.
- The silicon that the dose is measured with has higher μ/ρ and will therefore produce a higher dose to that of water. The high μ/ρ makes the detector susceptible to the low energy scatter and characteristic radiation produced in the build up cap.

6.2.2 Custom Built Cap

A custom made build up cap was made of aluminium and was made hemispherical in shape.

Aluminium was chosen as it has a density greater than water, but a relatively low Z (13), which makes it closer to water $Z(7)$ than other alternative materials. It is easily milled, chemically stable and robust. The build up cap has a thin plate (3 mm) high milled with a hole to fit a TN502 RD MOSFET. A cylindrical dome 8.00 mm radius is glued on top (Figure 6-1, Figure 6-2).

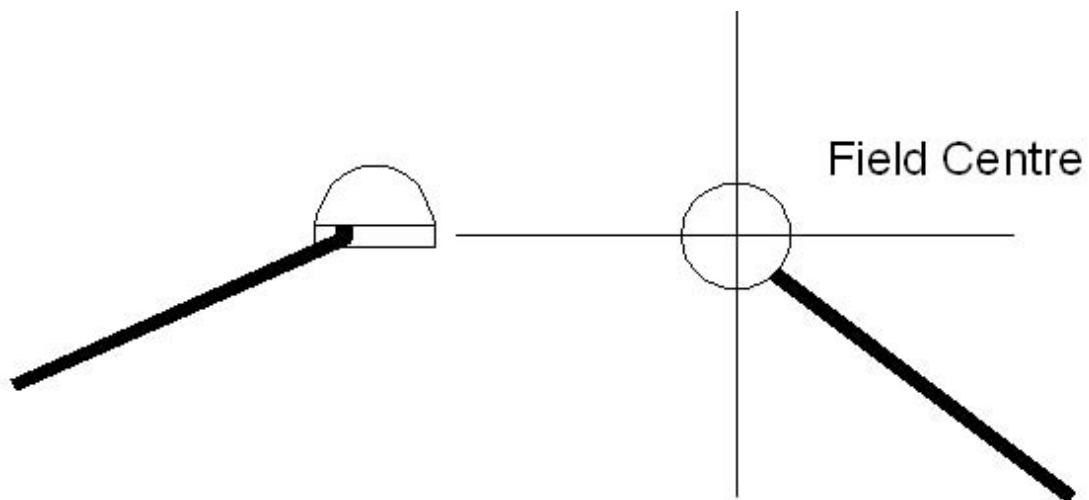


Figure 6-1: Build up cap Side View and Top View

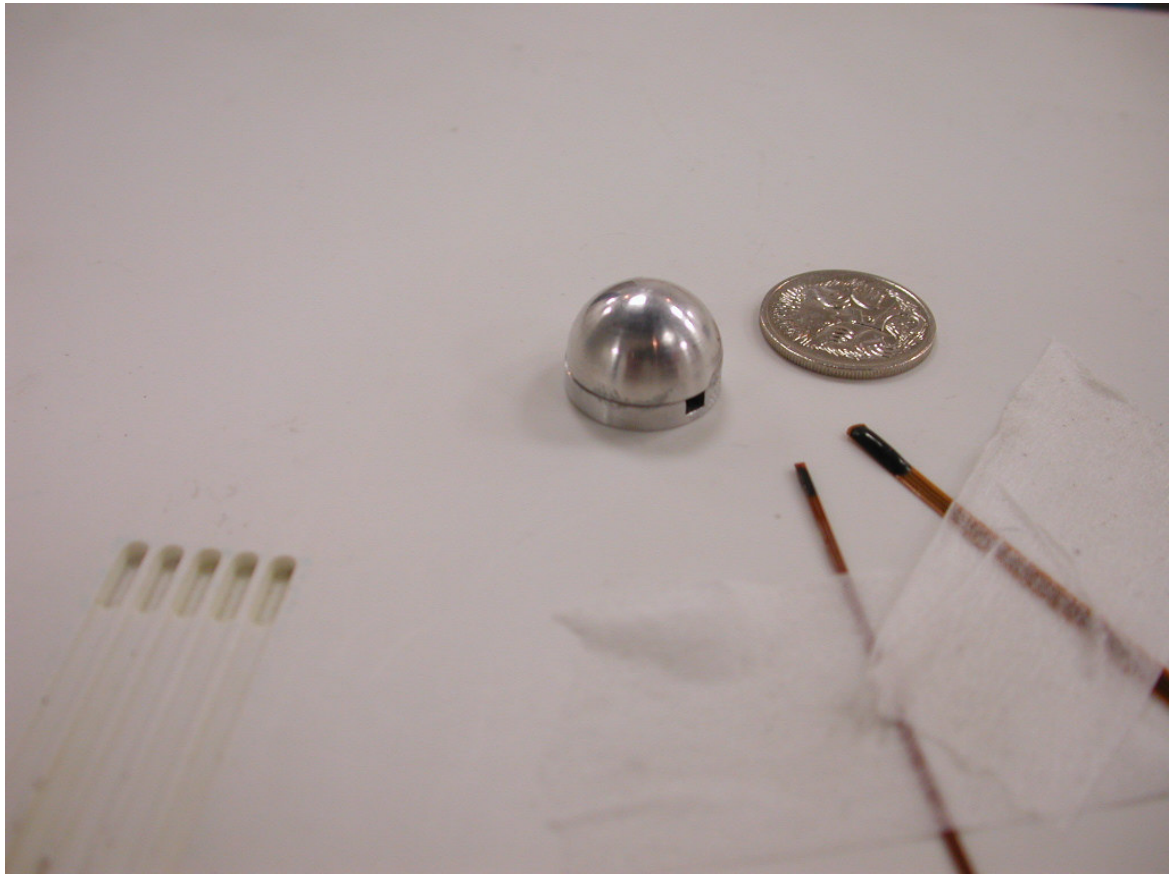


Figure 6-2: Build up cap with TN-502RD and TN-1002 RDM MOSFETs and RW3 with milled holes Au 5c used for scale.

As the mass absorption and transmission stopping power of aluminium is similar to water the water equivalent depth can be calculated roughly by the ratio of the densities of aluminium ($\rho=2.699$)(NIST, electronic resource) and water ($\rho=1$)(NIST, electronic resource). This gives an approximate water equivalent depth to the MOSFET of 2.16 mm, a depth greater than D_{\max} for 6 MV and slightly less than D_{\max} for 10 MV.

6.2.3 Build Up Cap Shadow

Build up caps perturb the dose below the cap as a portion of the dose is delivered to the build up cap. It is important to measure the extent of beam shadowing from the build up cap. This was done at D_{\max} depth for both 6 MV and 10 MV. Measurements were made with an ion chamber with and without the build up cap placed above. The percentage perturbation at D_{\max} was 6% for 6 MV and 4% for 10 MV. This is similar to the acceptable dose shadow of 5% to 6% (AAPM Report 87 2005, p15). For a treatment of 30 fractions this would result in less

than 0.5% difference to the dose in the shadowed region if a single measurement is made. If multiple measurements are needed the dose with the build up cap will have to be measured at different positions in the field.

6.2.4 CF_{ent} (Entrance Dose Calibration Factor)

$$CF_{ent} = \frac{R_{MOS, BUcap}}{R_{MOS, D_{max}}}$$

The ratio of the dose to the MOSFET in the build up cap on the surface of the patient to the reading of the MOSFET at D_{max} is CF_{ent} . The dose at D_{max} can be obtained by multiplying the MOSFET reading in the build up cap to CF_{ent} . CF_{ent} was measured by placing the MOSFET in Plastic Water® and irradiating it at D_{max} with 100cm SSD. The MOSFET was then irradiated with the build up cap at 100cm SSD. The ratio of the measurement with the build up cap to the measurement at D_{max} was taken as CF_{ent} . An average of 3 measurements was taken to ensure constancy. CF_{ent} was $1.006 \pm 0.8\%$ for 6MV and $1.088 \pm 0.1\%$ for 10MV. The reasons for the higher value for 10 MV could be varied, but this could be broken into two separate components

- SSD: As the MOSFET is 2.5+0.2 cm closer to the source it has a greater reading of approximately 5.4%
- Energy specific effects: The MOSFET is in a different energy spectrum to in RW3 and its reading will respond differently. It is not unusual for readings to be greater than the D_{max} reading. Changing the build up cap material can change results by 28% (Jornet et al. 2004), who also found for high energy X-Rays the reading is greater than at D_{max} .

6.2.5 CF_{SSD} (SSD Correction Factor)

$$CF_{SSD} = \frac{\left(\frac{R_{IC,D_{max}}}{R_{MOS,BU}} \right)_{SSD}}{\left(\frac{R_{IC,D_{max}}}{R_{MOS,BU}} \right)_{SSD=100cm}}$$

As the build up cap is placed on the surface of the patient there will be an inverse square law relationship with dose (CF_{SSD}): The MOSFET will be at a distance of $SSD-0.2$ cm, while the

point at D_{max} is at $SSD+1.5$ cm (6MV) or $SSD+2.5$ cm (10MV). The ratio $\frac{(SSD - 0.2)^2}{(SSD + D_{max})^2}$

will change with SSD (Figure 6-3). It is normalised to 1.000 at 100 cm SSD.

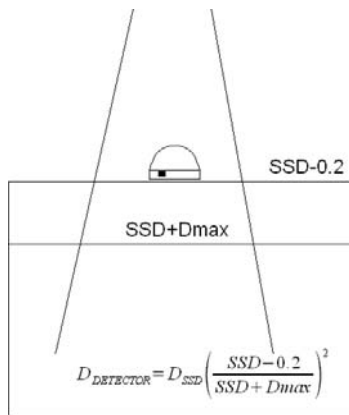


Figure 6-3: SSD Correction

The SSD correction factor depends on the build up cap used as well as the SSD (Jornet et al. 2004). Diodes have dose rate dependence, as the instantaneous dose per pulse results in recombination centres being occupied. Contaminating electrons from the collimators and flattening filter contribute to the surface dose. As there is often a lack of build up for in-vivo dosimeters these electrons contribute to the dose measured with the in-vivo dosimeters. These factors contribute to the significant SSD dependence found in diodes (Huyskens et al. 2001 p15, AAPM Report 87 p9).

SSD dependence of the build up cap was compared to an ion chamber at D_{max} . The ratio of the ion chamber reading to the MOSFET reading with build up cap was taken and plotted over the range of SSD's 85 cm to 115 cm. The results were normalised to the average ratio of all readings. No noticeable SSD dependence was found for 6MV or 10MV. The SSD dependence was found to be less than the 4 to 9% shown by Jornet et al. (2004), with a full range of $\pm 2\%$ for 6 MV and 10 MV (Figure 6-4). This is because MOSFETs do not suffer from dose rate dependence and the build up cap is large enough to remove most electron contamination.

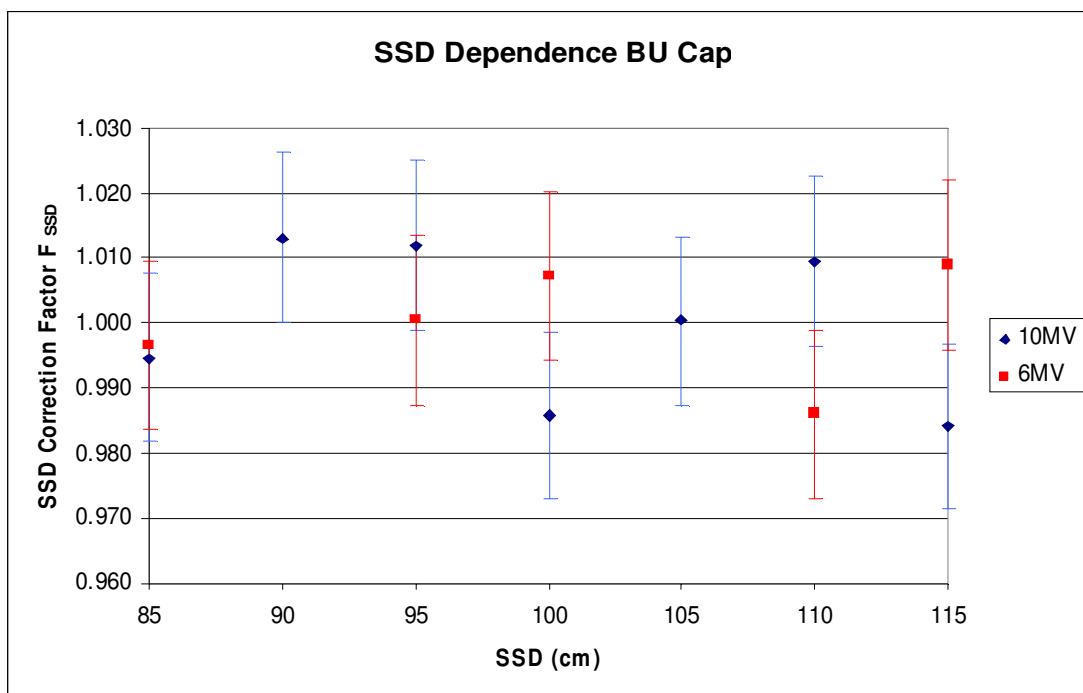


Figure 6-4: SSD Dependence of Build Up Cap

6.2.6 CF_{FS} (Field Size Correction Factor)

$$CF_{FS} = \frac{\left(\frac{R_{IC, D_{max}}}{R_{MOS, BU}} \right)_{FS}}{\left(\frac{R_{IC, D_{max}}}{R_{MOS, BU}} \right)_{FS=10}}$$

Typical values for CF_{FS} are less than 6% (Huyskens et al. 2001 p82., Luca Cozzi and Antonella Fogliata-Cozzi 1998, Jornet et al. 2004) indicating that there is seldom enough build up to remove electron contamination for IVD diodes (AAPM Report 82 2005, p36.). Other factors affecting the field size factor are build up and detector material types (AAPM Report 82 2005, p36). The presence of blocks has little effect on the field size factor (AAPM Report 82 p36).

The field size factor for the ion chamber was taken as the ratio of the dose to a field size to the dose for a 10 cm x 10 cm field at D_{max} . The field size factor for the MOSFET was taken as the measured reading with the MOSFET in the build up cap divided by the measured reading with the MOSFET in the build up cap for a 10 cm x10 cm field size and 100 cm SSD. The ion chamber used was a Scanditronix Wellhofer IC15 corrected for the effective point of measurement (IAEA TRS398 2000).

No noticeable field size dependence was found for 10MV (Figure 6-5)

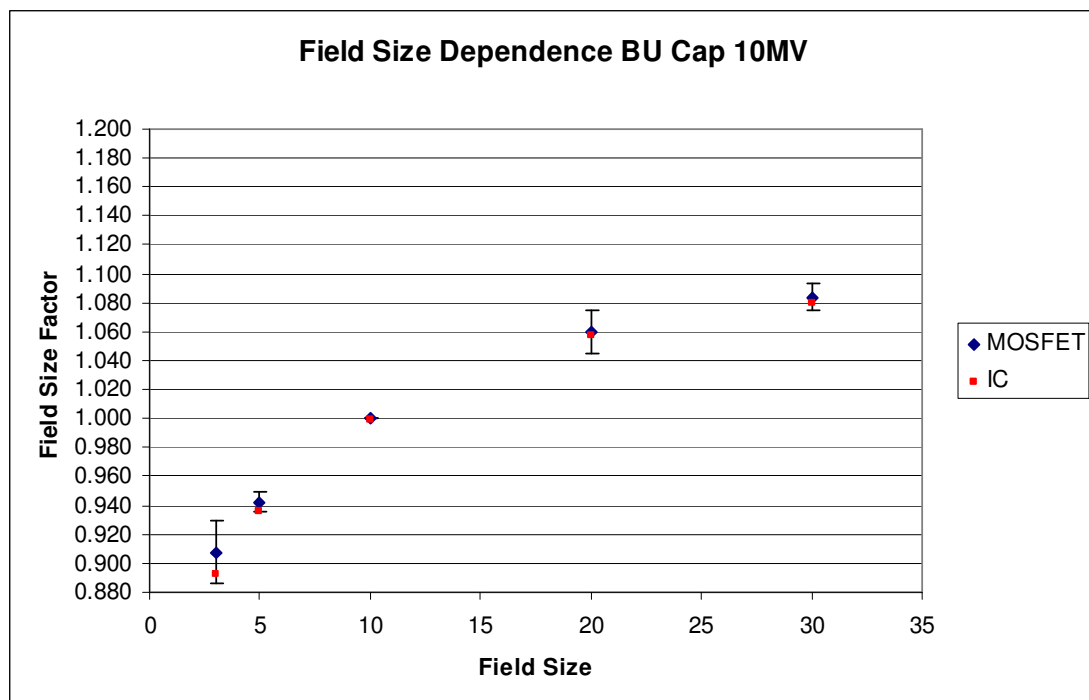


Figure 6-5: Field Size Dependence 10MV

A linear field size dependence was found for 6MV, with a smaller reading at larger field sizes. The total field size dependence over the range 3 cm x 3 cm to 30 cm x 30 cm was about 3%.

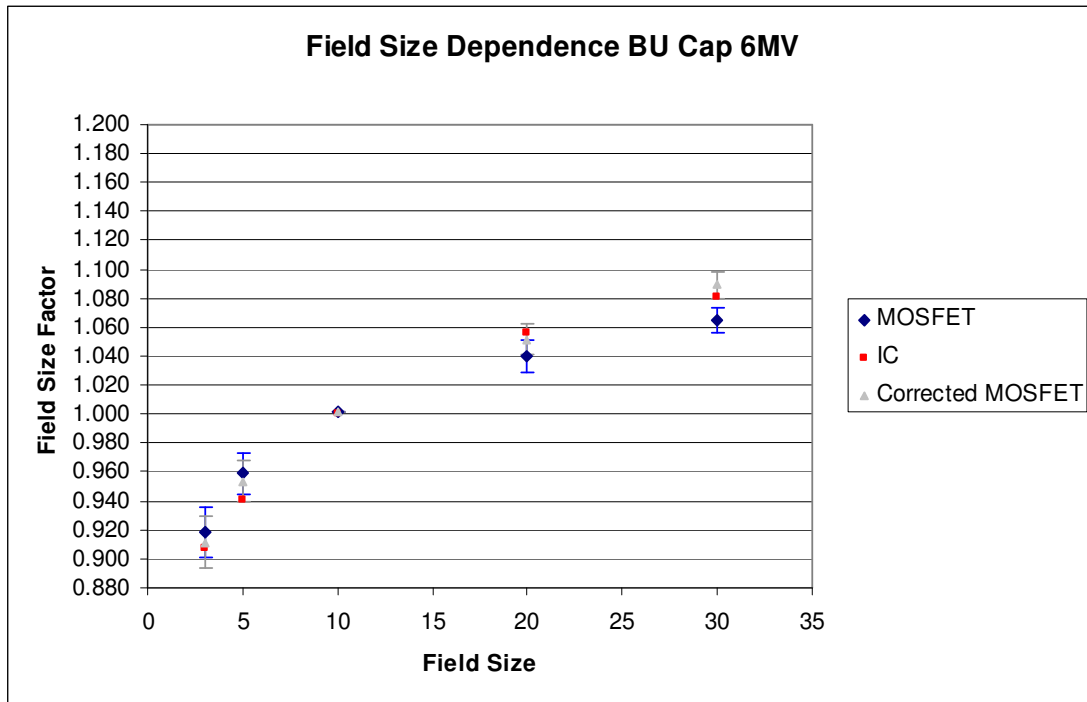


Figure 6-6: Field Size Dependence 6MV

A linear correction was applied to the field size dependence using least squares approximation of the points to a line. The correction was $CF_{FS} = 1 + (FS - 10) \times .00112$. This is a change of about 1% every 10cm² (Figure 6-6).

6.2.7 CF_{wedge} (Wedge Correction Factor)

$$CF_{wedge} = \frac{\left(\frac{R_{MOS,BU,10 \times 10 fs}}{R_{IC,D max,10 \times 10 fs}} \right)}{\left(\frac{R_{MOS,BU,wedge}}{R_{IC,D max,wedge}} \right)}$$

Beam hardening through the wedge will result in a different beam spectrum at the MOSFET in the build up cap. The presence of the steel wedge also increases the surface electron fluence. The increase in average beam energy as well as electron contamination can affect D_{max} . Jorner et al. (2004) noted that a 4% to 7% correction is necessary for 18 MV photons

using a variety of build up caps for a 60 degree wedge. Results were similar, but better for a 45 degree wedge (0.2% for us to 5.2% for Jornet et al. 2004). Measurement of the wedge factor showed no significant increase in wedge factor for low wedge angles. At higher wedge angles the wedge factor increases (the MOSFET reads lower than an ion chamber).

6 MV Wedge Factors

Wedge Angle	15	30	45	60
WF IC-15	0.682	0.516	0.312	0.341
WF BU CAP	0.684	0.514	0.314	0.331
IC-15/BU CAP	0.997	1.004	0.993	1.029
Uncertainty	0.014	0.011	0.012	0.015

Table 6-1: 6 MV Wedge Correction Factors

10 MV Wedge Factors

Wedge Angle	15	30	45	60
WF IC-15	0.731	0.581	0.378	0.408
WF BU CAP	0.737	0.579	0.370	0.398
IC-15/BU CAP	0.991	1.003	1.020	1.044
Uncertainty	0.014	0.013	0.021	0.021

Table 6-2: 10 MV Wedge Correction Factors

6.2.8 CF_{ang} (Angular Dependence Correction Factor)

Even if the detector had no angular dependence the presence of the build up cap will affect the beam profile and therefore could introduce an angular dependence. The angular dependence of the build up cap should therefore be checked as well as the detector. Typical angular dependence for diodes ranges from approximately 2% to 6% (Huyskens et al. 2001 p89-90) over the range 0 to +/- 75 degrees.

Angular dependence of the MOSFETs with the build up cap was negligible over the range 0 to 75 degrees, with a maximum angular dependence less than 2% (Figure 6-7).

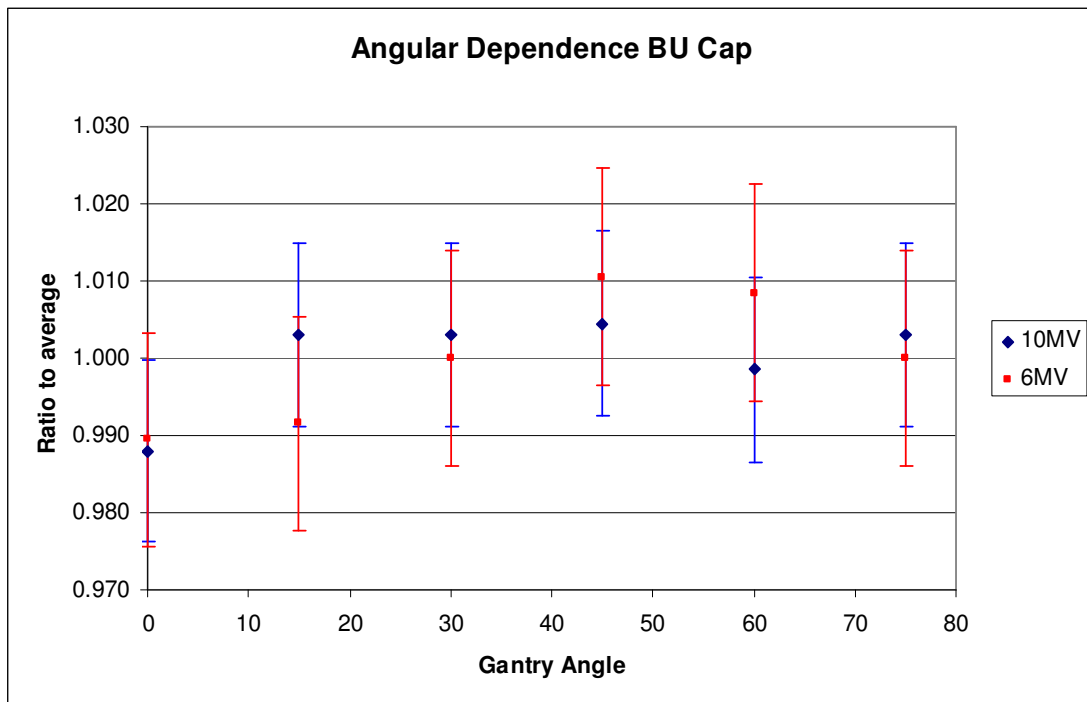


Figure 6-7: Angular Dependence of Build Up Cap

6.2.9 CF_{Tray} (Tray Correction Factor)

$$CF_{Tray} = \frac{R_{MOS,BU} \times IC_{D_{max},Tray}}{R_{MOS,BU,Tray} \times IC_{D_{max}}}$$

The presence of a tray in the beam will cause an increase of dose to the surface as photon interactions with the tray will cause an increase in contaminating electrons reaching the surface of the patient. The MOSFET was placed on the surface of a phantom in the build up cap in a 10 cm x 10 cm field, 100 cm SSD, and irradiated. The tray was then placed in the accessory holder and the same dose was delivered. The ratio of these two readings was taken and corrected for the treatment planning system tray attenuation factor (measured at D_{max}) for 6 MV and 10 MV. The tray correction factor was 0.971 for 6 MV and 1.009 for 10 MV. The reason why 10MV has a tray factor greater than 1.00 is probably because there is insignificant build up on the build up cap to reach D_{max} . As the tray acts like a “build up effect” type of modifier to the beam profile the dose to the MOSFET will be greater than if there was no tray.

For 6 MV the tray factor would be less as the depth would be greater than D_{max} for the beam energy.

6.3 Creation of a User Friendly Interface for Radiotherapists to Use

A spreadsheet was created to calculate the midline dose based on the TMR isocentric model. The information in the spreadsheet could be confusing to use and there is more information than the radiation therapists (RT's) need (Figure 6-8).

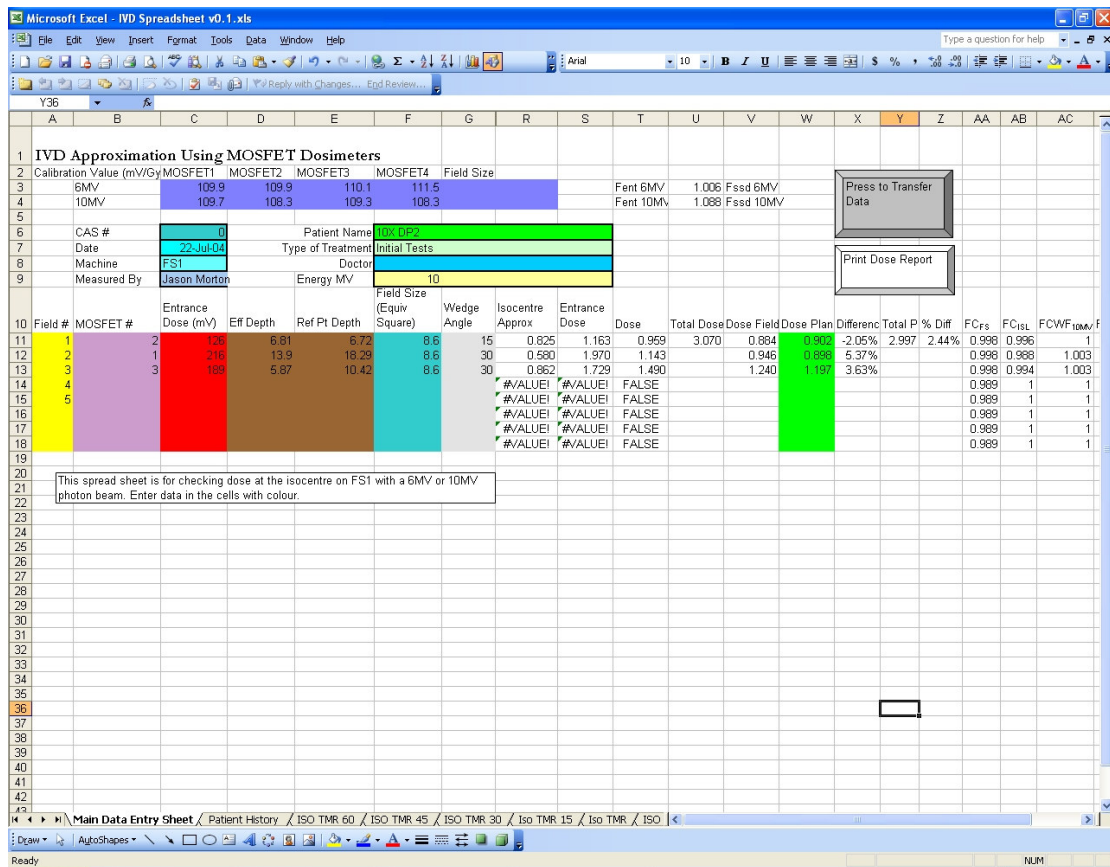


Figure 6-8: Data entry spreadsheet

The spreadsheet was redesigned, and a form based front end created for the radiation therapists to use. The form based front end simplified the data entry for the RT's. The in-vivo

dosimetry results are displayed on another form. Below are two pictures taken from the form based front end (Figure 6-9, Figure 6-10). An option was created so that the original data can be changed if there was an error entering the data. The information will automatically be backed up if the transfer data button is pressed. An automatic form printing macro was also written to print an In-Vivo-Dosimetry summary sheet with the results.

Data Entry Sheet 6MV

MOSFET In-Vivo-Dosimetry Data Entry Page

Enter the data in the boxes below and click on the next button for results.

Date: 0

Field #	MOSFET #	Effective Depth	Ref Pt Depth	Field Size Equivalent Square	Wedge Angle	MOSFET Reading mV	Planning System Dose (Gy)
1	2	6.81	6.72	8.6	15	126	.902
2	1	13.9	18.29	8.6	30	216	.898
3	3	5.87	10.42	8.6	30	189	1.197
4							
5							

Patient Surname: 10X DP2 Patient First Name: Doctor: [Dropdown]

Treatment Type: Initial Tests Machine: FS1 Energy: 10 MV

Next ->

Figure 6-9: Spreadsheet Form 1

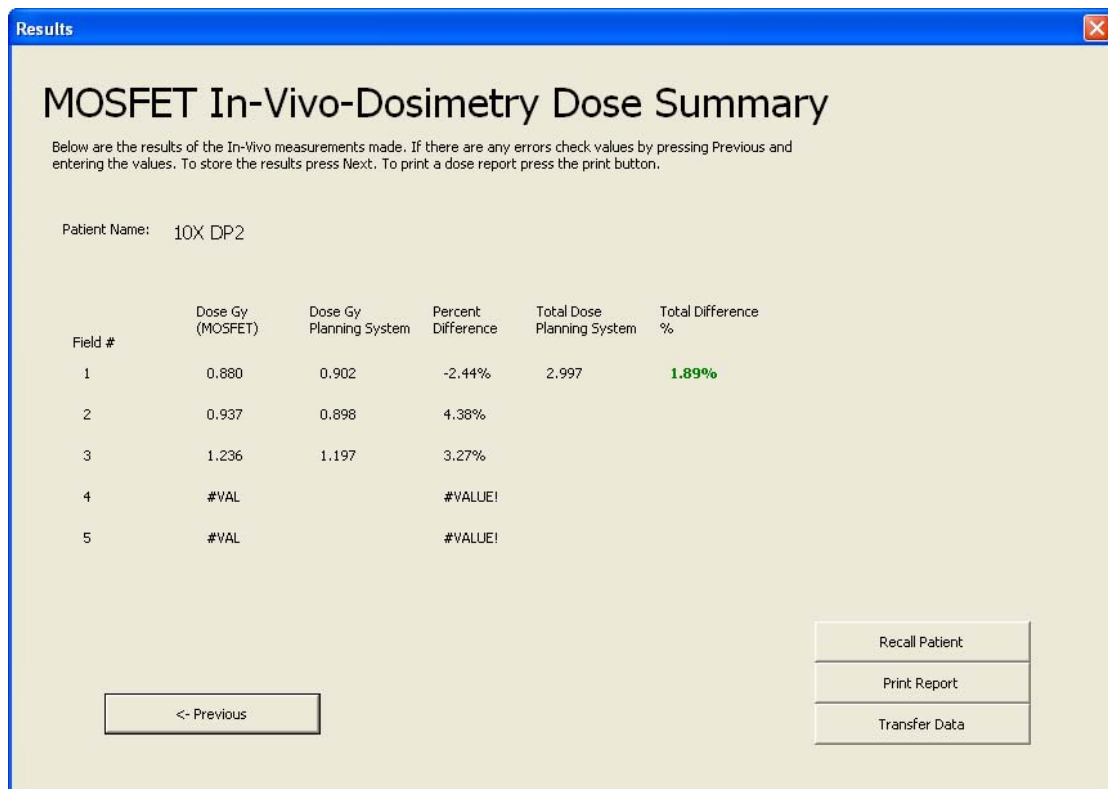


Figure 6-10: Spreadsheet form 2

From the above images the new interface has far less information and is far easier to use. Data is written with the use of text boxes and combo boxes. The tool also colours the total difference red if it is above the threshold percentage and green if it is below the threshold percentage. A message will also come up if the discrepancy on any individual field is greater than the threshold for the individual fields. As the data is stored creating a recall patient option is also possible.

A Commercial Software Package Used For MOSFET Measurements (Radcalc)

During the implementation of the MOSFET project a commercial MU checking system (Radcalc) was purchased. This MU checker had its own diode section which allowed for in-vivo dosimetry checks with diodes. This section was modified so that diode checks could be carried out with MOSFETs. As the implementation guidelines for the MOSFETs were the

same as those used for diodes (Leunens et al. 1994, Huyskens et al. 2001) it was easy to adapt Radcalc so that it could be used for entrance dose checks.

Results from lung/thorax measurements for the two separate systems were very similar, with both systems showing a systematic error of +2%, and a standard deviation of 3%. This is because both models use a full scatter medium and do not account for electron transport for low density materials.

Radcalc Vs. Spreadsheet MOSFET Measurement Results						
The results of IVD measurements in a Lung/Thorax phantom						
Plan	MOSFET Reading	Wedge	MOSFET Spreadsheet % difference	Average	Radcalc Diode % Difference	Average
dp1 6MV	78	0	-1.3%	-0.1%	-1.0%	-0.2%
dp1 6MV	107	60	-4.3%		-4.7%	
dp1 6MV	124	45	5.3%		5.0%	
dp2 6MV	95	15	0.4%	2.5%	0.4%	2.6%
dp2 6MV	160	30	3.0%		3.3%	
dp2 6MV	106	15	4.0%		4.0%	
dp3 6MV	282	0	3.5%	2.9%	3.2%	2.8%
dp3 6MV	177	15	5.9%		5.9%	
dp3 6MV	89	30	-0.7%		-0.7%	
dp3 6MV	183	0	3.5%	3.1%	3.7%	3.7%
dp3 6MV	98	15	-0.2%		0.5%	
dp3 6MV	204	30	5.9%		6.9%	
dp2 10MV	126	15	-1.3%	1.9%	-2.2%	0.8%
dp2 10MV	210	30	5.3%		5.0%	
dp2 10MV	189	30	1.5%		-0.4%	

Table 6-3: Comparison of Lung/Thorax phantom measurements in Radcalc and with spreadsheet

Spreadsheet	Radcalc
Average = 2.0%	1.9%
$\sigma = 3.1\%$	$\sigma = 3.3\%$
$2\sigma = 6.3\%$	$2\sigma = 6.7\%$

Table 6-4: Summary of Table 6-3

6.4 Implementation of Results in Radcalc

The correction factors measured before can be placed in Radcalc as the MOSFET IVD system follows the same principles as Diodes. As Radcalc can download SSD, effective depth, MLC information, as well as equivalent square field size directly from the planning system when checking treatment plans this information no longer needs to be placed manually into a spreadsheet.

Figure 6-11 shows the machine data entry page with the “Diode Data” tab selected. In this tab the information needed to implement diodes (or MOSFETs in this case) can be entered.

Machine Data Entry

Machine Info | Photon Energies | Jaw Settings | Gantry Angles | Collimator Angles | Couch Angles | Wedges | Attenuators | PDD Data | Sc Factors | Sp Factors | OAR Data | Diode Data | MLC Info

Machine: FS2 Energy Name: 6MV

Use Diode Correction Data?

Diode Calibration Value: 0.990

Attenuator Name: NONE Attenuator Correction:

Wedge Name: NONE Wedge Correction:

Field Size Correction Factors

Equiv Sq	CF _{FS}
3.00	0.992
5.00	0.994
10.00	1.000
20.00	1.011
30.00	1.022

SSD Correction Factors

SSD (cm)	CF _{SSD}
80.00	0.992
90.00	0.997
100.00	1.000
110.00	1.003
120.00	1.005

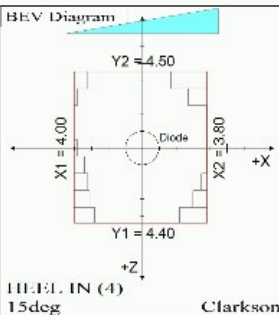
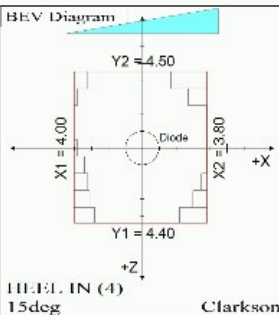
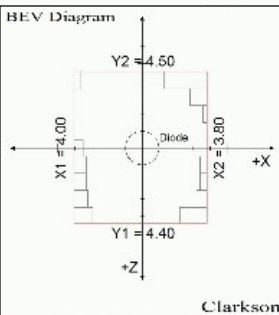
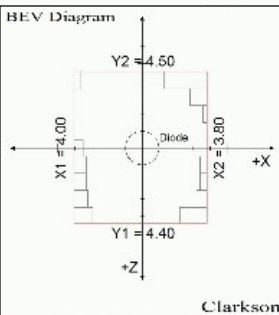
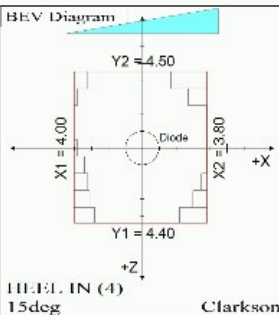
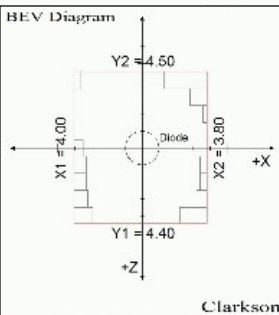
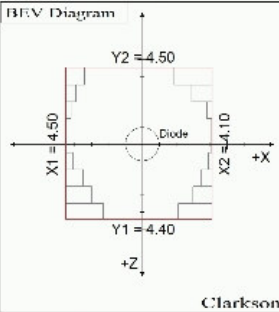
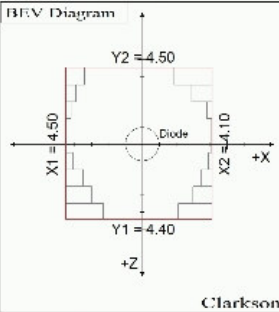
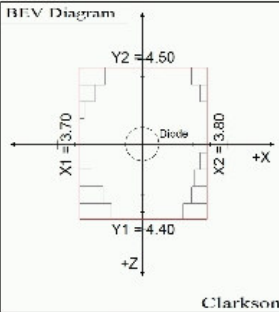
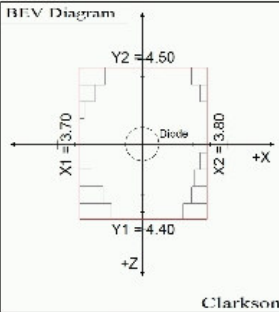
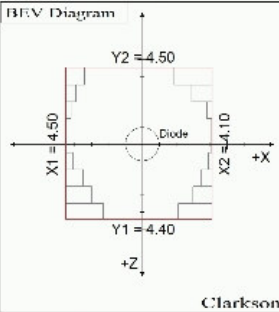
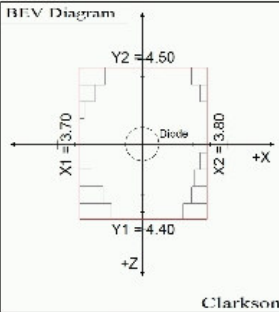
Save Machine Data Exit

Figure 6-11: Radcalc Diode Commissioning Page

Radcalc also prints out a copy of the results of measurements with the downloaded field shape and the MOSFET position (Figure 6-12). The MOSFET position can also be set by moving it on the plan. By default the MOSFET is placed at the dose point (not the centre of the field). The dose point is often the isocentre or close to the isocentre for high energy photon treatment planning.

**Photon
TLD/Diode Calc Sheet**

Patient Name: **Pat. ID#:**
Comment: _____

<table border="1" style="width: 100%; border-collapse: collapse;"> <tr> <td style="width: 30%;"><u>Field Description</u> rapo</td> <td>Accelerator: FS2 Energy Name: 10MV Gantry: 240</td> </tr> <tr> <td>Field ID: 1.1 Sc: 0.987 ISF: 1.467</td> <td>Collim.: 0 Couch: 0 SSD: 80.82 Depth: 2.50 Diode SSD: 80.82 At Skin, X/Z: 0.0/0.0</td> </tr> <tr> <td>Primary x OAF: 0.980 Scatter: 0.028</td> <td>Eq. Sq.: 8.31 Blk Eq Sq.: -6.15</td> </tr> <tr> <td>Cal. Factor: 0.00740 Dose Per MU: 0.01080 Delivered MU: 52 Dmax Dose: 0.562 Measured Dose: --- Percent Diff: -----</td> <td>  </td> </tr> </table>	<u>Field Description</u> rapo	Accelerator: FS2 Energy Name: 10MV Gantry: 240	Field ID: 1.1 Sc: 0.987 ISF: 1.467	Collim.: 0 Couch: 0 SSD: 80.82 Depth: 2.50 Diode SSD: 80.82 At Skin, X/Z: 0.0/0.0	Primary x OAF: 0.980 Scatter: 0.028	Eq. Sq.: 8.31 Blk Eq Sq.: -6.15	Cal. Factor: 0.00740 Dose Per MU: 0.01080 Delivered MU: 52 Dmax Dose: 0.562 Measured Dose: --- Percent Diff: -----		<table border="1" style="width: 100%; border-collapse: collapse;"> <tr> <td style="width: 30%;"><u>Field Description</u> rlat</td> <td>Accelerator: FS2 Energy Name: 10MV Gantry: 270</td> </tr> <tr> <td>Field ID: 1.2 Sc: 0.988 ISF: 1.455</td> <td>Collim.: 0 Couch: 0 SSD: 81.19 Depth: 2.50 Diode SSD: 81.19 At Skin, X/Z: 0.0/0.0</td> </tr> <tr> <td>Primary x OAF: 1.325 Scatter: 0.054</td> <td>Eq. Sq.: 8.31 Blk Eq Sq.: -6.21</td> </tr> <tr> <td>Cal. Factor: 0.00740 Dose Per MU: 0.01467 Delivered MU: 79 Dmax Dose: 1.159 Measured Dose: 1.159 Percent Diff: 0.1%</td> <td>  </td> </tr> </table>	<u>Field Description</u> rlat	Accelerator: FS2 Energy Name: 10MV Gantry: 270	Field ID: 1.2 Sc: 0.988 ISF: 1.455	Collim.: 0 Couch: 0 SSD: 81.19 Depth: 2.50 Diode SSD: 81.19 At Skin, X/Z: 0.0/0.0	Primary x OAF: 1.325 Scatter: 0.054	Eq. Sq.: 8.31 Blk Eq Sq.: -6.21	Cal. Factor: 0.00740 Dose Per MU: 0.01467 Delivered MU: 79 Dmax Dose: 1.159 Measured Dose: 1.159 Percent Diff: 0.1%	
<u>Field Description</u> rapo	Accelerator: FS2 Energy Name: 10MV Gantry: 240																
Field ID: 1.1 Sc: 0.987 ISF: 1.467	Collim.: 0 Couch: 0 SSD: 80.82 Depth: 2.50 Diode SSD: 80.82 At Skin, X/Z: 0.0/0.0																
Primary x OAF: 0.980 Scatter: 0.028	Eq. Sq.: 8.31 Blk Eq Sq.: -6.15																
Cal. Factor: 0.00740 Dose Per MU: 0.01080 Delivered MU: 52 Dmax Dose: 0.562 Measured Dose: --- Percent Diff: -----																	
<u>Field Description</u> rlat	Accelerator: FS2 Energy Name: 10MV Gantry: 270																
Field ID: 1.2 Sc: 0.988 ISF: 1.455	Collim.: 0 Couch: 0 SSD: 81.19 Depth: 2.50 Diode SSD: 81.19 At Skin, X/Z: 0.0/0.0																
Primary x OAF: 1.325 Scatter: 0.054	Eq. Sq.: 8.31 Blk Eq Sq.: -6.21																
Cal. Factor: 0.00740 Dose Per MU: 0.01467 Delivered MU: 79 Dmax Dose: 1.159 Measured Dose: 1.159 Percent Diff: 0.1%																	
<table border="1" style="width: 100%; border-collapse: collapse;"> <tr> <td style="width: 30%;"><u>Field Description</u> rapo</td> <td>Accelerator: FS2 Energy Name: 10MV Gantry: 305</td> </tr> <tr> <td>Field ID: 1.3 Sc: 0.990 ISF: 1.362</td> <td>Collim.: 0 Couch: 0 SSD: 84.27 Depth: 2.50 Diode SSD: 84.27 At Skin, X/Z: 0.0/0.0</td> </tr> <tr> <td>Primary x OAF: 1.318 Scatter: 0.056</td> <td>Eq. Sq.: 8.75 Blk Eq Sq.: -6.65</td> </tr> <tr> <td>Cal. Factor: 0.00740 Dose Per MU: 0.01371 Delivered MU: 20 Dmax Dose: 0.274 Measured Dose: --- Percent Diff: -----</td> <td>  </td> </tr> </table>	<u>Field Description</u> rapo	Accelerator: FS2 Energy Name: 10MV Gantry: 305	Field ID: 1.3 Sc: 0.990 ISF: 1.362	Collim.: 0 Couch: 0 SSD: 84.27 Depth: 2.50 Diode SSD: 84.27 At Skin, X/Z: 0.0/0.0	Primary x OAF: 1.318 Scatter: 0.056	Eq. Sq.: 8.75 Blk Eq Sq.: -6.65	Cal. Factor: 0.00740 Dose Per MU: 0.01371 Delivered MU: 20 Dmax Dose: 0.274 Measured Dose: --- Percent Diff: -----		<table border="1" style="width: 100%; border-collapse: collapse;"> <tr> <td style="width: 30%;"><u>Field Description</u> ap</td> <td>Accelerator: FS2 Energy Name: 10MV Gantry: 0</td> </tr> <tr> <td>Field ID: 1.4 Sc: 0.986 ISF: 1.254</td> <td>Collim.: 0 Couch: 0 SSD: 88.23 Depth: 2.50 Diode SSD: 88.23 At Skin, X/Z: 0.0/0.0</td> </tr> <tr> <td>Primary x OAF: 1.309 Scatter: 0.055</td> <td>Eq. Sq.: 8.14 Blk Eq Sq.: -6.54</td> </tr> <tr> <td>Cal. Factor: 0.00740 Dose Per MU: 0.01248 Delivered MU: 30 Dmax Dose: 0.374 Measured Dose: 0.361 Percent Diff: -3.6%</td> <td>  </td> </tr> </table>	<u>Field Description</u> ap	Accelerator: FS2 Energy Name: 10MV Gantry: 0	Field ID: 1.4 Sc: 0.986 ISF: 1.254	Collim.: 0 Couch: 0 SSD: 88.23 Depth: 2.50 Diode SSD: 88.23 At Skin, X/Z: 0.0/0.0	Primary x OAF: 1.309 Scatter: 0.055	Eq. Sq.: 8.14 Blk Eq Sq.: -6.54	Cal. Factor: 0.00740 Dose Per MU: 0.01248 Delivered MU: 30 Dmax Dose: 0.374 Measured Dose: 0.361 Percent Diff: -3.6%	
<u>Field Description</u> rapo	Accelerator: FS2 Energy Name: 10MV Gantry: 305																
Field ID: 1.3 Sc: 0.990 ISF: 1.362	Collim.: 0 Couch: 0 SSD: 84.27 Depth: 2.50 Diode SSD: 84.27 At Skin, X/Z: 0.0/0.0																
Primary x OAF: 1.318 Scatter: 0.056	Eq. Sq.: 8.75 Blk Eq Sq.: -6.65																
Cal. Factor: 0.00740 Dose Per MU: 0.01371 Delivered MU: 20 Dmax Dose: 0.274 Measured Dose: --- Percent Diff: -----																	
<u>Field Description</u> ap	Accelerator: FS2 Energy Name: 10MV Gantry: 0																
Field ID: 1.4 Sc: 0.986 ISF: 1.254	Collim.: 0 Couch: 0 SSD: 88.23 Depth: 2.50 Diode SSD: 88.23 At Skin, X/Z: 0.0/0.0																
Primary x OAF: 1.309 Scatter: 0.055	Eq. Sq.: 8.14 Blk Eq Sq.: -6.54																
Cal. Factor: 0.00740 Dose Per MU: 0.01248 Delivered MU: 30 Dmax Dose: 0.374 Measured Dose: 0.361 Percent Diff: -3.6%																	

Calculated By: Physics Physics 2006/3/20

Checked By: _____

Physician Signature: _____

Adelaide Radiotherapy - FPH

2006/3/20 08:56:41
RadCalc v4.3

Figure 6-12: Radcalc Printout

This can be used as a tool for checking the MLC field shape and identifying the correct field for measurement during the patient measurement. As Radcalc compares well with the spreadsheet there is no advantage gained from using the spreadsheet, and future spreadsheets

will not need to be made for each new commissioned linear accelerator, as the PDD's, wedges, and other information will be entered into Radcalc and checked as its primary function is an MU checker.

7 Clinical Results

7.1 Introduction

After the commissioning of the in-vivo dosimetry system using MOSFETs clinical trials of several radiotherapy treatment techniques were carried out. A total sample set of 23 patients was taken, with the majority of tests being prostate/pelvic treatments and breast treatments. Other treatments tested were lung/chest and head and neck. At least two fields were tested per treatment, with 3 fields tested for prostate patients. For tangential breast treatments both fields were measured.

7.2 Clinical Use

7.2.1 Patient Setup

The MOSFET was secured inside the build up cap with tape. Thus ensuring that the MOSFET was always in the same physical position inside the build up cap. The centre of the build up cap was marked. The build up cap was placed in the centre of the light field for all fields that were tested. Some treatments required measuring Posterior-Anterior (PA) fields. In these cases the beam passes through the couch. The SSD to the surface of the couch was therefore taken and the MOSFET placed on the posterior side of the treatment couch (for patient comfort). MOSFET measurements were performed by RT's without them knowing what the expected results should be.

7.2.2 RT Training

RT training was minimal and staff found it easy to set up the MOSFET. A single demonstration of a measurement was necessary before the first clinical measurements. After this demonstration the measurements were successfully carried out. A result sheet was made which required entering the treatment energy, patient name or UR number, field number /

description, MOSFET reading and SSD to the measurement surface. Time required to enter this information in the form was a factor which effected treatment time.

7.2.3 MOSFET Measurement process and time

The MOSFET was zeroed before each measurement and placed on the surface of the patient. The patient was then irradiated and the reading was taken. The time between irradiation and reading was less than 3 minutes to minimize fade (chapter 3).

Time savings are an important factor in a busy institution. The total time required to make the measurements was of the order of a few minutes, but even though a few minutes seems like a small amount of time radiation therapists found that they ran behind schedule after making measurements on three or more patients. Measuring every field on each patient would have significantly increased the treatment time per patient and therefore reduced the number of patients that could be treated per day.

7.3 Clinical Results

A total of 23 patients were treated. Below is a tabulation of treatment delivery types.

Treatment	Number of Patients	Number of fields
Breast	11	22
Prostate/Pelvis	8	24
Lung	3	6
Head and Neck	1	2
Total	23	54

Table 7-1: Treatment Summary

7.3.1 Breasts

Breast results were normally distributed around a mean, with an average of 1.8% and a standard deviation of 2.7%. This is similar to results found in other institutions with diodes, and is not worse than institutions implementing large scale diode in-vivo dosimetry (SD= 3.1 and 3.5% for Leuven and Milan respectively). There was no decrease in discrepancy with an

increase in dose implying that the MOSFET measurement uncertainty in the clinical range for breast treatments does not play a significant role in measurement accuracy.

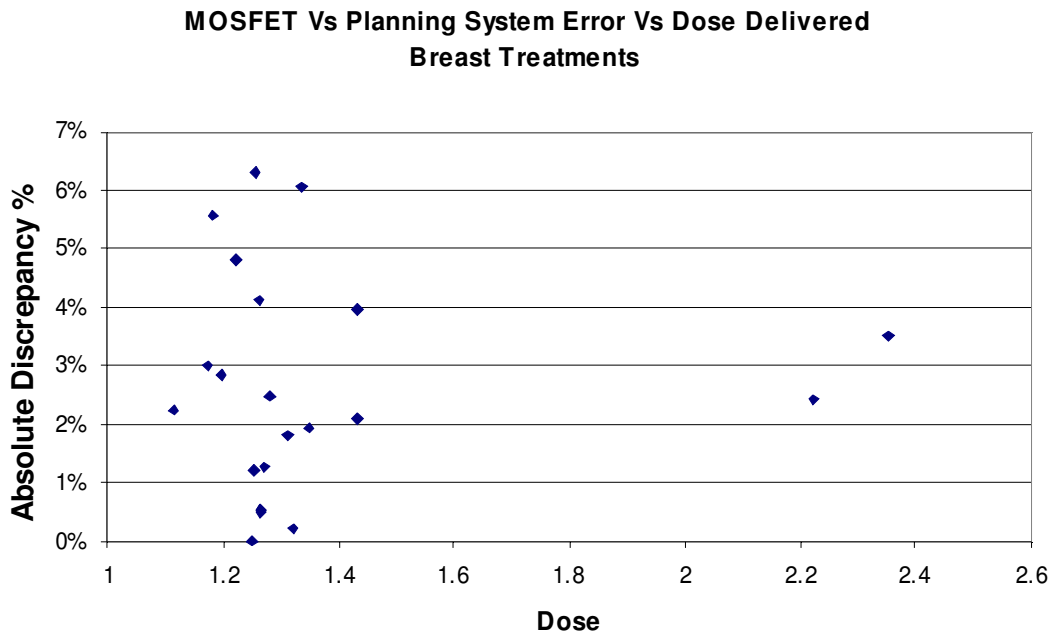


Figure 7-1: Breast Measurements

7.3.2 Prostates and Pelvis

Prostate/Pelvis treatments had results distributed around a mean, with an average of 1.3% and a standard deviation of 2.9%. This is similar to results found in other institutions (SD = 2.7% and 3.0% for Leuven and Milan respectively, Table 7-4), but worse than some diode studies might suggest (1.5% for Lanson et al. 1999 and 1.2% for Meijer et al. 2001). Absolute measurement discrepancy did not decrease with significantly increase in dose ($r=-0.269$, $P=0.225$), (Figure 7-2). This is probably because the smallest dose measured on the surface is 0.32 Gy. For a dose this small MOSFETs would have a larger standard deviation. If all 3 fields are considered per treatment the mean is 1%, and standard deviation 1.9%. This is comparable to the 1.5% S.D. reported by other studies (Lanson et al. 1999).

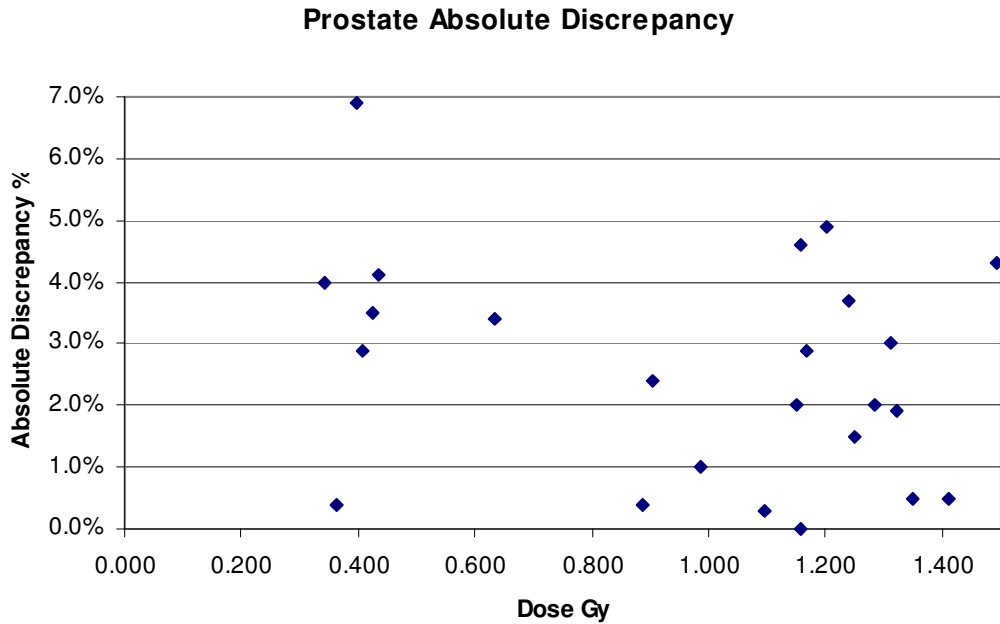


Figure 7-2: Prostate Measurements

7.3.3 Head and Neck, Lung

As there were too few head and neck and lung patients to compare individually they were all placed in a group. These techniques are complex and require excellent modelling from the planning system as well as placement of MOSFETs by RTs. The entrance dose for the fields was from 0.80 Gy to 2.10 Gy. Trays as well as wedges were used for many of the fields. The mean of all measurements was 0.8% with a standard deviation of 1.2%. This discrepancy is better than expected. The discrepancy also seemed to increase with dose, but with such a small sample size the error in this relationship is large.

7.3.4 All Results

All the results were distributed around a mean, with a mean of 1.3% and a standard deviation of 2.6% (Figure 7-4). The results were slightly negatively skewed with a skewness of -0.39 ± 0.33 (note tail end). The distribution of results was normal, with a kurtosis of 0.34 ± 0.67 . This is similar to the MOSFET commissioning results (Chapter 3). The average dose delivered per field was 1.167 Gy. The standard deviation of all measurements was 2.6%, slightly larger than the standard deviation of the MOSFET at that dose, showing that the

precision of measurements for MOSFETs could be a limiting factor in entrance dose in-vivo dosimetry measurements. As measurement means and standard deviations for diodes are similar to MOSFETs one can also say that the random error associated with patient setup is the limiting factor for entrance dose in-vivo dosimetry, and that the MOSFET precision, being of the same order of magnitude, does not increase the error associated with a measurement.

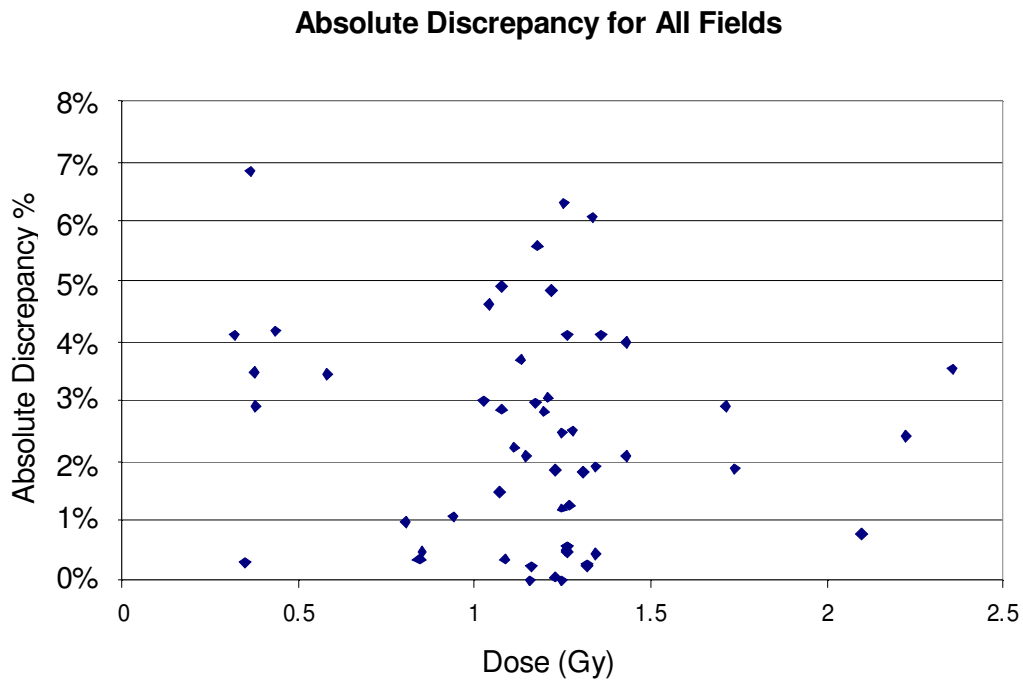


Figure 7-3: All Measurements

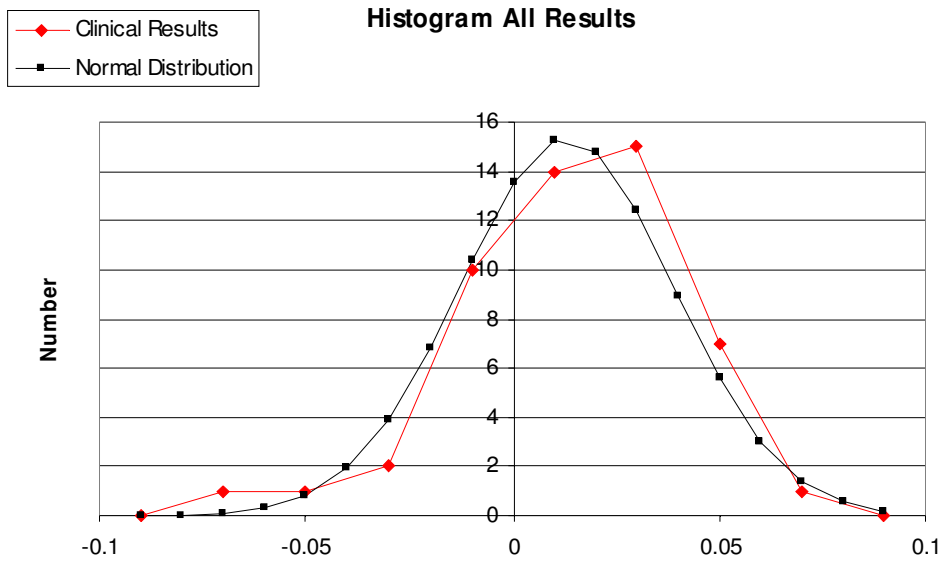


Figure 7-4: Histogram of results for all measurements

7.3.5 All Results without Breasts

Due to the increased discrepancies associated with breast treatments some institutions look at all treatments except breast treatments (Huyskens et al. 2001). With MOSFETs, when all treatments except breast treatments are considered the discrepancy/dose relationship shows an increase in the standard deviation of dose measurements with a decrease in dose (Figure 7-5).

This is similar to the commissioning results. If the theoretical standard deviation of

$\sigma = \frac{1.2836x^{-0.6485}}{3}$ is plotted against the results the graph shows that there is a good fit

between the theoretical standard deviation and the mean absolute discrepancy (Figure 7-5). If the results are broken into three groups (0.3-0.6 Gy, 0.8-1.4 Gy, 1.7-1.8 Gy) the standard deviations of the means fall along the theoretical standard deviation (Figure 7-5). This shows that the dose measured with the MOSFET is a factor affecting the accuracy of the entrance dose measurement. The uncertainty can be reduced by increasing the bias voltage across the MOSFET, but as the means and standard deviations are similar to other institutions there is little to gain by increasing the bias voltage and reducing the life expectancy of the MOSFET.

Dose/Discrepancy Relationship: All Fields Without Breasts

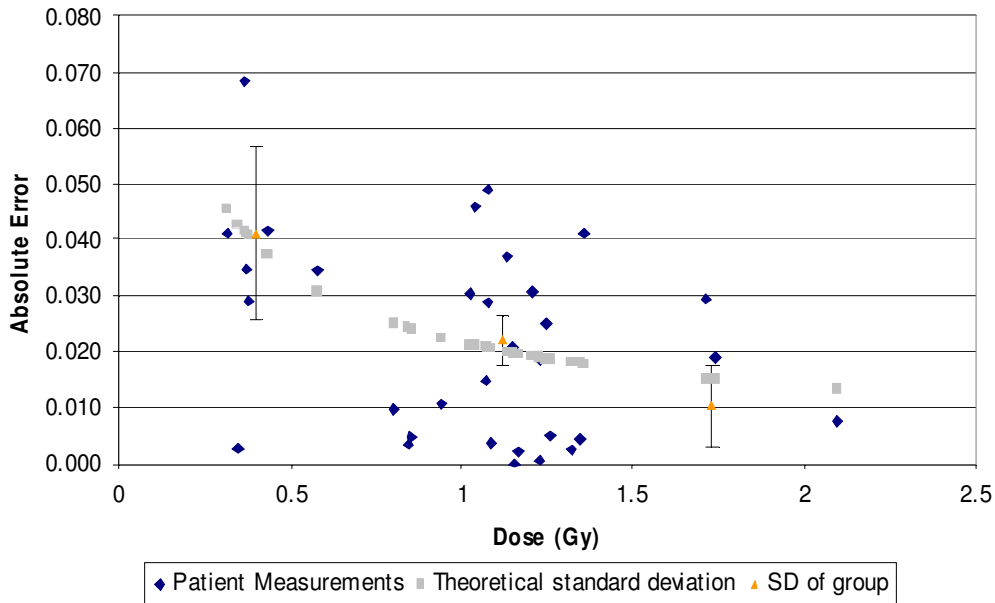


Figure 7-5: Absolute Discrepancy, all treatments excluding breast results

7.3.6 Error analysis

The standard deviation of a group of measurements in perfect phantom conditions should be less than the standard deviation of a group of measurements made on a patient. This is because of the added uncertainty involved in the patient positioning and detector placement. The standard deviation of a group of measurements for MOSFETs decreases with increasing dose and the 3σ uncertainty of a measurement of dose can be approximated with the equation

$$3\sigma = 1.283x^{-0.6485} \quad (7.1)$$

, where x is the dose in cGy.

Taking the MOSFET uncertainty associated with a measurement as the standard deviation from equation 7.1, the error that can not be contributed to the MOSFET reading can be separated using

$$\sigma_T = \sqrt{\sigma_M^2 + \sigma_S^2} \quad (7.2),$$

- σ_S is the contribution of error from setup and other factors.

- $\sigma_M = \frac{1.283x^{-0.6485}}{3}$ is the contribution to the error from the MOSFET
- σ_T is the total error for the reading
- x is the dose in cGy

7.3.6.1 Prostates

For prostates the readings were placed into two groups (Figure 7-2). The first group being fields of 0.8 Gy and above, and the second being the rest of the fields. The standard deviation of the average dose for the group was taken and compared to the standard deviation of the MOSFET (Table 7-2). The error associated with the treatment can therefore be checked and is constant at about 1.4%.

Fields	Average Dose	N	σ_T	Mean	σ_M	σ_S
>0.8 Gy	1.141	16	2.5%	1.26%	1.98%	1.5%
<0.8 Gy	0.404	7	4.1%	1.34%	3.88%	1.3%

Table 7-2: Patient Setup Error Summary for Prostates

7.3.6.2 Breasts

For breast treatments there was no distinct entrance dose regions that could be analysed. One treatment had two fields of 2 Gy, while the rest had two fields of about 1 Gy (Figure 7-1). The fields were averaged to get an indication of the typical dose delivered and therefore the typical error expected. The standard deviation of these was taken based on equation 7.1 using the average dose. This was compared to the standard deviation of the MOSFET measurements. The error in patient setup, or delivery is therefore about 2.0% (Table 7-3). This is greater than that found for prostate treatments. There are several reasons for this.

- The detector is hard to place as fields are tangential on a surface of high obliquity.
- The patient chest surface position is not constant as patient breathing will cause the detector to move in the direction of the wedge in wedged fields.

Average Dose	N	σ_T	Mean	σ_M	σ_S
1.364	22	2.7%	1.84%	1.77%	2.02%

Table 7-3: Patient Setup Error Summary for Breasts

7.3.6.3 Head and Neck

As only one patient was tested there was not enough information to analyse.

7.3.6.4 Lung

Only three patients (6 fields) were tested. The mean was 1.1%, with a standard deviation of 1.1%. The average dose was 1.47 Gy, but the fields were unevenly weighted with a spread of doses. Once again the small sample size offsets the error associated with measurement and if the sample size increased one would expect the standard deviation to increase.

7.3.7 Typical results for different techniques.

As in-vivo dosimetry for high energy photons in external beam radiation therapy is well established, with many papers and several booklets written on the topic. Results tend to vary from one centre to the next, but large studies in Europe, where in-vivo dosimetry is a regulatory requirement, will give a good indication of which results to expect.

The results depend on the field type and anatomical position. They are therefore often studied separately. Typically breast and head and neck treatments give poor results (AAPM 87 p 82. 2005, Fiorino 2000).

Paper/book	Technique	Mean	σ_T	Comments	
Quality assurance by systematic in vivo dosimetry: results on a large cohort of patients, Fiorino C et. al, Radiotherapy and Oncology, 2000	All	0.3%	3.0%		
	Tangential and breast	1.0%	3-4%		
	Vertebra	1.0%	2.1%		
	Brain	-0.7%	2.6%		
Implementation of an in vivo diode dosimetry program and changes in diode characteristics over a 4-year clinical history, Jursinic, Med Phys, 2001	All	0.5%	1.5%	If results were out the measurement was performed on a solid water phantom	
Accurate in vivo dosimetry of a randomized trial of prostate cancer irradiation, Meijer et al., Int Journ Rad Oncol Biol Physics, 2001	Prostate	0.9%	1.2%		
	ESTRO booklet 5, ESTRO, (Huyskens et al. 2001) Leuven	All excluding breast	0.31%		2.7%
	Breast mastectomy	3.5%	3.1%		
ESTRO booklet 5, ESTRO, (Huyskens et al. 2001) Milan	Breast lumpectomy	3.12%	4.7%		
	All	0.2%	3.1%		
	Breast	0.3%	3.5%		
	Brain	-1.0%	2.8%		
	Neck	1.1%	2.8%		
Tumour dose estimation using automated TLD techniques, Ferguson et al., Acta Oncologica, 1998.	Pelvis	0.5%	3.0%		
	All	-0.15%	3.0%		
	Pelvis	-0.83%	2.8%		
Breast	0.26%	2.9%			

Table 7-4: Institution means and Standard Deviations for external beam radiotherapy IVD

Paper/book	Technique	Mean	σ_T	Comments
Entrance and exit dose measurements with semiconductors and thermoluminescent dosimeters: a comparison of methods and in vivo results. Lancol et al., Radiotherapy and Oncology, 1996	All (diodes)	1%	2.8%	
	All (TLDs)	1.3%	4.1%	
Feasible measurement errors when undertaking in vivo dosimetry during external beam radiotherapy of the breast, Herbert C et al., Medical Dosimetry, 2003	Tangential Breast	4.3%	4.0%	Main source of error is diode positioning error
Quality assurance in radiation oncology. A study of feasibility and impact on action levels of an in vivo dosimetry program during breast cancer irradiation, Cozzi and Cozzi, Radiotherapy and Oncology 1998	Breast (corrections)	-1.9%	2.4%	
	Breast (no corrections)	-1.2%	2.7%	
In vivo dosimetry during conformal radiotherapy. Requirements for and Findings of a routine procedure, Lanson et al., Radiotherapy and Oncology 1999	Prostate	1.2%	1.5%	(total treatment dose)
	Parotid	1.3%	2.0%	(total treatment dose)
The implementation of in vivo dosimetry in a small radiotherapy department Radiotherapy and Oncology 1998, Voordeckers M et al.	All	-1.3%	4%	
Selective in vivo dosimetry in radiotherapy using P-type semiconductor diodes: a reliable quality assurance procedure., Howlett S et al., Medical Dosimetry, 1999	All	0.5%	2.2%	
	Breast/chest	0.5%	2.3%/3.3%	
	Prostate	0.1%	1.7%	

Table 7-5: Institution means and Standard Deviations for external beam radiotherapy IVD

7.4 Conclusion

Clinical results from MOSFETs for in-vivo dosimetry are comparable to results from TLD's and diodes, which are the two currently accepted techniques at present. For simple techniques such as prostate fields the spread of results (standard deviation) is limited by the minimum spread for the MOSFET (Figure 7-5). For complex techniques such as breasts, the limiting factor in the measurement is the technique as there is no decrease in error with increasing dose (Figure 7-1). All fields were within the required tolerances set in Chapter 5. These tolerances are acceptable and similar to the limits set by other institutions (Chapter 5).

8 Conclusion

MOSFETs can be used for external beam radiotherapy in-vivo dosimetry. With the use of a custom made build up cap and measurements of the following dependencies:

- field size correction factor
- wedge correction factor
- angular dependence
- tray correction factor
- SSD correction factor
- Entrance dose calibration factor

MOSFETs can be used to accurately determine and test doses given to patients as part of a regular QA programme, or as part of quality assurance when testing new techniques. Results are similar to other large scale studies, but the dose dependence of the standard deviation of measurements for MOSFETs is a limiting factor at low doses (Chapter 7).

8.1 Considerations

8.1.1 Time

In-vivo dosimetry is a time consuming process. When clinical trials were being performed the linear accelerators ran behind schedule after 4 to 5 patients. This is a significant factor as the patient's were allowed extra time for the in-vivo dosimetry and only some of the fields were tested. To test all fields would have taken longer. For a busy department the time spent checking entrance dose is significant and would affect the amount of patients treated daily. As the test only needs to be carried out at the start of treatment to detect errors though, this is acceptable.

8.1.2 Error and Precision

MOSFETs have an interesting dose-error relationship, showing a non-stochastic relationship between dose received and the measurement precision. They have small absolute error though, with few correction factors needed for raw dose measurements.

8.1.3 MOSFET Robustness

MOSFETs are not as robust as other detectors, but as they are only used for a while before replacement (20 000 mV), breakage is not as important as it is for diodes. During the commissioning and characterization of the MOSFETs three MOSFETs were damaged. The main way the MOSFET was damaged was by pressing it too hard. This happened with wax for the angular dependence measurements. Care should therefore be taken not to press the bulbous end of the MOSFET too hard as this could lead to MOSFET failure.

8.1.4 Long Term Stability

Although MOSFETs can be kept for a long time without any significant changes in reproducibility they become unreliable if left attached to the bias for a long period of time (approximately six months) without being used. It is advisable that the MOSFETs be left unplugged from the bias if not in use for a long period of time.

8.2 Future Project Considerations

This project is complete for photons, but electrons could be investigated for surface dosimetry. Electron in-vivo dosimetry could also be investigated and implemented. As the stopping power ratio for silicon is similar to that of water and tissue for high energy electrons the relative dose for electrons requires less investigation than for photons. MOSFETs have a distinct advantage over diodes for electron in-vivo dosimetry as diodes result in a dose

shadow that is too large for in-vivo dosimetry when placed on the surface (Gibson and Langmack, 2004).

MOSFET measurements have also shown that MOSFETs have few dependencies in high energy photon fields. Their small size and versatility would make them an excellent choice of detector for anthropomorphic phantom measurements. They can also be used in conjunction with film in IMRT QA. They are tissue equivalent in the build up region for photons. As they can be surgically placed during treatment they can be used in-situ during treatment to get a true tumor dose.

9 References

AAPM Report 87, “*DIODE IN VIVO DOSIMETRY FOR PATIENTS RECEIVING EXTERNAL BEAM RADIATION THERAPY*”, Feb 2005, Published for the American Association of Physicists in Medicine, Medical Physics Publishing

AAPM TG 40., 1994, “*AAPM report no. 46 Comprehensive QA for Radiation Oncology*”. Published for the American Association of Physicists in Medicine by the American Institute of Physics, April

Andreo, P Evans, M.D.C Hendry, J.H. Horton, J.L. Izewska, J. Mijnheer, B.J. Mills, J.A. Olivares, M. Ortiz López, P Parker, W Patrocínio, H Podgorsak, E.B. Podgorsak, M.B Rajan, G. Seuntjens, J.P Shortt, K.R. Strydom, W. Suntharalingam, N. Thwaites, D.I. Tolli, H., 2005, “*Review of Radiation Oncology Physics: A Handbook for Teachers and Students*”, INTERNATIONAL ATOMIC ENERGY AGENCY, VIENNA

Attix F H, 1986, “*Introduction to Radiological Physics and Radiation Dosimetry*” John Wiley and Sons, Inc ISBN 0-471-01146-0

Benson C, Price RA, Silvie J, Jaksic A, Joyce MJ., 2004, ‘Radiation-induced statistical uncertainty in the threshold voltage measurement of MOSFET dosimeters.’, *Phys Med Biol.* 21;49(14):3145-59.

Brauer-Krisch E, Bravin A, Lerch M, Rosenfeld A, Stepanek J, Di Michiel M, Laissue JA., 2003 ‘MOSFET dosimetry for microbeam radiation therapy at the European Synchrotron Radiation Facility.’, *Med Phys.* Apr;30(4):583-9

Butson MJ, Rozenfeld A, Mathur JN, Carolan M, Wong TP, Metcalfe PE, 1996, ‘A new radiotherapy surface dose detector:the MOSFET.’, *Med Phys.* May;23(5):655-8.

Chuang CF, Verhey LJ, Xia P., 2002, ‘Investigation of the use of MOSFET for clinical IMRT dosimetric verification.’, *Med Phys.* Jun;29(6):1109-15.

Cheung T, Butson MJ, Yu PK., 2004, ‘Effects of temperature variation on MOSFET dosimetry.’, *Phys Med Biol.* Jul 7;49(13):N191-6.

Cozzi L, Cozzi A F, 1998, “Quality assurance in radiation oncology. A study of feasibility and impact on action levels of an in vivo dosimetry program during breast cancer irradiation”, *Radiotherapy and Oncology* 47, p 29–36

Dobbs J, Barrett A, Ash D, 1999, “*Practical Radiotherapy Planning*”, Third Edition, Oxford University Press, Arnold

Edwards CR, Green S, Palethorpe JE, Mountford PJ., 1997, ‘The response of a MOSFET, p-type semiconductor and LiF TLD to quasi-monoenergetic x-rays.’, *Phys Med Biol.* Dec;42(12):2383-91.

Ferguson HM, Lambert GD, Gustard D, Harrison RM., 1998, “Tumour dose estimation using automated TLD techniques.”, *Acta Oncologica,* ;37(5):479-84.

- Francescon P, Cora S, Cavedon C, Scalchi P, Reccanello S, Colombo F., 1998, 'Use of a new type of radiochromic film, a new parallel-plate micro-chamber, MOSFETs, and TLD 800 microcubes in the dosimetry of small beams.', *Med Phys.* Apr;25(4):503-11.
- Fiorino C, Corletto D, Mangili P, Broggi S, Bonini A, Cattaneo GM, Parisi R, Rosso A, Signorotto P, Villa E, Calandrino R., 2000, 'Quality assurance by systematic in vivo dosimetry: results on a large cohort of patients.', *Radiother Oncol.* Jul;56(1):85-95.
- Gibson, BJ, Langmack, KA, 2004, "AN ASSESSMENT OF THE CHARACTERISTICS OF N-TYPE DIODES FOR USE IN ELECTRON BEAM RADIOTHERAPY", *Medical Dosimetry*, Vol 29 No. 3, 161-165,
- Gladstone DJ, Chin LM., 1991, 'Automated data collection and analysis system for MOSFET radiation detectors.', *Med Phys.* May-Jun;18(3):542-8.
- Grusell E and Rikner G., 1986, 'Evaluation of temperature effects in p-type Si semiconductor detectors.', *Phys Med Biol.*
- Herbert CE, Ebert MA, Joseph DJ., 2003, "Feasible measurement errors when undertaking in vivo dosimetry during external beam radiotherapy of the breast.", *Medical Dosimetry*, Spring;28(1):45-8.
- Holms-Siedle A, 1974, "The Space Charge Dosimeter", *Nucl. Inst. Meth.* 169-179, cited in Gladstone and Chin 1990
- Hosseini-Pooya M, Jafarizadeh M., 2004, 'Effect of reader and oven annealing on the glow curve structure and fading of aLiF:Mg,Cu,P TL dosimeter.', *J Radiol Prot.*, Jun;24(2):173-8.
- Howlett S, Duggan L, Bazley S, Kron T. 'Selective in vivo dosimetry in radiotherapy using P-type semiconductor diodes: a reliable quality assurance procedure.' *Med Dosim.* 1999 Spring;24(1):53-6.
- Huyskens DP, Bogaerts R, Verstraete J, Lööf M, Nyström H, Fiorino C, Broggi S, Jornet N, Ribas M, Thwaites DI, 2001, '*Practical guidelines for the implementation of in vivo dosimetry with diodes in external radiotherapy with photon beams (entrance dose)*', First edition ESTRO , ISBN 90-804532-3
- IAEA TRS 381, 1997, ANDREO P.,ALMOND P.R. ,MATTSSON O., NAHUM A.E., ROOS M., (IAEA TRS 381), Dec 1997 , "*THE USE OF PLANE-PARALLEL IONIZATION CHAMBERS IN HIGH-ENERGY ELECTRON AND PHOTON BEAMS. AN INTERNATIONAL CODE OF PRACTICE FOR DOSIMETRY*", International Atomic Energy Agency,
- IAEA: TRS 398, 2000, "*Absorbed Dose Determination in External Beam Radiotherapy An International Code of Practice for Dosimetry Based on Standards of Absorbed Dose to Water*" , International Atomic Energy Agency, Vienna
- ICRU (1976), 1976, "*Determination of absorbed dose in a patient irradiated by beams of x- or gamma-rays in radiotherapy procedures,*" ICRU Rep. 24, International -Commission on Radiation Units and Measurement, Bethesda,

MD. 1976

IPEM Report 81, 1999, “*Physics Aspects of Quality Control in Radiotherapy*” The Institute of Physics and Engineering in Medicine, Fairmount House, 230 Tadcaster Road, ISBN 0 904181 91 X

Jornet N, Carrasco P, Jurado D, Ruiz A, Eudaldo T, Ribas M., 2004, ‘Comparison study of MOSFET detectors and diodes for entrance in vivo dosimetry in 18 MV x-ray beams.’, *Med Phys.* Sep;31(9):2534-42.

Jurisnic P A, 2001, “Implementation of an in vivo diode dosimetry program”, *Medical Physics*, Aug;28(8):1718-26.

Kirby TH, Hanson WF, Johnston DA., 1992, ‘Uncertainty analysis of absorbed dose calculations from thermoluminescence dosimeters.’, *Med Phys.* Nov-Dec;19(6):1427-33.

Khan FM, Sewchand W, Lee J, Williamson JF, 1980 “Revision of tissue-maximum ratio concepts for cobalt 60 and higher energy x-ray beams”, *Med Phys.* 7(3) May/June

Kron T, Duggan L, Smith T, Rosenfeld A, Butson M, Kaplan G, Howlett S, Hyodo K., 1998, ‘Dose response of various radiation detectors to synchrotron radiation.’, *Phys Med Biol.* Nov;43(11):3235-59.

Lanson J H , Essers M, Meijer G J , Minken A W H, Uiterwaal G J , Mijnheer B.J., 1999, “In vivo dosimetry during conformal radiotherapy. Requirements for and Findings of a routine procedure”, *Radiotherapy and Oncology* 52 51-59

Leunens G, Van Dam J, Dutreix A, Van der Schueren E., 1994, “Importance of in vivo dosimetry as part of a quality assurance program in tangential breast treatments.” *Int J Radiat Oncol Biol Phys.* Jan 1;28(1):285-96.

Loncol T, Greffe JL, Vynckier S, Scalliet P., ‘Entrance and exit dose measurements with semiconductors and thermoluminescent dosimeters: a comparison of methods and in vivo results.’, *Radiother Oncol.* 1996 Nov;41(2):179-87.

Mayles WPM, Lake R, McKenzie A, Macaulay EM, Morgan HM, Jordan TJ, Powley SK, 1999, ‘*Physics Aspects of Quality Control in Radiotherapy*’, The Institute of Physics and Engineering in Medicine, Fairmount House, 230 Tadcaster Road, York YO24 1ES

Masterson-McGary EM ‘Patient Dosimetry (IVD)’, AAPM 2003, electronic reference, <<http://www.aapm.org/meetings/03AM/pdf/9854-64117.pdf>>

Meijer GJ, Minken AW, van Ingen KM, Smulders B, Uiterwaal H, Mijnheer BJ, 2001, “Accurate in vivo dosimetry of a randomized trial of prostate cancer irradiation.”, *Int J Radiat Oncol Biol Phys.* Apr 1;49(5):1409-18

NIST Physical Reference Database, Electronic Resource
<http://physics.nist.gov/PhysRefData/XrayMassCoef/tab1.html>

NIST Physical Reference Database, Electronic Resource
<http://physics.nist.gov/PhysRefData/XrayMassCoef/tab2.html>

Quach KY, Morales J, Butson MJ, Rosenfeld AB, Metcalfe PE., 2000, 'Measurement of radiotherapy x-ray skin dose on a chest wall phantom.', *Med Phys.* Jul;27(7):1676-80.

Ramaseshan R, Kohli KS, Zhang TJ, Lam T, Norlinger B, Hallil A, Islam M., 2004, 'Performance characteristics of a microMOSFET as an in vivo dosimeter in radiation therapy.', *Phys Med Biol.* Sep 7;49(17):4031-48.

Ramaseshan R, T.Lam, G.Perkins, R.Heaton and M.Islam, 2002, "In-Vivo dosimetry for IMRT using MOSFET dosimeter.", Presentation, 6th Annual MOSFET User Group Meeting

Rowbottom CG, Jaffray DA., 2004, 'Characteristics and performance of a micro-MOSFET: an "imageable" dosimeter for image-guided radiotherapy.', *Med Phys.* Mar;31(3):609-15

Scalachi P, Francescon P., 1998, 'Calibration of a MOSFET detection system for 6-MV in vivo dosimetry.' *Int J Radiat Oncol Biol Phys.* Mar 1;40(4):987-93.

Sessions JB, Roshau JN, Tressler MA, Hintenlang DE, Arreola MM, Williams JL, Bouchet LG, Bolch WE., 2002, 'Comparisons of point and average organ dose within an anthropomorphic physical phantom and a computational model of the newborn patient.', *Med Phys.* Jun;29(6):1080-9.

Soubra M, Cygler J, Mackay G., 1994, 'Evaluation of a dual bias dual metal oxide-Si semiconductor field effect transistor detector as radiation dosimeter.', *Med Phys.* Apr;21(4):567-72.

Tabachnick, B. G., & Fidell, L. S., 1996. "Using multivariate statistics (3rd ed.)". New York: Harper Collins, p18. cited in, Questions and Answers About Language and Statistics
<http://www.jalt.org/test/bro_1.htm>

Tello V M, Tailor R C, Hanson W F, 1995, "How water equivalent are water-equivalent solid materials for output calibration of photon and electron beams?", *Med Phys.* 22(7), July

Thomson and Nielsen Technical Note No.3, 1995, "Reproducibility Using Model TN-RD-19 Dual Sensitivity Bias Supply" Thomson and Nielsen Ottawa

Thomson and Nielsen Users Manual, 1998, 'Operators Manual Patient Dose Verification System Model TN-RD-50', Thomson and Nielsen Eighth Publication.

Thomson and Nielsen Technical Note No.3, 2002, 'Reproducibility Using Model TN-RD-22 Dual Sensitivity Bias Supply', Thomson and Nielsen Ottawa.

Van Dam J, Marinello G, 1994 'Methods for in-vivo Dosimetry in external Radiotherapy', 1st edn, ESTRO and Garant

Voordeckers M, Goossens H, Rutten J, Van den Bogaert W, 1998, "The implementation of in vivo dosimetry in a small radiotherapy department", *Radiotherapy and Oncology* 47, p45-48

Wang B, Kim CH, Xua XG., 2004, 'Monte Carlo modelling of a high-sensitivity MOSFET dosimeter for low- and medium-energy photon sources.' *Med Phys.* May;31(5):1003-8.

Wood JJ, Mayles WP, 1995, 'Factors affecting the precision of TLD dose measurements using an automatic TLD reader.' *Phys Med Biol.* Feb;40(2):309-13.

Williams JR, Thwaites DI, Redpath AT, 1993, "*Chapter 8: Radiotherapy Physics In Practice*", Oxford University Press, Oxford, New York

Appendix A

A An analysis on the effect of phantom scatter on isocentric midline dose estimates for entrance and midline dose prediction

A.1 Definitions:

Tissue Maximum ratio (TMR): The ratio of the dose at D_{\max} on a reference point on the central axis to the dose to the same point at a different depth in a phantom.

TMR: Ratio of the dose at depth z to the dose at D_{\max}

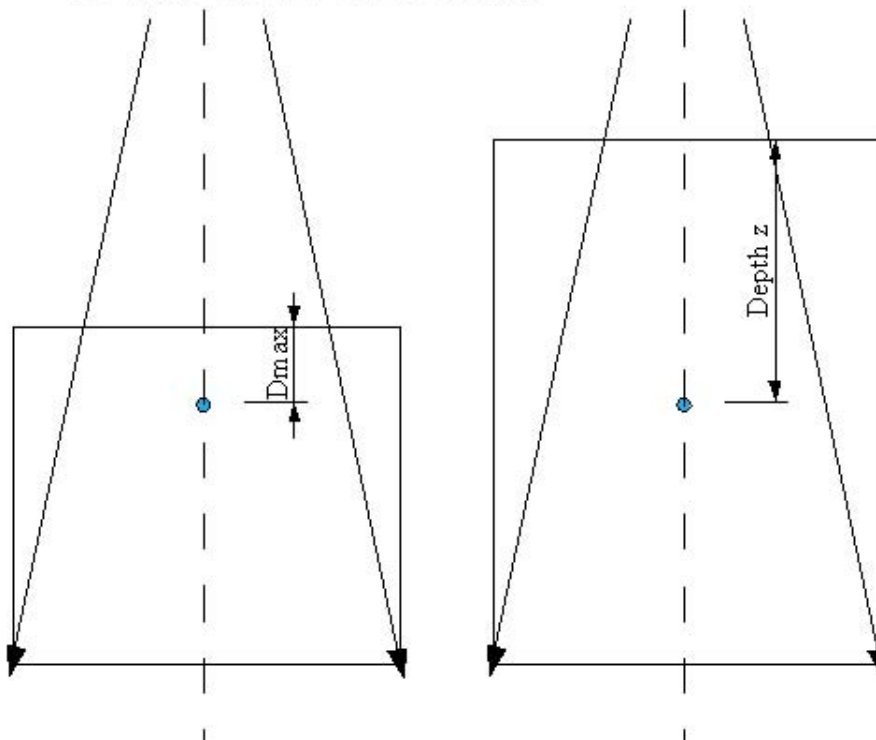


Figure A-1: Setup for measuring TMR

Total scatter correction factor: $S_{c,p}(r)$ is the scatter contribution to the dose at depth originating from the collimating system and the phantom for field size r . r_0 is the reference field size (10 cm x 10 cm).

Collimator scatter correction factor: $S_c(r)$ is the ratio of the effective primary dose for a given collimator field size r (Figure A-2). r_0 is the reference field size (10 cm x 10 cm).

Effective primary dose $P_c(r)$: Dose due to the primary beam as well as photons scattered from the collimating system (including source, target, flattening filter, collimator and other scatterers in the beam) Khan 1980*.

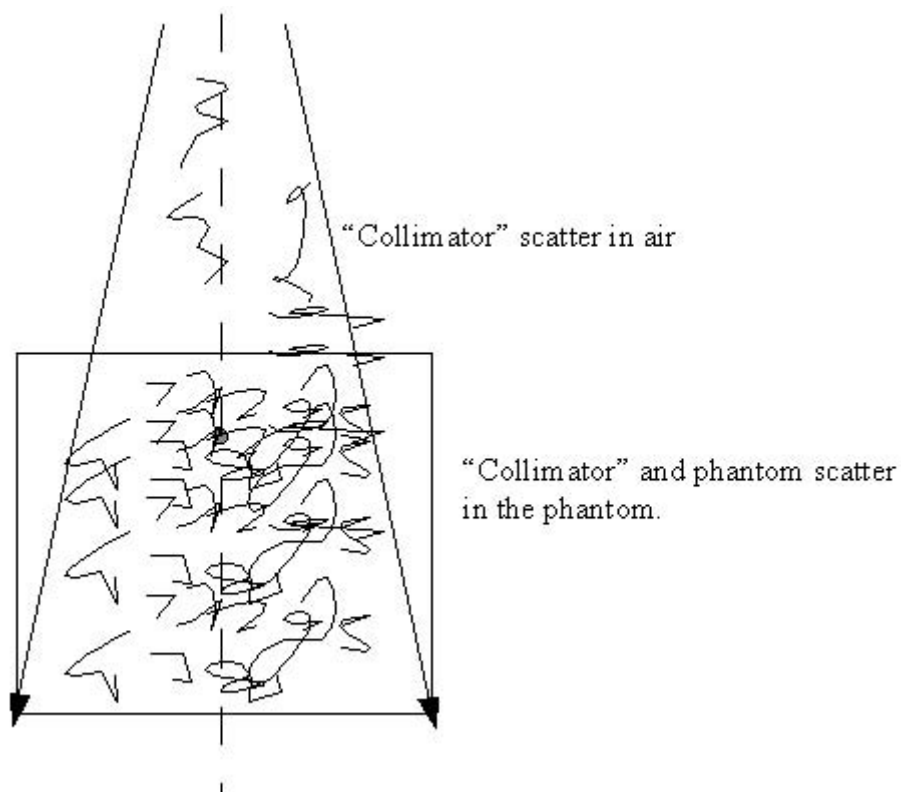
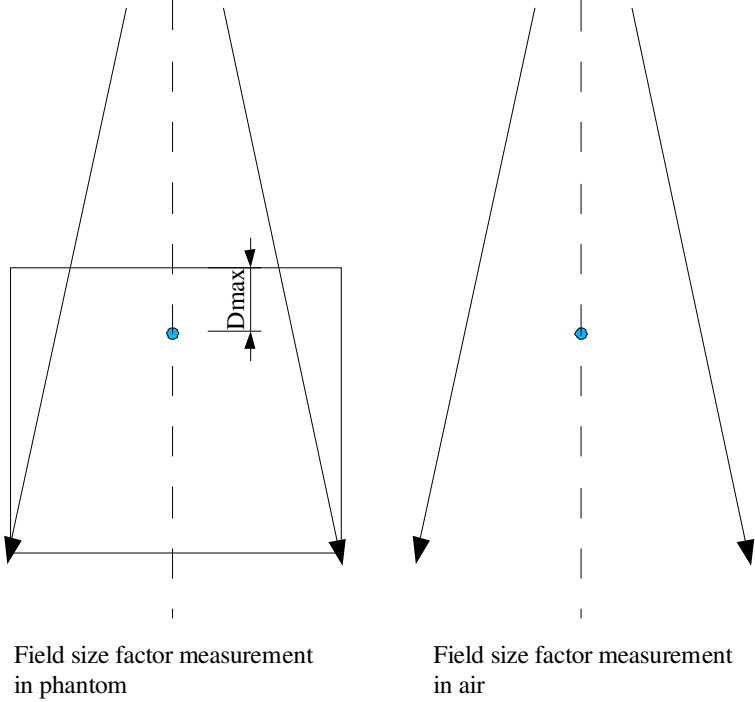


Figure A-2: Scatter from collimator and phantom

Back Scatter Factor $BSF(r)$: The ratio of the dose to D_{max} in a phantom with field size r to the dose in a mini phantom in air of the same field size.

* Khan M F, Sewchand W, Lee J, Williamson J F, 'Revision of tissue-maximum ratio and scatter-maximum ratio concepts for cobalt 60 and high energy x-ray beams', Medical Physics, 1980

Setup for phantom scatter factor measurement.



Scatter Contributions 6 MV

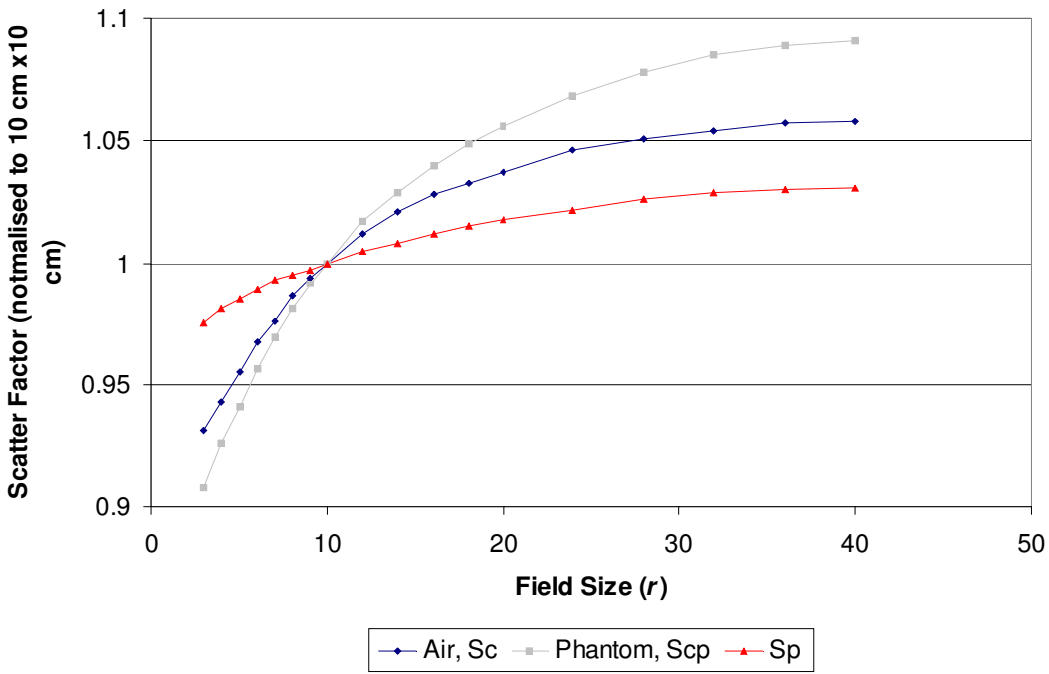


Figure A-3: S_c and $S_{c,p}$ measurements

Figure A-3 shows the setup for measuring S_c and $S_{c,p}$. The field size factor is normalised to a 10x10 field size. Measurements are made in air with a mini phantom for determining S_c .

Measurements are made in water at a fixed reference depth for determining $S_{c,p}$.

A.2 Procedure

A.2.1 Separating Collimator and Phantom Scatter

A.2.1.1 Collimator Scatter

The collimator scatter factors can be derived from measurements in air with an ion chamber and a build up cap such that the external diameter of the cap is large enough to achieve electronic equilibrium (D_{\max}) (Figure A-3).

$S_c(r) = \frac{P_c(r)}{P_c(r_0)} = \frac{1 + f_c(r)}{1 + f_c(r_0)}$, where $f_c(r)$ is the fraction of the primary dose scattered by the

collimating system (Khan 1980). $S_c(r)$ is therefore the ratio of the reading for field size r to the reading for the 10x10 field.

A.2.1.2 Total Scatter (Collimator Scatter and Phantom Scatter)

The total scatter correction factor can be derived from measurements in a phantom at the reference depth (Figure A-3). If r_0 is the reference field size the total scatter correction factor

becomes $S_{c,p}(r) = \frac{P_c(r)}{P_c(r_0)} \frac{[1 + f_p(r)]}{[1 + f_p(r_0)]}$ (Figure A-2 setup B), where $f_p(r)$ is the fraction of the

effective primary dose modified (attenuation and scattering) by the overlying and underlying phantom material (Khan 1980).

From the above relationships the equation below emerges.

$$S_{c,p}(r) = \frac{P_c(r)}{P_c(r_0)} \frac{[1 + f_p(r)]}{[1 + f_p(r_0)]} = S_c(r) \frac{[1 + f_p(r)]}{[1 + f_p(r_0)]}, \text{ as } S_c(r) = \frac{P_c(r)}{P_c(r_0)}$$

A.2.1.3 Phantom Scatter

Therefore

$$\frac{S_{c,p}(r)}{S_c(r)} = \frac{[1 + f_p(r)]}{[1 + f_p(r_0)]}, \text{ which is the phantom scatter correction factor } S_p(r).$$

A.2.2 The case when the reference depth is D_{\max} (Field back scatter)

If the reference depth is the depth of dose maximum, $S_p(r)$ is then $\frac{BSF(r)}{BSF(r_0)}$.

The contribution of the back scatter can then be calculated from the normalised phantom scatter correction factors. The back scatter contribution of field size r to field size r_0 can therefore be derived from $S_p(r)$ (Table A-1).

Siemens Primus 6MV				Siemens Primus 10MV			
FS (r)	$S_c(r)$	$S_{cp}(r)$	$S_p(r)$	FS (r)	$S_c(r)$	$S_{cp}(r)$	$S_p(r)$
3	0.931	0.908	0.975	3	0.916	0.892	0.974
4	0.943	0.926	0.981	4	0.936	0.921	0.984
5	0.955	0.941	0.985	5	0.949	0.935	0.985
6	0.967	0.956	0.989	6	0.962	0.951	0.989
7	0.976	0.969	0.993	7	0.973	0.965	0.992
8	0.986	0.981	0.995	8	0.983	0.978	0.995
9	0.994	0.991	0.997	9	0.993	0.99	0.996
10	1.000	1.000	1.000	10	1.001	0.999	0.998
12	1.012	1.017	1.005	12	1.015	1.017	1.002
14	1.021	1.029	1.008	14	1.026	1.03	1.004
16	1.028	1.04	1.012	16	1.033	1.041	1.008
18	1.033	1.049	1.015	18	1.04	1.05	1.009
20	1.037	1.056	1.018	20	1.046	1.057	1.011
24	1.046	1.068	1.022	24	1.053	1.069	1.015
28	1.051	1.078	1.026	28	1.057	1.076	1.018
32	1.054	1.085	1.029	32	1.061	1.082	1.02
36	1.057	1.089	1.03	36	1.062	1.086	1.023
40	1.058	1.091	1.031	40	1.065	1.088	1.021

Table A-1: 6 MV and 10 MV scatter contributions normalised to 10x10 FS

A.2.3 Error in midplane dose approximation (Entrance and Exit)

For midplane dose approximation the contribution of backscatter that can be attributed to a change in field size can therefore be calculated. The back scatter correction for the exit dose is the ratio of the field back scatter for the exit field size to the entrance field size, B_{A',A_0} (chapter 3).

$$T_{exit} = \frac{TMR_{(A',Z-d_{max})} \times f_1 \times B_{A',A_0}}{TMR_{(A',d_{max})} \times f_2 \times B'_{A'}} \quad (\text{chapter 3}),$$

The back scatter contribution B_{A',A_0} (chapter 3) increases approximately linearly with patient thickness, with a maximum contribution of 0.7% for a patient 25 cm thick (Figure A-4).

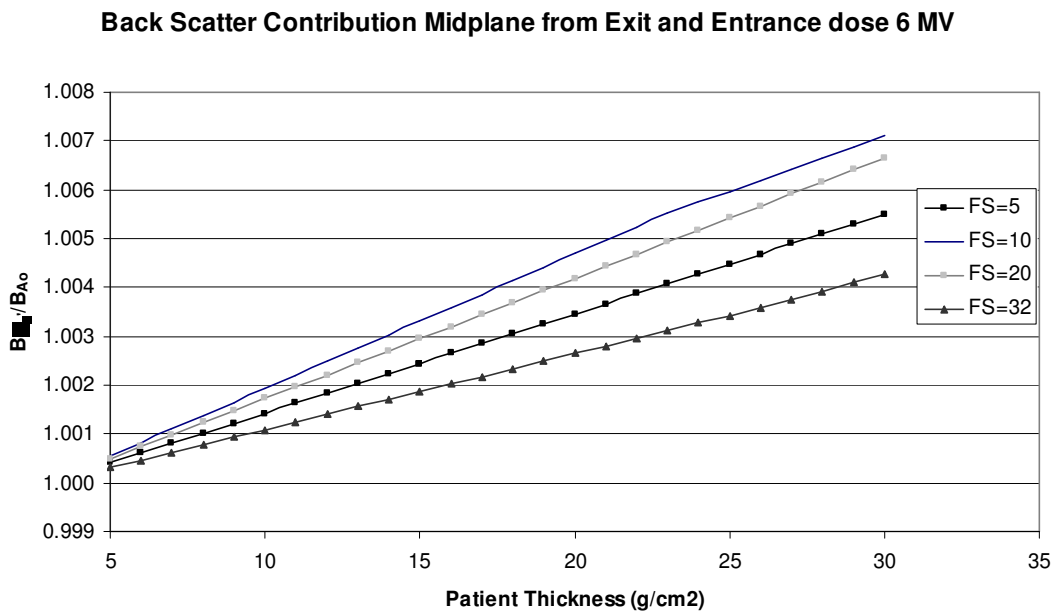


Figure A-4: Back Scatter contribution, TMR midplane

A.2.4 Error in isocentric dose approximation (Entrance only)

For isocentric dose approximation the contribution of backscatter that can be attributed to a change in field size can be calculated. The back scatter correction for the isocentric is the ratio of the field back scatter for the isocentric field size to the entrance field size, B_{A',A_0} .

$$T_{iso} = \frac{TMR_{(A,z)} \times f_1 \times B_{A,A_0}}{(SAD)^2}, \text{ where } B_{A,A_0} = \frac{B_A}{B_{A_0}}$$

The back scatter contribution B_{A,A_0} increases approximately linearly with isocentric depth, with a maximum contribution of 0.6% for an isocentric depth of 20.0 cm (Figure A-5).

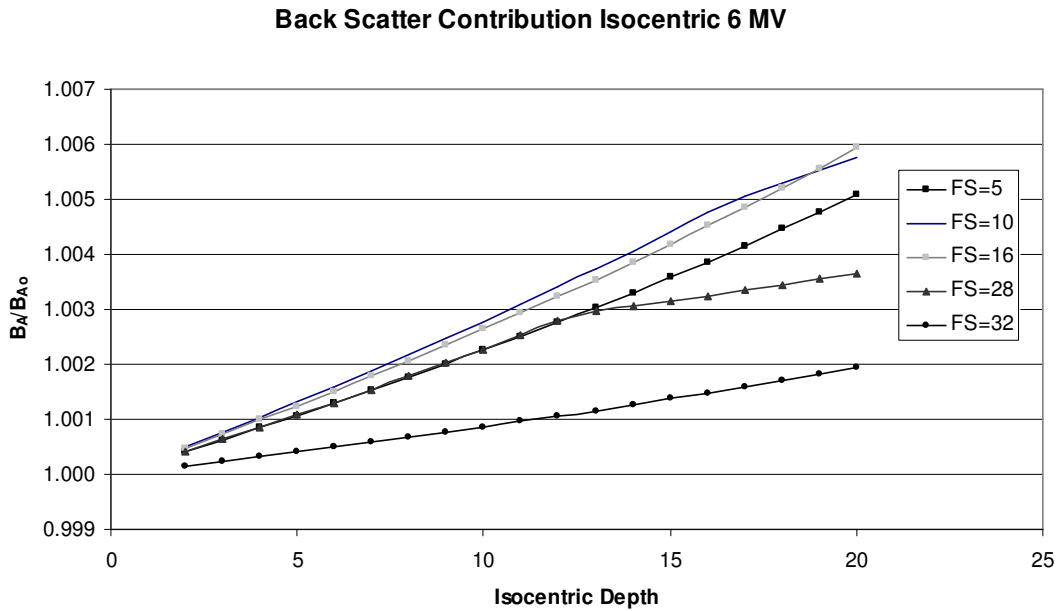


Figure A-5: Back scatter contribution for isocentric treatment